# PARAMETER IDENTIFICATION WITH UNKNOWN INPUT AND INCOMPLETE MEASUREMENTS

**WANG XIAOJUAN**

**NATIONAL UNIVERSITY OF SINGAPORE**

**2013**

# PARAMETER IDENTIFICATION WITH UNKNOWN INPUT AND INCOMPLETE MEASUREMENTS

**WANG XIAOJUAN**

*B. Eng.*
*(Tongji University, China)*
*M. Eng.*
*(Xi'an Jiaotong University, China)*

**A THESIS SUBMITTED**
**FOR THE DEGREE OF DOCTOR OF PHILOSOPHY**
**DEPARTMENT OF CIVIL AND ENVIRONMENTAL ENGINEERING**
**NATIONAL UNIVERSITY OF SINGAPORE**
**2013**

# DECLARATION

I hereby declare that this thesis is my original work and it has been written by me in its entirety.

I have duly acknowledged all the sources of information which have been used in the thesis.

This thesis has also not been submitted for any degree in any university previously.

Ph.D. Candidate: _____ Date: _____

Wang Xiaojuan

# Acknowledgements

I would like to express my sincerest gratitude to my advisor, Prof. Koh Chan Ghee, for his profound vision, research philosophy, invaluable guidance, and encouragement in conducting this research work. I will never forget Prof. Koh's enthusiasm in research. From him, I not only learn how to do research, but also gain ability to deal with real engineering problems.

When carrying out experimental validation in the Structural Engineering Laboratory, I received professional and kind help from the staffs there, who are gratefully acknowledged.

I also would like to appreciate the generous financial support from the National University of Singapore and the American Bureau of Shipping during my PhD study.

In this beautiful tropical country, the happy moments spent with my friends and colleagues, constitute my memory for Singapore.

Finally, I must acknowledge the long-lasting understanding, patience, encouragement and support from my family: my parents, husband and younger brother. In my hard time, they always give me warm and powerful support. Without them, the completion of the thesis would not have been possible.

# Summary

Continuous monitoring and early damage detection of engineering structures are of practical importance since failures of structures may cause great casualties and property loss. The ‘health’ status of a structure can be evaluated with the values of key parameters determined by structural identification based on observed structural response. Nevertheless, difficulty in numerical convergence poses a great challenge to identify a large and complex structural system globally due to considerable number of unknown parameters and degrees of freedom (DOFs) involved. To this end, substructural identification strategy based on the concept of ‘divide and conquer’ provides a novel way to improve numerical convergence due to largely reduced number of unknowns and DOFs.

Although the idea of substructural identification is not new and seems straightforward, the main challenge lies in acquiring complete dynamic measurements at interface, as input to the substructure of concern. Since it is difficult or expensive to obtain complete interface measurements, particularly for beam and plate substructures involving angular accelerations, a recovery method is developed in this study to compute angular accelerations via measurements of strains and translational accelerations. Incorporating this recovery method, an improved genetic algorithm (GA) based on a search space reduction method (SSRM) is employed to identify unknown substructural parameters. Numerical

studies of parameter identification on beam and plate substructures are conducted to validate the effectiveness of the proposed identification strategy.

The difficulty in excitation measurement poses another great challenge in many identification methods for structural or substructural systems. To address this issue, an iterative identification algorithm, involving the use of Tikhonov regularization method and SSRM, is proposed to identify structural parameters without excitation measurements. In each iteration of the strategy, Tikhonov regularization method is adopted to identify the unmeasured excitation forces in state space while structural or substructural parameters are updated with the identification results from SSRM. Numerical studies for global structural identification as well as substructural identification without measurement of excitation forces on a beam and a plate demonstrate the performance of the proposed strategy. Its effectiveness is further verified by an experimental study on a 10-storey frame in laboratory.

Finally, an iterative strategy is developed for substructural identification to address the simultaneous absence of complete interface measurements and excitation forces. The strategy is successfully tested for parameter identification of beam and plate substructures with limited interface measurements and unmeasured excitations. Experimental studies conducted on a 10-storey frame and a small-scale jack-up model further verify the effectiveness of the proposed strategy.

# Contents

**Acknowledgements** ..... **i**

**Summary** ..... **iii**

**Contents** ..... **v**

**List of Tables** ..... **ix**

**List of Figures** ..... **xi**

**List of Symbols** ..... **xv**

**Chapter 1. Introduction** ..... **1**

1.1 Overview of structural identification methods ..... 3

1.2 Classical identification methods ..... 5

1.2.1 Least-square methods ..... 5

1.2.2 Maximum-likelihood estimation ..... 7

1.2.3 Kalman filter methods ..... 8

1.3 Non-classical identification methods ..... 10

1.3.1 Simulated annealing ..... 10

1.3.2 Tabu search ..... 13

1.3.3 Ant colony optimization ..... 15

1.3.4 Particle swarm optimization ..... 18

1.3.5 Neural network ..... 20

1.3.6 Genetic algorithm ..... 24

1.4 Structural identification with unknown input ..... 28

1.5 Substructural identification methods ..... 31

1.6 Objectives and scope ..... 37

1.7 Research significance ..... 39

1.8 Thesis outline ..... 41

**Chapter 2. Substructural Identification with Measurements of Strains and Translational Accelerations ..... 45**

2.1 Substructure method with the concept of 'quasi-static displacement' ..... 48

2.2 Angular acceleration recovery method ..... 51

2.3 Search space reduction method ..... 53

2.4 Substructural identification strategy ..... 59

2.5 Numerical examples ..... 61

2.5.1 Substructural damage identification on a simply supported beam ..... 62

2.5.2 Substructural identification on a cantilever plate ..... 70

2.6 Discussion ..... 76

2.6.1 Differentiation error ..... 76

2.6.2 Sensitivity studies ..... 78

2.7 Summary ..... 81

**Chapter 3. Global Structural Identification with Unknown Input ..... 83**

3.1 Discrete time state space form for global structure ..... 84

3.2 Tikhonov regularization ..... 86

3.3 Iterative global structural identification strategy ..... 88

3.4 Numerical examples ..... 92

3.4.1 Damage identification on a simply supported beam ..... 93

3.4.2 Structural identification on a cantilever plate ..... 99

3.5 Experimental study ..... 101

3.5.1 Stiffness measurements ..... 103

3.5.2 Dynamic test ..... 107

3.5.3 Global frame identification with unknown input force ..... 112

3.6 Estimation of force ..... 115

3.7 Summary ..... 121

**Chapter 4. Substructural Identification with Unknown Input ..... 125**

4.1 Discrete time state space form for substructure with concept of 'quasi-static displacement' ..... 126

4.2 Iterative substructural identification strategy ..... 129

4.3 Numerical examples ..... 132

4.3.1 Substructural damage identification on a simply supported beam ..... 132

4.3.2 Substructural identification on a cantilever plate ..... 137

4.4 Experimental study ..... 140

4.5 Summary ..... 143

**Chapter 5. Substructural Identification with Incomplete Interface Measurements ..... 145**

5.1 Discrete time state space form for substructure with integration technique ..... 147

5.2 Identification strategy ..... 150

5.3 Numerical examples ..... 153

5.3.1 Damage identification on a simply supported beam ..... 154

5.3.2 Substructural identification on a cantilever plate ..... 157

5.4 Experimental study ..... 160

5.4.1 Substructural identification on frame without interface acceleration and excitation force ..... 161

5.4.2 Substructural identification on a small-scale jack-up without interface angular accelerations ..... 164

5.5 Estimation of interface acceleration ..... 170

5.6 Summary ..... 174

**Chapter 6. Conclusions and Recommendations ..... 177**

6.1 Conclusions ..... 177

6.2 Recommendations for future study..... 180

**References ..... 183**

**Appendix A Tikhonov Regularization Method with L-curve for Determination of Regularization Parameter ..... 199**

**Appendix B Strain-to-Displacement Relation in Beam Element ..... 201**

# List of Tables


| | | Pages |
|---|---|---|
| Table 2.1 | GA parameters used for identification of SS1, SS2 and SS3 | 65 |
| Table 2.2 | Absolute identification errors of SS1 and SS2 in undamaged and damaged states | 67 |
| Table 2.3 | Absolute identification errors for Case 1 and Case 2 of SS3 in undamaged and damaged states | 69 |
| Table 2.4 | GA parameters used for identification of SS1 and SS2 | 73 |
| Table 2.5 | Absolute identification error of SS1 and SS2 | 74 |
| Table 3.1 | GA parameters used for global beam and plate identification | 93 |
| Table 3.2 | Absolute identification errors with respect to noise level and iteration number | 95 |
| Table 3.3 | Absolute identification errors with respect to noise level | 101 |
| Table 3.4 | Measured stiffness by static test | 105 |
| Table 3.5 | Natural frequencies computed from measured stiffness by static test | 105 |
| Table 3.6 | Specifications of the accelerometers installed on the frame | 108 |
| Table 3.7 | Identification results of the frame with force measurements | 111 |
| Table 3.8 | Identification results of the frame without force measurements | 113 |
| Table 4.1 | Absolute identification errors of undamaged and damaged SS3 after 20 iterations | 134 |
| Table 4.2 | Measurement set 1 and set 2 | 137 |
| Table 4.3 | Absolute identification errors of SS2 with respect to noise level | 139 |
| Table 4.4 | Identification errors of SS1 with force measurements | 141 |
| Table 4.5 | Identification errors of SS1 without force measurements | 143 |
| Table 5.1 | Absolute identification errors of undamaged and damaged SS3 | 155 |
| Table 5.2 | Measurements of SS2 | 159 |

| | | |
|---|---|---|
| Table 5.3 | Measurement set 1 and set 2 | 159 |
| Table 5.4 | Absolute identification errors of SS2 with respect to noise level | 160 |
| Table 5.5 | Stiffness of SS1 by static test and dynamic test | 161 |
| Table 5.6 | Identification errors of SS1 with unknown forces and interface accelerations | 163 |
| Table 5.7 | Structural parameters for the experimental model | 166 |
| Table 5.8 | Specifications of the installed accelerometers on the jack-up | 167 |
| Table 5.9 | Absolute errors (%) of the identification results of SS1 | 170 |

# List of Figures


| | | Pages |
|---|---|---|
| Figure 1.1 | Flowchart of GA | 25 |
| Figure 1.2 | Organization of thesis | 44 |
| Figure 2.1 | Flowchart of SSRM | 55 |
| Figure 2.2 | Flowchart of iGAMAS | 57 |
| Figure 2.3 | Flowchart of substructural identification strategy using measurements of strains and translational accelerations | 59 |
| Figure 2.4 | A simply supported beam (a) Without damage, (b) With damage and (c) Its numerical model | 63 |
| Figure 2.5 | Three different substructures with sensor placements (a) SS1, (b) SS2 and (c) SS3 | 64 |
| Figure 2.6 | Identified damage extent of SS1 | 66 |
| Figure 2.7 | Identified damage extent of SS2 | 66 |
| Figure 2.8 | Identified damage extent of SS3 (Case 1) | 68 |
| Figure 2.9 | Identified damage extent of SS3 (Case 2) | 69 |
| Figure 2.10 | A cantilever plate model with excitation at a corner | 71 |
| Figure 2.11 | (a) A cantilever plate, (b) SS1 and (c) SS2 | 72 |
| Figure 2.12 | Stiffness identification results of SS1 | 73 |
| Figure 2.13 | Stiffness identification results of SS2 | 74 |
| Figure 2.14 | Exact and recovered interface angular acceleration at node 8 of SS3 | 77 |
| Figure 2.15 | Two different sensor placements for damage identification of SS3 | 79 |
| Figure 2.16 | Sensitivity of translation acceleration at node 3 and angular acceleration at node 4 to elemental stiffness K1, K3, K5 and K7 of SS3 | 80 |
| Figure 3.1 | Flowchart of global structural identification strategy with unknown input | 88 |
| Figure 3.2 | Algorithm of global structural identification with unknown input | 91 |

| | | |
|---|---|---|
| Figure 3.3 | The simply supported beam (a) Numerical mode and (b) Sensor placement | 94 |
| Figure 3.4 | Identified damage extent of the simply supported beam | 94 |
| Figure 3.5 | Identification results of elements 1-8 in undamaged beam, 0% noise | 96 |
| Figure 3.6 | Identification results of elements 9-16 in undamaged beam, 0% noise | 97 |
| Figure 3.7 | Identified flexural rigidity and its search space of element 8, 0% noise | 98 |
| Figure 3.8 | (a) Numerical mode of a cantilever plate (b) Sensor placement | 100 |
| Figure 3.9 | Stiffness identification results of the cantilever plate | 100 |
| Figure 3.10 | The 10-storey steel frame | 102 |
| Figure 3.11 | (a) Illustration of a 10-storey steel frame and (b) The lumped-mass model | 103 |
| Figure 3.12 | Instrumentation of the static test | 104 |
| Figure 3.13 | Natural frequencies of the frame | 106 |
| Figure 3.14 | Instrumentation of the dynamic test | 107 |
| Figure 3.15 | Installed accelerometers on the frame | 108 |
| Figure 3.16 | Sensor placements in the frame | 109 |
| Figure 3.17 | Three random forces applied to the frame at level 10 | 110 |
| Figure 3.18 | Identified stiffness of the frame with force measurements | 111 |
| Figure 3.19 | Sensor placements for frame identification without force measurements | 112 |
| Figure 3.20 | Identified stiffness of the frame without force measurements | 114 |
| Figure 3.21 | Identified force after 1 iteration, 0% noise | 115 |
| Figure 3.22 | Identified force after 5 iterations, 0% noise | 116 |
| Figure 3.23 | Identified force after 20 iterations, 0% noise | 116 |
| Figure 3.24 | Identification errors in estimated forces and flexural rigidities, 0% noise | 117 |
| Figure 3.25 | Identified force, 5% noise | 118 |
| Figure 3.26 | Identified force, 10% noise | 119 |
| Figure 3.27 | FFT results of the identified forces, 5% noise | 119 |
| Figure 3.28 | FFT results of the identified forces, 10% noise | 120 |
| Figure 3.29 | Filtered results of the identified force, 10% noise | 121 |

| | | |
|---|---|---|
| Figure 4.1 | Functions of different measurement sets | 130 |
| Figure 4.2 | (a) The simply supported beam, (b) SS3 and the sensor placement and (c) Numerical model of SS3 | 133 |
| Figure 4.3 | Identified damage extent of SS3 | 134 |
| Figure 4.4 | Identification results of undamaged SS3, 5% noise | 135 |
| Figure 4.5 | Identified flexural rigidity and its search space of element 8 in each iteration, 5% noise | 136 |
| Figure 4.6 | (a) The cantilever plate and (b) SS2 and the sensor placement | 138 |
| Figure 4.7 | Identification results of SS2 | 138 |
| Figure 4.8 | SS1 and the sensor placement | 140 |
| Figure 4.9 | Identified stiffness of SS1 with force measurements | 141 |
| Figure 4.10 | Identified stiffness of SS1 without force measurements | 142 |
| Figure 5.1 | Flowchart of proposed strategy for substructural identification | 152 |
| Figure 5.2 | (a) Numerical model of the simply supported beam, (b) SS3 and the sensor placement and (c) Numerical model of SS3 | 154 |
| Figure 5.3 | Identified damage extent of SS3 | 155 |
| Figure 5.4 | Identification results of undamaged SS3, 10% noise | 156 |
| Figure 5.5 | Identified flexural rigidity and its search space of element 8 in each iteration, 10% noise | 157 |
| Figure 5.6 | (a) The cantilever plate and (b) SS2 and the sensor placement | 158 |
| Figure 5.7 | Identification results of SS2 | 160 |
| Figure 5.8 | SS1 and the sensor placement | 162 |
| Figure 5.9 | Identified stiffness of SS1 with unknown forces and interface accelerations | 163 |
| Figure 5.10 | Experimental model for the jack-up | 164 |
| Figure 5.11 | Illustration of the experimental jack-up model(Wang, 2012) | 165 |
| Figure 5.12 | Installed accelerometers in SS1 | 167 |
| Figure 5.13 | Substructure model of SS1 and the sensor placement | 168 |
| Figure 5.14 | Identified flexural rigidities of SS1 | 169 |
| Figure 5.15 | Identified angular acceleration at node 12 after 1 iteration, 0% noise | 171 |
| Figure 5.16 | Identified angular acceleration at node 12 after 5 iterations, 0% noise | 171 |

| | | |
|---|---|---|
| Figure 5.17 | Identified angular acceleration at node 12 after 20 iterations, 0% noise | 172 |
| Figure 5.18 | Identified angular acceleration on node 12, 5% noise | 173 |
| Figure 5.19 | Identified angular acceleration on node 12, 10% noise | 173 |

# List of Symbols

| | |
|---|---|
| $[C_{rr}]$ | Damping matrix of a substructure |
| $D_i$ | Damage extent for element $i$ |
| $\{d\}$ | Deformation |
| $f$ | Fitness function |
| $err_{mean}^{iter}$ | Absolute mean error after $iter$ iterations |
| $EI_{i\_u}$ | Flexural rigidity of element $i$ before damage occurrence |
| $EI_{i\_d}$ | Flexural rigidity of element $i$ after damage occurrence |
| $iter$ | Iteration number |
| $[K_{rr}]$ | Stiffness matrix of a substructure |
| $K_i^{iter}$ | Identified $i^{th}$ parameter after $iter$ iteration |
| $K_i$ | Stiffness of storey $i$ |
| $L$ | Length of an acceleration time history |
| $[M_{rr}]$ | Mass matrix of a substructure |
| $M$ | Number of measurements |
| $N$ | Number of unknown parameters |
| $Noise$ | Randomly generated noise vector |
| $[R]$ | Mapping matrix |
| $\{s\}$ | Strain |
| $\{U\}$ | $\{\{u\} \quad \{\dot{u}\} \quad \{\ddot{u}\}\}^T$ displacement, velocity and acceleration response of a structure |
| $\{\ddot{u}_j\}$ | Interface acceleration response of a substructure |
| $\{\ddot{u}_r\}$ | Internal acceleration response of a substructure |
| $\{\dot{u}_r\}$ | Internal velocity response of a substructure |
| $\{u_r\}$ | Internal displacement response of a substructure |

| | |
|---|---|
| $\{u_w\}$ | Translational displacement |
| $\{u_\theta\}$ | Angular displacement |
| $\ddot{u}_m$ | Measured acceleration response |
| $\ddot{u}_e$ | Estimated acceleration response |
| $W$ | Applied weight |
| $X$ | Contaminated signal vector |
| $X_{clean}$ | Clean signal vector |
| $\{y\}$ | Measurements used for force identification |
| $\{r\}$ | Rigid body motion |
| $[\Phi_\alpha]$ | Rigid body modes |
| $\{\alpha\}$ | Rigid body amplitudes |
| $\alpha$ | Newmark constant $\alpha = 1/4$ |
| $\delta$ | Newmark constant $\delta = 1/2$ |
| $\Delta t$ | Time interval |
| $\Delta x_i$ | Displacement difference between level $i$ and $i-1$ |

# Chapter 1. Introduction

During the last few decades, health monitoring and damage identification of engineering systems during their service life has attracted increasing attention in the fields of mechanical, aeronautical and civil engineering. Continuous health monitoring and early damage detection on the existing and ageing infrastructure is of significant importance since sudden failure of structures causes great casualties and property loss. Therefore, it is necessary to conduct health monitoring and damage assessment for in-service structures to ensure safe operation.

In early years, visual inspection has been widely applied for structural health monitoring and damage detection. However, it has some inherent drawbacks. It is difficult to inspect large and complex structures due to the inaccessibility of many parts. Moreover, most damage, initiating from the inside of structural components, cannot be detected by naked eyes. Furthermore, structural condition assessment by visual inspection is largely based on subjective criteria. In addition, the visual inspection procedure can be very tedious and time consuming. To complement visual inspection, local non-destructive evaluation (NDE) techniques have been developed. In general, local NDE is based on experimental methods, such as acoustic or ultrasound methods, magnetic field methods, radiography, eddy-current methods and thermal field methods (Doebling et al., 1996). These methods usually require location of possible structural damage to be known as a priori (Zou et al., 2000). Furthermore, service is often interrupted when such monitoring is conducted.

In addition, local NDE is more suitable for individual structural components instead of large and complex structures.

Due to the limitations of visual inspection and local NDE, vibration-based NDE has been proposed as a global identification technique based on the idea that the measured structural vibration responses reflect its dynamic characteristics (Farrar et al., 2001). From mathematical point of view, vibration-based NDE is an inverse problem with the aim of identifying unknown structural parameters from measured vibration data. System identification is extensively employed to solve this inverse problem. When system identification is applied to a structural system with the aim of determining its physical parameters (mass, stiffness and damping), based on measured input (excitation) and output (structural response), it is generally known as structural identification. By employing structural identification methods, continuous health monitoring and damage detection of a structure system with constant dynamic measurements are possible. Damage inside a structure, which adversely affects current or future performance of that structure system, is generally assumed to cause decrease in structural stiffness. By recording and comparing the identified stiffness, the damage inside a structure can be located and quantified.

In recent years, rapid advances of technology in many areas have facilitated development of structural identification. For instance, exponential increase in computer capacity and scientific computation speed has made system identification feasible for very large structures; Advances in sensor technology, PC-based data acquisition systems, wireless communication techniques and broadband data transmission have made real application of structural identification possible. With

primary results by structural identification, health status of structures can be evaluated and appropriate repair and maintenance work can be accordingly planned.

## 1.1 Overview of structural identification methods

There are many comprehensive reviews (Doebling et al., 1996, 1998; Farrar et al., 2001; Sohn et al., 2004) on structural identification methods. During past two decades, significant progress has been achieved on modal-based methods using natural frequencies and their changes since frequencies can be cheaply acquired from measured vibration responses (Kim et al., 2003; Carden and Fanning, 2004; Fan and Qiao, 2011). The fundamental idea of modal-based methods is that damage-induced changes in physical parameters (mass, damping, and stiffness) will cause detectable changes in modal parameters (natural frequencies, modal damping, and mode shapes). Nevertheless, the detected natural frequency changes alone may not be sufficient for a unique identification of structural damage since lower frequency modes are insensitive to small levels of local damage (Salawu, 1997). To address this issue, considerable research works were presented by using other supplementary modal measurements such as mode shape (Ratcliffe, 1997), mode shape curvature (Pandy et al., 1991; Wahab et al., 1999) and some combinations of frequency and mode shape information of structures, e.g. modal strain energy (Shi et al., 1999, 2002), frequency response function (Wang et al., 1997; Hwang and Kim, 2004), frequency response function curvature (Sampaio et al., 1999), flexibility (Alvandi and Cremona, 2006) and flexibility curvature (Lu et al., 2002). From practical point of view, however, it is inconvenient to apply these methods for in-service structures since it is difficult to accurately extract modal parameters from vibration data

without excitation force measurements. Furthermore, the identification results of most modal-based methods largely depend on the accuracy of measurements, and they are normally insensitive to small damage in structures. In addition, the accuracy of identification results can be improved by incorporating measurements of higher modes, mode shape curvature etc., but these supplementary modal measurements are difficult to accurately acquire in practice.

In the last decade, frequency and time domain methods have been extensively explored for structural parameter identification. Frequency domain methods often deal with measurements of structural frequency response function while time domain methods often directly handle measured structural vibration signals. These two groups of methods estimate parameters of the mathematical model describing the structure by minimizing the error between the predicted and observed output. The frequency and time domain methods only require limited vibration responses measurements in structures. Furthermore, since measurements of frequency response function and vibration signals contain global information of structures, these methods are in principle capable of identifying large and complex structures. In practice, since structural responses are directly measured by a variety of sensors, e.g. accelerometers, strain gauges etc., frequency domain methods have to convert the measured response data into the frequency domain by one of the Fourier methods (Caravani et al., 1997). Time domain methods are generally capable of capturing detailed information and adjusting the structure parameters so that the predicted output matches the time-evolving measurements as closely as possible (Koh and Shankar, 2003).

Structural identification methods can be categorized in other ways according to their characteristics and purposes, e.g. parametric and non-parametric models, deterministic and stochastic methods, classical and non-classical methods. In this research, structural identification methods will be reviewed firstly based on a classical and non-classical categorization, followed by discussion of structural identification without input and substructural identification methods.

## 1.2 Classical identification methods

Most classical methods have sound mathematical basis. Some typical classical methods are least-square method, maximum-likelihood technique and the extended Kalman filter. These three classic methods will be reviewed in the context of structural identification as follows.

### 1.2.1 Least-square methods

Least-square method is perhaps the first classical method applied for structural identification. It estimates the unknown parameters of structural systems by minimizing the sum of squared errors between the predicted and measured outputs. In the field of structural identification, the equation of motion for a structural system can be reformulated into an algebraic equation with unknown stiffness and damping coefficients to be determined by solving the algebraic equation with sufficient measurements. Since the idea and implementation of this method are quite simple and straightforward, it has been widely applied for structural identification and damage assessment.

Stiffness and damping coefficients of a three-DOF structure system was identified by use of least-square method (Agbabian et al., 1991). Least-square method was used to identify the fundamental parameters of a simple mathematical model for a mechanical subsystem of a large shaking table such as the effective mass, effective horizontal stiffness (Ozcelik et al., 2008). Classical least-square methods are able to identify constant parameters, but they are inapplicable to track time-varying system parameters. To address this issue, some improved least-square methods were further developed for complicated identification problems. A recursive least-square method with an updated least-square fit technique incorporated was employed to identify stiffness and damping parameters of a building subjected to dynamic excitations (Caravani et al., 1997). Their results show that the identified parameters converge to the accurate values with 5% noise contaminated dynamic measurements. Recursive least-square method was applied for damage assessment on a three-floor shaking table benchmark model experimentally (Chu and Lo, 2011). Furthermore, this method was employed in identifying time-varying modal properties of a real building in Taiwan. Their results show that global damage behaviour due to weak element or components failure can be revealed with the proposed recursive least-square method. The location and extent of the structural damage in continua were correctly identified by using only a limited amount of measurements of incomplete modal data (Chen and Bicanic, 2000). A new adaptive tracking technique based on the least-square estimation approach (Yang and Lin, 2005) was proposed to identify the time-varying structural parameters. Their simulation results demonstrate that the proposed technique is capable of tracking the parametric change of structures induced by damages. Significant achievements have been made on applying the

least-square method to structural identification and damage detection, but the noise contaminated data and the requirements of sufficient measurements impair its performance and limit its applications in this field.

### 1.2.2 Maximum-likelihood estimation

In statistics, maximum-likelihood estimation is a well-known and widely applied approach to the problem of estimating parametric models by maximizing the probability of predicted and observed data. This probability refers to the likelihood function of the measurements. Since likelihood function is monotonically increasing, the parameters are determined by minimizing the logarithm of likelihood function for ease of manipulation. Compared with the least-squares method, maximum-likelihood estimation is superior in determining parameters with non-liner model and non-normal data due to its advantages such as sufficiency, consistency, efficiency and parameterization invariance (Myung, 2003; Franklin, 2005).

Mathematical formulation of back analysis for soil and rock parameters with field instrumentation data with a maximum-likelihood framework was presented (Ledesma et al., 1996) and the formulation was applied to identify parameters in a tunnel excavation problem (Gens et al., 1996). The maximum-likelihood method employed in identification procedure provided an estimation of the reliability of identified Young's modulus of three layers and the ratio of horizontal to vertical in-situ stress in the excavation zone. They also found that reasonable agreement has also been achieved between the stiffness values estimated from field measurement and those measured in laboratory. The frequency response functions for non-

parametric identification of rotor-bearing systems with random or multi-sine excitation were estimated based on the maximum-likelihood estimator, considering noise in multiple-input and multiple-output (Peeters et al., 2001a). An identification procedure based on frequency response functions with maximum likelihood estimation method was developed to yield modal parameters with uncertainties (Peeters et al., 2001b) and was applied for an experimental rotor rig excited by random or multi-sin forces. Their results show that the modal parameters of the rotor rig can be accurately estimated. An automatic identification and tracking procedure based on a frequency domain maximum-likelihood estimator was proposed (Verboven et al., 2002) and applied for damage assessment in a slat track of an Airbus A320 commercial airplane (Parloo et al., 2002). Their results indicate that high accuracy and confident bounds for the estimated parameters are obtained by applying frequency-domain maximum-likelihood algorithm with noisy measurements. In maximum-likelihood estimation, a good initial guess of unknown parameters is very important, since the likelihood function is usually a nonlinear function of the parameters.

### 1.2.3 Kalman filter methods

The Kalman filter, firstly introduced by Kalman (1960), is an algorithm which operates recursively on streams of noisy input data to produce a statistically optimal estimation of the underlying system state by minimizing the mean-square error. A linear dynamic system can be modeled by a Markov chain discretely in time domain, and Kalman filter provides optimal estimation in each discrete time increment for the linear system subjected to Gaussian white noise disturbances. The

standard Kalman filter is inapplicable for non-linear systems due to its linear assumption. To further apply it to nonlinear dynamic systems, extended Kalman filter is proposed to avoid divergent estimation of the parameters and provide acceptable estimation results.

The extended Kalman filter has been widely applied for nonlinear state estimation and parameter identification based on vibration measurements in civil engineering due to its advantages such as high efficiency and accuracy. The extended Kalman filter, incorporated with a weighted global iteration procedure in an objective function for stable and convergent estimation, was applied to system identification for multiple-DOF linear systems, bilinear hysteretic systems, and equivalent linearization of bilinear hysteretic systems (Hoshiya and Saito, 1984). Their proposed approach gives fairly satisfactory estimation for parameters of these systems. Later on, to obtain stable solutions and fast convergence to optima, extended Kalman filter weighted local iteration procedure was proposed and applied for parameter identification in a linear single-DOF model under various noise conditions (Hoshiya and Sutoh, 1992).

An extended Kalman filter approach with an adaptive tracking technique incorporated was proposed to identify the structural parameters and their changes after damage events with vibration data (Yang et al., 2006). Their simulation results demonstrated that the proposed approach is applicable of, and effective in, tracking the changes of system parameters with measured vibration data for both linear and nonlinear structures. In addition, the proposed approach was further applied to identify the structural parameters with unknown inputs (Yang et al., 2007). Their

simulation results for linear and nonlinear structures demonstrate that the proposed approach is capable of identifying the structural parameters, parameters variations as well as unknown excitations. To produce better state estimation and parameter identification, an unscented Kalman filter approach was proposed and applied to structural identification for highly nonlinear systems (Wu and Smyth, 2007). Their numerical studies show that the unscented Kalman filter is more robust to noise contaminated measurements, applicable to non-differentiable function and highly computationally efficient.

## 1.3 Non-classical identification methods

Non-classical methods are based on some heuristic or meta-heuristic concepts (e.g. evolutionary principles) and often depend on computer power for the extensively and hopefully robust search. Generally, many non-classical methods support complex optimization with multi-objectives, uncertainty, nonlinearity, discontinuity or discreteness while many aforementioned classic methods are inapplicable for these complex optimization problems. Comprehensive surveys on meta-heuristic optimization methods were conducted (Blum and Roli, 2003; Rani and Moreira, 2010). In this study, simulated annealing, tabu search, ant colony optimization, particle swarm optimization, neural networks and genetic algorithm are reviewed as the representatives for non-classical methods.

### 1.3.1 Simulated annealing

The simulated annealing strategy, initially introduced for optimization problems by Kirkpatrick et al. (1983), mimics the physical annealing procedure which involves

heating and controlled cooling of a material to increase its crystal size as well as reduce its defects. The thermal equilibrium at any given temperature can be finally reached through heating which causes the atoms to wander randomly to higher energy state from their initial positions as well as cooling which allows them to find states of lower internal energy. The optimization problem with simulated annealing is to find the global minimum of a complicated function of all atomic coordinates. A comprehensive review on convergence of the simulated annealing algorithm to an optimal solution was given by Lundy and Mees (1986).

Kirkpatrick et al. (1983) applied the method for two combinatorial optimization problems: the travelling salesman problem and the layout of chips in circuit design. Furthermore, the simulated annealing strategy was also applied for other optimization problems, such as groundwater management optimization (Dougherty et al., 1991), optimization examination timetabling problem (Thompson et al., 1998), and optimal ship routing (Kosmas and Vlachos, 2012). In structural engineering, the simulated annealing method was intensively applied for optimization design of various structural systems. Amongst, the strategy was developed for discrete optimization of a three-dimensional 6-storey, unsymmetrical steel frames subjected to gravity and seismic loads (Balling, 1991). Furthermore, a 10-storey frame of two or eight variables was optimized with a simulated annealing algorithm incorporating sensitivity analysis and automatic reduction of the search range (Pantelides and Tzan, 1997). In addition, a distributed simulated annealing algorithm was applied for optimal design of a 21-storey irregular steel braced frame subjected to multiple constraints including stress, maximum displacement, and inter-storey drift (Park and Sung, 2002).

Simulated annealing is also intensively applied in the field of structural identification and damage detection. Simulated annealing algorithm was employed to identify parameter structure in a one-dimensional groundwater flow model (Zheng and Wang, 1996). This approach was further extended to identify both the parameter structure and the parameter values. In addition, the technique of simulated annealing was applied to locate and quantify damages in a simulated test structure with experimental data obtained from cracked steel cantilever beams by minimizing the appropriate cost function in terms of the parameters (Ruotolo et al., 1997). An adaptive simulated annealing global optimization technique was developed to estimate the location and severity of damages in a simply supported reinforced concrete beam with experimental modal data from an I-40 Bridge (Bayissa and Haritos, 2007).

Although simulated annealing algorithm is good at hill climbing for optimal solutions and widely applied for various optimization problems, its convergence speed is very slow (Jeong and Lee, 1996; Zhou and Yi, 2007). To improve the convergence speed, some hybrid optimization algorithms have been proposed. Adaptive simulated annealing genetic algorithm incorporating simulated annealing and genetic algorithm was proposed for system identification (Jeong and Lee, 1996). A hybrid algorithm combing an adaptive real-parameter genetic algorithm with simulated annealing was proposed to detect damages in beam-type structures with static displacement responses and natural frequencies information (He and Hwang, 2006). To enhance global searching ability, a new method called genetic simulated annealing algorithm syncretizing the genetic algorithm and simulated annealing was presented for identification of structural parameters of frames (Zhou and Yi, 2007).

Their results show that these proposed algorithms preserve the merits of each algorithm while not substantially altering their identities, and speeds up the convergence.

### 1.3.2 Tabu search

Tabu search algorithm was initially proposed and applied for employee scheduling problem by Glover and McMillan (1986). A local dynamic neighborhood search procedure embedded in tabu search algorithm was employed to find an improved solution in the neighborhood of current solution, until the stopping criterion has been satisfied. The memory structures embodied in tabu search algorithm allows the method to go beyond points of local optima by admitting non-improving moves (Glover, 1990). It enhanced the performance of tabu search method over most conventional local search methods. Three-tier memory structure, e.g. short, intermediate and long-term structures, serves to intensify and diversify the search to achieve superior performance.

Tabu search algorithm was widely applied for various optimization problems, such as travelling salesman problem (Fiechter, 1994; Gendreau et al., 1998), graph partitioning (Rolland et al., 1996), vehicle routing problem (Gendreau et al., 1994, 1996), quadratic assignment problem (Misevicius, 2005). Some research works were also reported on its applicability to structural engineering optimization problems. Amongst, tabu search was employed for weight minimization of two-dimensional frame structures considering multiple load conditions with stress, displacement and local/global buckling constraints, and multiple objective functions in the problem formulation (Bennage and Dhingra, 1995). The cross-sectional areas of a space truss

were taken as variables for optimal structural design in terms of weight minimization with tabu search algorithm (Bland, 1998). In addition, tabu search algorithm was applied for optimization of 3-storey/3-bay, 9-storey/5-bay, and 20-storey/5-bay steel moment resisting frames (Kargahi et al., 2006). They found that tabu search optimization was able to achieve a larger weight reduction for these three frames than commercially available programs (Kargahi and Anderson, 2006).

Tabu search algorithm was extendedly applied for parameter identification of different engineering systems. The parameter structure and parameter values for one-dimensional groundwater flow model were successfully identified with tabu search algorithm while most of traditional gradient-based methods were not applicable for this type of inverse problem (Zheng and Wang, 1996). To achieve faster and more efficient search, an adaptive tabu search was proposed for identification of mechanical system such as hot-air tube, system with torsional resonance, static nonlinearity and inverted pendulum (Puangdownreong et al., 2002). In addition, tabu search algorithm was employed to determine the optimal parameter values of different processes to be modeled (Bagis, 2006). Their results demonstrate that tabu search algorithm is fast and efficient for system identification problems with appropriate value of initial solution, type of move, size of neighborhood, tabu list size, aspiration criterion, and stopping criterion.

From mechanism point of view, tabu search algorithm climbs the hill in the steepest direction and stops at the top then goes downwards to search for another hill to climb. Therefore, a considerable number of iterations are spent on climbing hills rather than searching for the tallest hill. For complex and difficult problems, the

computational resources for tabu search algorithm spent on unwanted search areas exploration are un-negligible. In addition, tabu search algorithm is not guaranteed to achieve optimal solutions. However, it is fortunate that tabu search algorithm can be readily to be integrated with other methods to improve the convergence speed as well as the solution quality. A new integrated genetic algorithms, based on tabu search and simulated annealing method was proposed to solve the unit commitment problem (Mantawy et al., 1999). Their results show that the proposed algorithm performs high speed of convergence and high quality of solutions compared with individual genetic algorithm, simulated annealing and tabu search methods. Recently, a new hybrid algorithm combining enhanced continuous tabu search with elitism based genetic algorithm was proposed and applied to parameter estimation problems (Ramkumar et al., 2011). Their proposed hybrid algorithm yielded unbiased estimation for parameters with the presence of colored noise.

### 1.3.3 Ant colony optimization

Ant colony optimization was initially introduced by Dorigo (1992) to find an optimal path in graph through the behaviour of ants seeking a good (i.e., short) path from their nest to a food source. Ants initially explore the area for food around their colony randomly. As soon as the food is found, a chemical pheromone trail is laid down on the ground of the trip back to their nest so that the location of food source can be found by other ants through tracking pheromone. The quantity of pheromone deposited may depend on the quantity and quality of the food. However, the pheromone trail evaporates with time, thus a long path back to the nest costs more time for pheromone evaporation to a lower density compared with a short path. In

addition, the density of pheromone in shorter path will become higher due to frequently march. As a result, when a shortest path is found by one ant, other ants are more likely to follow that path, and the positive feedback eventually leads all ants to follow that single path (Dorigo and Blumb, 2005).

Ant colony optimization is a typical meta-heuristic algorithm based on stochastic search procedures, which are used to obtain sufficiently good solutions to many optimization problems with reasonable computational time. It has been successfully applied to combinatorial optimization problems such as traveling salesman problem (Dorigo and Gambardella, 1997), routing problem in a computer network (Di Caro and Dorigo, 1998), quadratic assignment problem (Maniezzo and Colorni, 1999), sequential ordering problem (Gambardella and Dorigo, 2000) and shop scheduling problems (Blum and Sampels, 2004).

In the field of structural engineering, ant colony optimization was widely applied to optimization of various structures. Amongst, it was utilized to design space trusses (Camp and Bichon, 2004) and steel frames (Camp et al., 2005) by minimizing the total weight or cost of the structure while satisfying design constraints such as allowable stresses in members and/or nodal deflection limits. Ant colony optimization has been extended and applied for continuous and mixed discrete-continuous optimization problems recently (Socha, 2004). A new ant colony algorithm was proposed to solve dynamic continuous optimization problems (Tfaili and Siarry, 2008). The effectiveness of the proposed algorithm was proved through good performance in their experiment on a set of dynamic continuous test functions. In addition, an improved ant colony optimization algorithm was proposed and

applied to a series of constrained engineering problems, including the design problem of trapezoidal channels, tension/compression string, welded beam, pressure vessel and 10-bar truss (Kaveh and Talatahari, 2008).

In the field of structural health monitoring, ant colony optimization algorithm was adopted to identify the parameters of a concrete dam (Li et al., 2003). They found that the algorithm is more efficient and robust in converging to the global minima for model parameter estimation than gradient-type methods. Furthermore, ant colony optimization algorithm was used for identifying single and multiple damages in a 2-storey rigid frame (Yu and Xu, 2010). Their identification results show that the algorithm is very effective in locating and quantifying the severity of the structural damages. Later on, the effectiveness and robustness of ant colony algorithm was further verified experimentally on a building model of a 3-storey steel frame structure fabricated in laboratory (Yu and Xu, 2011). The experimental results converged quickly in identifying damage location and extent for four different damage patterns. In addition, the ant colony optimization was employed for structural as well as substructural damage identification (Hu and Zhang, 2011). Their results demonstrate that this algorithm is very efficient and stable for structural damage identification.

Ant colony optimization has advantages in giving positive and rapid feedback in process of searching the solution, thus it can find optimal solution for various complicated optimization problems. However, disadvantages of using the algorithm do exist such as difficult theoretical analysis, uncertain convergence in spite of

convergence is guaranteed and the changing probability distribution by iteration (Ziad et al., 2012).

### 1.3.4 Particle swarm optimization

Particle swarm optimization, originally proposed by Kennedy and Eberhart (1995), mimics the social behaviour in flock of birds, bees and fishes on correcting their movements to avoid predators or seek food sources. It searches a space through adjusting the trajectories of individual particles, stochastically approaching toward the positions of the best previous performance of their own and neighbors (Clerc and Kennedy, 2002; Kameyama, 2009).

Particle swarm optimization is a population-based stochastic search algorithm with evolutionary advantages through sharing information among individual particles. Recently, it was widely applied in diverse engineering optimization problems, such as power systems design (del Valle et al., 2008; Alrashidi and El-Hawary, 2009), controllers design (Gaing, 2004; Zamani et al., 2009), mechanical systems design (He et al., 2004). The algorithm was further applied in the field of structural size and shape optimization. Standard size and shape optimization for 2-bar plane truss, 10-bar plane truss, 25-bar space truss and torque arm selected from literature were conducted to evaluate performance of particle swarm optimization algorithm (Fourie and Groenwold, 2002). Furthermore, the optimization algorithm was employed for the optimal sizing design of convex 10-bar truss, non-convex 25-bar truss and convex 36-bar truss (Schutte and Groenwold, 2003). Design of three different truss systems was taken as benchmark optimization tasks with particle swarm optimization algorithm (Perez and Behdinan, 2007).

Particle swarm optimization algorithm was further introduced to detect the location and extent of damage in structural systems due to its major advantages including high reliability and stability, independence of initial estimates of heuristic parameters. The location and extent of single and multi-damage in a 2-storey rigid frame were accurately detected with an improved particle swarm optimization algorithm (Yu and Wan, 2008). A damaged stiffness matrix in a simulated cantilever beam model was identified with this optimization algorithm (Abdalla, 2009). A new particle swarm optimization algorithm was introduced to determine the damage location and extent in a 10-bar truss and a cracked free-free beam (Begambre and Laier, 2009), where the optimization algorithm was able to locate the global optimum with great accuracy and confidence by a small number of function evaluations compared with simulated annealing algorithm. Recently, a two-stage method incorporating particle swarm optimization algorithm was proposed to identify the location and extent of multiple damages in structural systems (Seyedpoor, 2012). In the first stage, a modal strain energy based index was presented to locate damages while in the second stage a particle swarm optimization algorithm was adopted to determine the damage extent. Numerical results of a cantilevered beam and 31-bar planar truss demonstrated that the proposed two-stage method is able to accurately identify multiple structural damages. Besides, a multi-stage optimization approach based on the swarm intelligence algorithm was presented to precisely identify the locations and extents of damages in a 15-element cantilevered beam, a 31-bar planar truss and a 63-element space frame based on natural frequency changes in these structures (Seyedpoor, 2011).

Particle swarm optimization algorithm has become increasingly popular due to its simplicity and high convergence speed. However, some unexpected results may appear when the optimization algorithm is applied for multiple objectives problems. The non-dominated points on the Pareto front are difficult to locate since the velocity and position of each individual is guided by more than one criterion (Coello et al., 2004). Therefore, different modifications have been introduced to standard particle swarm optimization algorithm to improve its performance. A multi-objective particle swarm optimization algorithm, incorporated with techniques including storage and continuous modification of potential solution in external repository, self adaptive mutation, and a simple yet efficient constraint handling methodology, was proposed to identify a real one storey and one bay reinforced concrete frame (Perera et al, 2010). Their results show that the proposed modified algorithm can handle damage identification problems with modeling error in finite element model as well as multiple objectives in the optimization model. A hybrid optimization algorithm combining particle swarm optimization algorithm with genetic algorithm was proposed to identify multiple crack damages in a thin plate using an inverse time-domain formulation with the objective of minimizing the difference between the measured and theoretically predicted accelerations (Sandesh and Shankar, 2010). Their numerical identification results show that the proposed hybrid algorithm obtains more accurate identification results.

### 1.3.5 Neural network

Research on neural network (NN) has recently drawn considerable attention and the way it works is to imitate how brain operates. NN models are made up of

interconnected processing elements called neurons which respond in parallel to a set of input signals given to each. An NN model consists of three main parts, namely neurons, weighted interconnections between neurons and activation functions that act on the set of input signals at neurons to produce output signals. Training of an NN model refers to the determination of weights in the model using some training algorithms which are essential to most NN models. NN has unique capability to be trained to recognize given patterns and to classify other untrained patterns. Therefore, NN operates as a black-box, model-free and adaptive tool to capture and learn significant structures of data.

NN method gives an approximate solution to a problem instead of solving the problem in a rigorous mathematical sense. It has many advantages such as massive parallelism, adaptability, robustness, and the inherent capability to handle nonlinear systems (Chen et al., 1995). Therefore, it has been extensively studied and successfully applied to various problems including face detection (Rowley et al., 1998), river flow prediction (Karunanithi et al., 1994), and image classification (Lu and Weng, 2007). The applications of NN in the field of civil engineering were comprehensively reviewed by Flood and Kartam (1994a; 1994b), Rafiq et al. (2001) and Adeli (2001).

Adeli and Park (1995a) developed a neural dynamic model for structural optimization. Later this model was applied to optimal plastic design of low-rise steel frames (Park and Adeli, 1995). Their results show that the proposed model is able to yield stable results with randomly selected starting points. In addition, a nonlinear neural dynamics model for structural optimization with highly nonlinear and

complicated constraints was proposed and applied to a minimum weight design of space trusses subjected to stress and displacement constraints and multiple loading conditions (Adeli and Park, 1995b). The proposed model was further extended for optimal design of cold-formed steel beams and applied to three commonly used shapes (hat, I, and Z) according to the American Iron and Steel Institute allowable stress design or load and resistance factor design specifications (Adeli and Karim, 1997).

In the field of structural identification and damage detection, the capability of NN was demonstrated (Wu et al., 1992) through a simple 3-storey frame, modeled as a 'shear building', with girders assumed to be rigid and columns being flexible. In their study the computed acceleration time histories were used as measured responses of the structure, which then were passed through a Fast Fourier Transform (FFT) process and the resulting Fourier spectra of the acceleration time histories were used as input to NN. Their results indicate that NN is capable of learning the behaviour of undamaged and damaged structures and identifying the damaged member with evaluated damage extent based on the frequency response of the structure. They also pointed out a big challenge remaining to be resolved before this approach becomes a truly viable method of structural damage assessment in complex structures: a considerate amount of samples is required in NN for training process due to large number of unknown parameters involved.

A NN-based substructural identification (Yun and Bahng, 2000) was conducted to estimate stiffness parameters of a complex structural system, particularly for the case with noisy and incomplete measurements of modal data. In their study,

substructural identification and sub-matrix scaling factor were employed to overcome the issues associated with many unknown parameters in a large structural system. In addition, Latin hypercube sampling and component mode synthesis method were adapted for efficient pattern generation for training the NN, which can adequately establish the relationship between stiffness parameters and modal information. Two numerical studies on a two-span truss and a multi-storey frame show that the substructural technique and the concept of sub-matrix scaling factor are very efficient to reduce the number of unknown stiffness parameters to be estimated. Besides, the identified results were acceptable even with noisy measurements.

Since training NN with samples is time-consuming, to reduce the number of training samples without significantly affecting the accuracy of neural network prediction, orthogonal arrays selection (Chang et al., 2002) for samples training was developed to improve computational efficiency. To demonstrate the efficiency of orthogonal arrays method, four other sample selection methods were also employed for comparison, namely the full factorial selection, the hypercube selection, the linear selection and the random selection. The comparisons results of two cases including a simply supported T beam and a circular plate indicated that the orthogonal arrays selection is most efficient. An adaptive multiplayer perceptron technique (Xu et al., 2001) and a progressive NN (Liu et al., 2002b) were proposed to detect cracks and determine the elastic constants of anisotropic laminated plates. In their study, a modified back-propagation learning algorithm with a dynamically adjusted learning rate and an additional jump factor was developed to speed up the training process for the NN model. Furthermore, to reduce the number of training data, they adopted the

concept of orthogonal array to generate the representative combinations of elastic constants. Although many efforts have been put on improving the performance of NN, the computational efficiency of NN does not compare well with those of other non-classic methods, such as genetic algorithm and particle swarm optimization.

### 1.3.6 Genetic algorithm

Genetic Algorithm (GA) is a very powerful and efficient global optimization method based on the principle of 'survival of the fittest', which imitates biological evolution by natural selection, random crossover and mutation. GA implements a stochastic searching procedure and operates with a population of chromosomes, which represent a set of trial parameters of the target problem. In general, GA starts with an initial population, usually obtained through random sampling, followed by three GA operations, shown in Fig. 1.1. In the selection operation, members of the chromosomes that give the best value of objective function are chosen as the fittest. By using other two genetic operators, crossover and mutation, GA continuously explores potential feasible chromosomes. In GA operation, through selection, crossover and mutation on current population, a likely better new population will be generated. In general, chromosomes are encoded in binary or real number. However, when GA is implemented for engineering problems, long and unwanted computational time is spent on coding and encoding these binary numbers. Moreover, binary coded GA may find it difficult to make some jumps in the search space, due to the limitation of representation ability of binary strings.

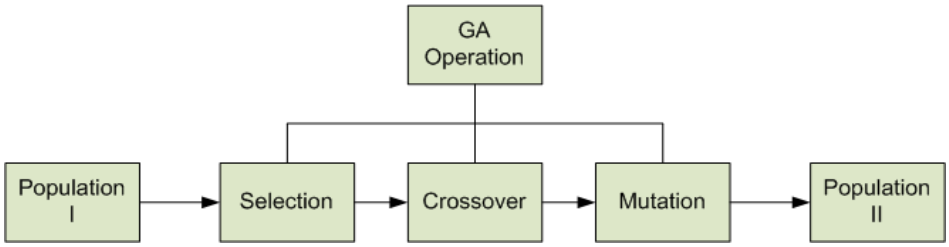


Figure 1.1 Flowchart of GA

Selection operation is to determine which chromosome in current population to be placed in the mating pool, and it also decides that chromosomes with better fitness will be given more copies in the mating pool. Generally, there are two different selection ways, proportion based and ranking based. The proportion based selection decides the number of copies for the chromosomes by the proportion of fitness to the sum of fitness for whole current population, which may potentially lead to a premature solution. The ranking based selection arrays chromosomes by the value of fitness function, and determines the number of copies by its ranking in current population. It avoids being trapped in local optima by allowing the algorithm to limit differences of selection proportions between fitter and less fit chromosomes. Crossover is usually performed on randomly selected pairs of chromosomes in the mating pool. In fact, the single-point crossover is favourable for binary-coding GA. It randomly selects a crossover point and exchanges the information of two chromosomes after that point. The arithmetic crossover may be more effective for the real-coding GA. It performs a linear combination of two chromosomes. After crossover, the new population is then subjected to mutation to further explore available space for variables to avoid premature solution. After these three GA operations, a new generation is evolved.

GA was widely applied in the field of structural health monitoring owing to its inherent advantages, such as global search capacity due to the population-to-population search scheme, fairly loose requirement on initial guess and ease of implementation for parallel computing. Fruitful achievements have been accomplished on the application of GA for structural identification and damage detection. GA was employed to detect the location and magnitude of the damage on a statically indeterminate truss bridge by minimizing difference of measured and predicted static displacements (Chou and Ghaboussi, 2001). The presence, size and degree of flaw in the core layer of sandwiches plates were successfully detected with GA based on the time-harmonical response of the plate to harmonic excitation (Liu and Chen, 2001). A combined GA and nonlinear least-square method was proposed to determine the material property of composite plate (Liu et al., 2002a). A real parameter-coded micro-GA was proposed to inversely determine material constants of composite laminates using dynamic response at one point on the plate surface (Liu et al., 2005). To determine the material constants of the laminated cylindrical shells, a uniform crossover micro-GA was employed as the inverse operator with transient dynamic displacement responses obtained at only one receiving point on the outer surface of shells (Han et al., 2002). By minimizing a global error derived from dynamic residual vectors, GA was applied for parameter identification in three different structures, namely a two-dimensional truss, a cantilever beam and a portal frame (Rao et al., 2004). Based on a continuum damage model, GA was adopted as search engine for health assessment in a simply supported concrete beam with measured modal data (Perera and Torres, 2006).

To further improve the performance of GA, some efforts have been made to incorporate other search algorithms or alter the architecture of GA. To obtain good identification results for systems with many unknown parameters, a hybrid computational strategy was proposed (Koh et al., 2003a), which combines GA with a compatible local search operator. In the study, two hybrid methods were formulated and illustrated by numerical studies to perform significantly better than GA method without local search. A fairly large structure was identified with good results, with incomplete measurements and noisy data taken into consideration. To improve the accuracy and computational efficiency, a modified GA by search space reduction method (SSRM) based on migration and artificial selection was proposed for parameter identification of multiple-DOF structural systems (Perry et al., 2006). This modified GA achieves significant improvement in terms of identification accuracy and computational speed compared with a standard GA. Later on, this modified GA was applied in an output-only strategy for identifying structural parameters and damage in a system of buildings numerically as well as a 7-storey steel frame experimentally based on incomplete, noise-contaminated acceleration measurements (Perry and Koh, 2008). Several sampling methods such as random uniform distribution, Latin hypercube, orthogonal array and Hammersley sequence sampling (Zhang et al., 2010a) and some local search methods such as conjugate gradient method, Broyden-Fletcher-Goldfarb-Shanno method and simulated annealing (Zhang et al., 2010b) were incorporated to reduce the search space for parameters and enhance the convergence speed of GA. Their results show that Hammersley sequence sampling and Broyden-Fletcher-Goldfarb-Shanno method achieve substantial improvement of GA in terms of efficiency and accuracy.

## 1.4 Structural identification with unknown input

Generally, information of excitations are required and taken as input information in most of structural identification methods. However, it is often difficult or even impossible to measure excitations when structural systems are subjected to wind forces or earthquake loads etc. In this regard, some structural identification methods were proposed without excitation measurements.

A considerable number of methods, such as Ibrahim time domain method (ITD), random decrement technique (RDT), Natural Excitation Technique (NExT) and Eigensystem Realization Algorithm (ERA), were proposed to extract natural frequencies, modal damping ratios and mode shapes of a structure from measured vibration signals. Structural parameters are then identified through the extracted modal properties. ITD technique was proposed (Ibrahim, 1977) to extract structure modal parameters directly from measured structure free-decay response signals. Nevertheless, in practice, it is difficult to acquire free-decay response when the structure is under operation. To overcome this difficulty, RDT was proposed (Cole, 1971) to extract free vibration signals from ambient vibration measurements. With extracted modal parameters from combined ITD and RDT, structural mass, damping and stiffness matrices were identified (Huang et al., 1999; Lin et al., 2001). The mathematical basis was proposed (Vandiver et al., 1982) to show that displacement responses of system are equivalent to free-decay responses of the system when input excitation is stationary Gaussian white noise process. RDT incorporated with ITD method were successfully applied to Hakucho suspension bridge in Japan (Siringoringo and Fujino, 2008) with recorded ambient vibration data. The basic

principle of NExT method (Farrar and James III, 1997) involves a time domain curve algorithm to formulate a cross-correlation function between various response measurements on an ambiently excited structure to estimate the resonant frequencies and modal damping. When the structure is subjected to ambient vibration, the cross-correlation function between two response measurements has the same analytical form as the impulse response function (or free vibration response) of the structure. ERA method (Juang and Pappa, 1985), developed to analyze impulse response functions, was applied for cross-correlation functions to obtain resonant frequencies and modal damping of structures. Reliable modal parameters of Hakucho bridge were obtained through NExT combined with ERA (Siringoringo and Fujino, 2008).

In the aforementioned several methods, the accuracy of extracted modal parameters suffers from approximation of external excitations to be stationary Gaussian white noise process. In some situations, this approximation is unrealistic when the structures are subjected to earthquake induced ground motion, strong wind and impact forces etc. In addition, the natural frequencies of first few modes may not change significantly even in presence of major defects, indicating low sensitivity for detecting damage.

Extended Kalman filter (EKF) was adopted to identify system parameters without input excitation on various systems, multiple degree-of-freedom linear systems, bilinear hysteretic systems, and equivalent linearization of bilinear hysteretic systems (Hoshiya and Saito, 1984) when the system was subjected to harmonic excitation or Gaussian white noise excitation. A weighted global iteration (WGI) procedure was developed by them to improve the efficiency and accuracy of

identification results of EKF. They further developed a weighted local iteration (WLI) to improve the performance of EKF in parameter identification of plain strain problems (Hoshiya and Sutoh, 1993). An algorithm (Shi et al., 2000) in the nature of EKF for system identification was proposed to simultaneously estimate system parameters and input power spectral density without requirement of an assumption of input excitation form. Without any restriction on unknown input excitation, an iterative least square (ILS) method was proposed (Wang and Haldar, 1994) to simultaneously identify parameters of an earthquake excited structure and the ground motion. This approach was validated on different types of structures including shear-type building, plane trussed and frames. Nevertheless, application of this approach is limited since the output response measurements at all structural DOFs are necessary. Generally, it is virtually impossible to acquire response measurements at every one DOF especially when a large number of DOFs are involved in a structural system. To address this issue, a technique of combination of ILS and EKF (Wang and Haldar, 1997) was proposed to identify unknown structural parameters at element level with limited observations. A modified ILS method (Chen et al., 2004) was developed to identify both structural parameters and input time history with complete and noise free as well as incomplete and noise slightly contaminated output measurements. The application of their approach was limited to clean or slightly polluted measurements.

An iterative gradient-based model updating method (Lu and Law, 2007) based on dynamic response sensitivity was proposed to identify input excitation force and physical parameters of a structure. Both sinusoidal and impulsive forces on a single-span beam and a two-span beam were studied in their numerical examples. In their

approach, Newmark method was used to compute structural dynamic response and its sensitivities with respect to different parameters of the system. Instead of Newmark method in their previous work, the state-space approach (Lu et al., 2011) was adopted to compute both structural dynamic responses and responses sensitivities with respect to structural parameters as well as force parameters. An iterative damped least-squares method (Zhang and Law, 2009) was applied to simultaneously identify structural parameters and unknown orthogonal coefficients in Chebyshev polynomial approximation which was used to model the support excitation. In their study, local damage and unknown support excitation in a 15-storey shear building and a 5-storey steel frame structure were accurately detected from only a few dynamic responses of the structures. Nevertheless, the numerical convergences posed large difficulties due to the introduced considerable number of unknown coefficients in Chebyshev polynomial approximation.

## 1.5 Substructural identification methods

In practice, it is impossible to identify all unknown structural parameters for a large complex system at one time. Numerical convergence poses the first difficulty due to large number of unknown parameters to be identified. Furthermore, modeling error affects the accuracy of identification results since it is rather difficult to build a very accurate mathematic model for a complex structural system. In addition, the process of identification is extremely time-consuming since structural dynamic response will be computed repeatedly for a system with a large number of DOFs.

To address these difficulties, substructural identification, based on the concept of 'divide and conquer' strategy, provides a feasible solution to identify a large and complex structure system progressively. With substructure approach, a large and complex structure is partitioned into many substructures, each with far fewer DOFs and unknown parameters, so that system identification can be carried out for each substructure of manageable size independently. There are several advantages of substructural identification: (1) The speed and capability of numerical convergence to accurate solution can be significantly improved due to reduced number of unknowns as well as DOFs involved in system identification. (2) Far few sensors are required to be installed in the substructure of concern. (3) Modeling errors can be largely reduced since complicated boundary condition and connection of different structural parts are excluded in substructure. (4) It is unnecessary to measure the excitations if they are outside of the substructure of interest. (5) The identification efficiency of substructures can be largely improved with parallel computing by carrying out system identification for each substructure independently.

Many classical methods were employed as search engines for substructural identification during the last two decades. The earliest work on substructural identification in time domain was reported by Koh et al. (1991) who identified the stiffness and damping coefficients using extended Kalman filter with a weighted global iteration algorithm. In their study, substructural identification was carried out on three types of structures, namely a shear building, a plane frame building and a plane truss bridge. Their results show that substructure approach performs much better than global structural identification in terms of accuracy and efficiency. Extended Kalman filter with weighted global iteration was also employed for

substructural identification in a simple shear building (Orate and Tanabe, 1993) and 2-storey plane frames (Orate and Tanabe, 1994). A discrete auto-regressive, moving average mode with stochastic input and sequential prediction error method was applied for parameter estimation of substructures in a multi-storey building and a truss bridge (Yun and Lee, 1997).

The eigen-system realization algorithm and Kalman filter identification were employed for parameter identification based on the first- and second-order substructure model (Tee et al., 2005). Numerical studies of a 12-DOF system and a larger structural system with 50 DOFs with noise contaminated responses as well as laboratory experiments of an 8-storey frame model illustrated that the proposed methodology is able to locate and quantify the damage fairly accurately. However, response measurements of accelerations are required at all DOFs for this method. From application point of view, it is difficult even impossible to obtain complete measurements due to limited available number of sensors. To eliminate the requirement of complete measurements, an improved substructural identification strategy (Tee et al., 2009) was developed by integrating condensation model identification with a recovery method (Koh et al., 2006). Numerical simulation on a multi-storey shear buildings and a 50-DOF structure system with limited number of sensors as well as experimental study on an 8-storey steel plane frame subjected to shaker and impulse hammer excitations were performed to examine effectiveness and efficiency of the strategy. Both the numerical and experimental results show that the proposed strategy yields reasonably accurate identification in terms of location and extent of damages. However, a considerable number of sensors are still required for this approach and the maximum noise level allowed is limited to only 5%. In

addition, at least one internal force is required to be applied within the substructure, thus it is inapplicable for substructural identification when input excitation is applied outside the substructure of concern.

A combination of a modified iterative least-square technique for substructural identification in the first stage and extended Kalman filter with a weighted global iteration for global structural identification in the second stage was proposed without measurements of input excitation (Katkhuda and Haldar, 2008). Although the approach avoids the measurements of input forces, responses at all DOFs of the substructure and the location of the applied excitation are necessary to implement their proposed substructural identification. Incorporated with discrete adjoint variable method and virtual distortion method, parameter identification of concerned substructure from a global structure was carried out by assuming fixed boundaries of the isolated substructure and applying virtual forces on these boundaries (Hou et al., 2005). The virtual forces were computed by assuming the substructural responses at all DOFs with the modeled fixed boundary conditions to vanish. A numerical example of a frame-truss with 5% and 10% noise levels and an experiment of a cantilever beam were conducted to illustrate success of the isolation methodology in terms of computational efficiency and identification accuracy compared with global structural identification. However, in the study, it is necessary to measure the responses at all DOFs of the substructure, which constrains applicability of the method in case of a hardly accessible boundary.

Compared with application of classical methods in substructural identification, the emerging non-classical methods are more promising in terms of effectiveness,

efficiency and robustness. With rapid development of computer capacity in recent years, an increasing number of non-classical methods were employed, especially NN and GA, for substructural identification.

NN for estimating substructural stiffness was first studied by Yun and Bahng (2000). Natural frequencies and mode shapes were used as input patterns to NN for element-level identification with incomplete measurements of mode shapes. The effectiveness of the proposed method was validated by substructural identification of a 2-span truss and a multi-storey frame structure. However, in the numerical example of a multi-storey frame, limited number of sensors, unavailable angular DOFs measurements and severely contaminated observed data yielded largely deteriorated estimations for substructural stiffness. NN for substructural identification was further applied for joint damage assessment in a numerical study of 2-bay 10-storey frame and an experimental study of a 2-storey frame (Yun et al., 2001). Their results show that joint damages can be reasonably estimated even in case where measured modal vectors were limited to a localized substructure and data were severely corrupted by noise. NN was further employed to develop a substructural identification methodology in time domain with direct use of the acceleration measurements instead of observed natural frequencies and mode shapes (Xu and Du, 2006). The effectiveness of the proposed method was validated through reasonably accurate estimation of stiffness and damping coefficient for the substructure in a shear building. In addition, a multi-stage NN was presented to detect location and extent of damage in a two-span continuous concrete slab and a 3-storey portal frame based on substructure approach with measured modal parameters such as frequencies and mode shapes as input to NN (Bakhary et al., 2010a, 2010b).

Their identification results show that the approach can successfully detect damages in substructures under different damage scenarios.

Due to its robustness and ease of implementation, GA was employed as a search engine for substructural identification and progressive structural identification of a fairly large system of 50 DOFs (Koh et al., 2003b). In their study, the substructure model based on the concept of 'quasi-static displacement' was proposed to eliminate the requirement of time signals of displacement and velocity at the interface. Known-mass and unknown-mass systems with up to 102 unknown parameters were successfully identified even with incomplete and noisy measurements. Due to the difficulty of obtaining complete interface measurements, particularly angular responses at the interface of beam/frame structures, a new substructural identification method with GA embedded was developed in frequency domain to determine the unknown parameters, which completely eliminates the need of interface measurements (Koh and Shankar, 2003). The applicability of the proposed method was validated through numerical studies of a uniform beam containing two substructures and a non-uniform beam with five substructures. The parameter identification of nonlinear structures with GA in time domain has been carried out based on substructural approach from relatively simple lumped mass systems to complex truss systems (Kumar and Shankar, 2009). It is worthwhile to apply GA to substructural identification due to its inherent advantages, such as globally numerical convergence induced by population-to-population search, no requirement for initial condition and gradient information as well as ease of implementation.

## 1.6 Objectives and scope

Based on literature review, excitation measurements are required and treated as input in many structural identification methods. Nevertheless, it is difficult or even impossible to acquire measurement data of excitations in some situations such as natural forces. The absence of excitation measurements poses a huge challenge in the application of many structural identification methods.

Substructural identification approach has shown its advantages in terms of efficiency and accuracy compared with global structural identification due to fewer DOFs and unknowns involved. But complete interface measurements are necessary in most substructural identification methods. From practical point of view, they are not always possible to obtain. In particular, for beam and plate substructures, it is difficult or expensive to accurately measure the considerable number of angular accelerations at interface. The absence of complete interface measurements causes another great difficulty in achieving reliable identification results.

In view of the above challenge and difficulty, the main objectives of this study are:

(1) Develop effective structural and substructural identification strategies without excitation measurements.

(2) Propose applicable identification strategy for beam and plate substructures with incomplete interface measurements.

To achieve these objectives, the scope of this research includes:

(1) Present a substructural identification strategy for beam and plate substructures without measurements of interface angular accelerations, by employment of measurements of strains and translational accelerations.

(2) Propose an iterative identification strategy for parameter identification of structural systems without excitation measurements.

(3) Further develop the proposed strategy in (2) for substructural identification without measurements of forces applied within substructures.

(4) Develop a substructural identification strategy without complete interface measurement as well as excitation force measurements.

(5) Investigate the performance of identification strategies in (1), (2), (3) and (4) through numerical studies.

(6) Validate the effectiveness of identification strategies in (2), (3) and (4) through experimental studies.

In summary, from practical point of view, the identification strategies proposed in this study are to address the insufficiency or absence of input information such as the excitation forces as well as interface responses especially the angular accelerations.

## 1.7 Research significance

The main challenge in structural and substructural identification lies in the fact that excitation forces are difficult or even impossible to measure accurately in practice. The requirement of complete interface measurements poses another great challenge in the application of substructural identification, particularly for beam and plate substructures where angular accelerations at interface are needed but not necessarily measureable. The main significance of this research is to overcome these two challenges through development of innovative identification strategies. The original contributions are summarized as follows.

(1) The proposed recovery method is capable of accurately computing interface angular accelerations via measurements of strains and translational accelerations, so as to provide complete interface measurements required for parameter identification of beam and plate substructures. The method has the advantage of avoiding measurement of angular accelerations at interface, which is more difficult or more expensive to measure than translational accelerations.

(2) The recovery method recovers angular accelerations not only at interface but also at some internal DOFs. The accuracy of identification results is significantly improved by involving these recovered internal angular accelerations in fitness function since angular accelerations are more sensitive to the change of substructural parameters than internal translational accelerations.

(3) Savitzky-Golay differentiation algorithm is introduced for computing the second-order derivatives of strain measurements due to its simple idea of least-squares polynomial fitting and ease of implementation with well-established coefficients. Differentiation error may be significant in the beginning part of signals due to insufficient data. This problem is effectively mitigated in the GA-based identification by ignoring the initial part of simulated and measured signals in fitness function.

(4) Force measurements are difficult or even impossible to obtain in some cases. An iterative identification strategy, incorporating Tikhonov regularization method and SSRM, is proposed for identification of global structures and substructures with no need for force measurements. Tikhonov regularization method is introduced for force identification whereas SSRM is employed for parameter identification.

(5) It is not always possible to obtain complete interface measurements. The iterative strategy is further developed for substructural identification when the interface measurements are insufficient or even absent. The unmeasured interface accelerations are treated in a similar way to unknown forces, which are identified with Tikhonov regularization method.

(6) Finally, combining the above two strategies, i.e., (4) and (5), leads to the iterative identification strategy that is capable of accurately identifying the

time history of unknown excitation forces and unmeasured interface accelerations.

## 1.8 Thesis outline

The thesis consists of six chapters, arranged according to the progressive development and application of different proposed substructural identification strategies.

In the first chapter, the background of structural identification is introduced, followed by literature review on various structural identification methods categorized into classical and non-classical methods. Then the reviews on structural identification with unknown input and substructural identification methods are conducted. Finally, the objectives and scope, research significance and outline of the thesis are provided.

In Chapter 2, to eliminate the requirement of angular acceleration measurements at the interface of beam and plate substructures, a substructural identification strategy is presented by use of translational acceleration and strain measurements. A recovery method is developed to compute angular accelerations from measured strains and translational accelerations. Then the unknown substructural parameters are identified with SSRM. Numerical studies of parameter identification in beam and plate substructures are conducted to validate the effectiveness of the proposed identification strategy.

In Chapter 3, an iterative identification strategy for parameter identification of structural systems is developed to address absence of input excitation measurements. First, the equation of motion of structural systems is formulated into discrete time state space form according to the locations of sensors installed. A strategy incorporating the Tikhonov regularization method and SSRM is proposed to identify the unknown structural parameters. Tikhonov regularization method is employed to identify the excitation forces and SSRM is applied for parameter identification of the structural system in each iteration. To validate the effectiveness of the proposed identification strategy, numerical simulations are carried out on a simply supported beam and a cantilever plate without measurements of applied forces. An experimental study of structural identification on a 10-storey frame is conducted to further verify the proposed identification strategy.

In Chapter 4, a new strategy, incorporating the ideas proposed in Chapter 2 and 3, is developed for substructural identification without measurements of excitation forces applied within substructures as well as without interface angular accelerations which are computed from the measured strains and translational accelerations with the recovery method in Chapter 2. First, the discrete time state space form for substructures with the concept of 'quasi-static displacement' is established to facilitate force identification with Tikhonov regularization method while SSRM is employed as the search engine for substructural parameter identification. Numerical studies of parameter identification in beam and plate substructures and the experimental study for substructural stiffness identification on a 10-storey frame are carried out to validate the effectiveness of the proposed strategy.

In Chapter 5, an iterative substructural identification strategy is developed to simultaneously address the issues of incomplete interface measurements and unknown excitations. The unknown interface accelerations and the unmeasured excitation forces within the substructure are updated with Tikhonov regularization method while substructural parameters are identified with SSRM. Two numerical examples of parameter identification in beam and plate substructures as well as two experimental studies on a 10-storey frame and a laboratory fabricated jack-up are carried out to further investigate the performance of the proposed identification strategy.

The last chapter concludes the thesis with key findings. Some recommendations for future work are outlined.

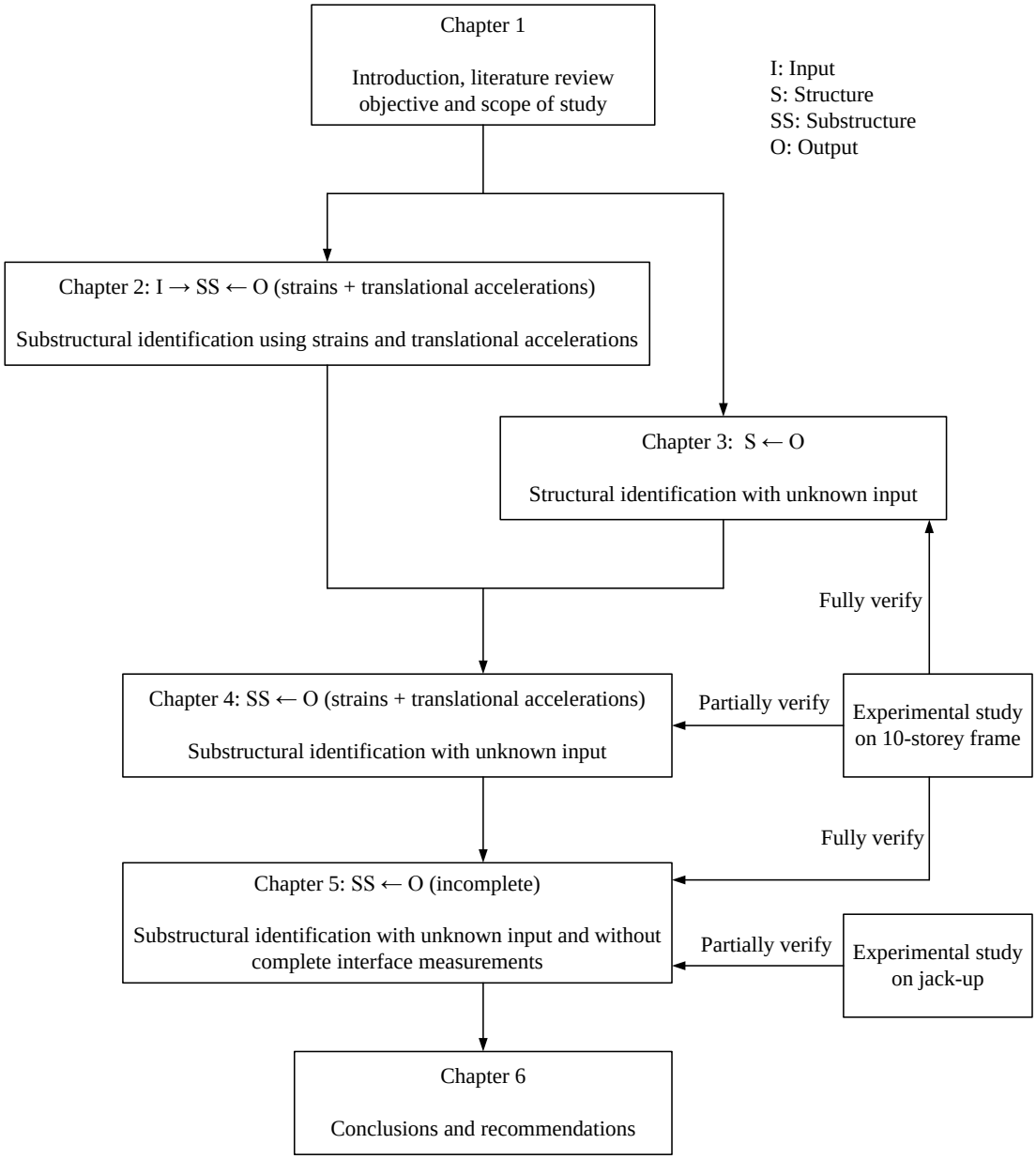


Figure 1.2 Organization of thesis

# Chapter 2. Substructural Identification with Measurements of Strains and Translational Accelerations

Theoretically, given sufficient dynamic measurements, it is possible to identify all unknown parameters for large and complex structural systems at one time. Nevertheless, numerical convergence poses the first challenge due to large number of unknown parameters and degrees of freedom (DOFs) involved. Furthermore, for a complex structural system, it is rather difficult to build a very accurate mathematic model. Thus the accuracy of identification results will be inevitably affected by the modeling error. Additionally, parameter identification for a structure with a large number of DOFs will be extremely time-consuming since structural dynamic responses are needed to be computed repeatedly in the process of identification. To this end, based on the novel concept of 'divide and conquer', substructural identification strategy is adopted to reduce the number of unknowns and DOFs, so as to improve the numerical convergence to the optimal solution, reduce the modeling error and enhance the computational efficiency.

The idea of substructural identification appears straightforward by dividing a large and complex structure into many substructures which can be identified separately. The main difficulty lies, however, in obtaining interface forces at interface DOFs which are necessary to compute dynamic responses of the concerned substructure,

separated from the remaining part of structure. The complete displacement, velocity and acceleration measurements at interface DOFs should be gathered to compute the substructural interface forces. Although the interface displacement and velocity can be obtained from the measured acceleration at interface by applying integration techniques, the accuracy of integrated displacement and velocity is inevitably affected by noise in the acceleration measurements. To avoid measuring interface displacement and velocity, Koh et al. (2003b) proposed a concept of 'quasi-static displacement' to compute the interface force with the measured interface acceleration by neglecting the damping force, which is usually small compared to the inertia force in typical civil engineering structures subjected to dynamic loads. With this concept, the substructural parameters are successfully identified numerically and experimentally without interface displacement and velocity measurements.

Although it is unnecessary to measure the interface displacement and velocity, the complete acceleration measurements at interface DOFs are still required to compute interface forces for substructural forward analysis. At the interface of beam and plate substructures, it is necessary to measure not only translational accelerations but also angular (rotational) accelerations. In principle, angular acceleration can be obtained indirectly by post-processing the available angular displacement or velocity signal (Ovaska and Valiviita, 1998). Nevertheless, angular displacement or velocity sensors of various kinds have disadvantages such as complicated design, high cost or low precision (Liang et al., 2010). For instance, capacitive sensors have high demands on processing; optical sensors have limitations for their integration in miniature mechanical systems (Khiat et al., 2010). Although some numerical

differentiation algorithms and filtering methods were developed to alleviate the noise amplification effect in process of differentiation, these effects are unfavourable since the main noise in angular acceleration comes from the quantization of angular displacement and velocity signal during the approximate differentiation. Angular accelerometers have not been widely used in commercial application due to their limited angular measurement range or high cost as their major drawbacks, although they measure angular accelerations in a direct way (Wolfaardt, 2005). For instance, a high precision of miniature force balance angular accelerometer Columbia SR-220 RNP weights 113g, whose mass effect is negligible for application to large structures, but may not be small enough for application to small structures and substructures. Although some microelectromechanical systems (MEMS) angular accelerometers have been invented and developed, their performance cannot be compared to that of conventional sensors (Aizawa et al., 2008). Therefore, from application point of view, it is not easy to accurately acquire complete angular accelerations directly at interface while they are required as input for substructural identification.

In contrast, with the advantages of being small in size and mass, easy attachment, high sensitivity and low in cost, strain gauge is one of the most widely applied sensors in research and industry. In addition, the technology and application of fiber sensors have progressed rapidly in the last two decades due to their advantages over other types of sensors in terms of electrically passive operation, electromagnetic interference immunity, high sensitivity, and multiplexing capabilities (Kersey et al., 1997). For structural health monitoring, impact detection, shape control and vibration damping, fiber Bragg grating (FBG) optical strain sensors are widely

applied in bridges, mines, marine vehicles and aircrafts, as demonstrated by Rao (1999). Therefore, in practice, strains can be readily obtained by applying strain gauges in most cases and FBG optical strain sensors for some special conditions such as harsh environments and long-range, long-term deployments.

To overcome the difficulty of obtaining angular acceleration directly with expensive angular accelerometers or indirectly with angular displacement sensors or gyroscopes (angular rate sensors), a recovery method is proposed to compute interface angular accelerations by use of measured strains and translational accelerations. Incorporating with this recovery method, SSRM is applied to identify the unknown substructural parameters. Numerical studies of substructural identification in a simply supported beam and a cantilever plate are conducted to validate the effectiveness of the proposed identification strategy.

## 2.1 Substructure method with the concept of 'quasi-static displacement'

This method was proposed by Koh et al. (2003b), briefed as follows. Generally, the motion of a multi-DOF dynamic system can be described as

$$[M]\{\ddot{u}\}+[C]\{\dot{u}\}+[K]\{u\}=\{P\} \tag{2.1}$$

where $[M]$, $[C]$ and $[K]$ are mass, damping and stiffness matrices of the structural system, respectively. $\{\ddot{u}\}$ , $\{\dot{u}\}$ , $\{u\}$ represent the acceleration, velocity and displacement responses when the structure is subject to excitation forces $\{P\}$.

The procedure of structural identification involves computing dynamic responses repeatedly, when the system involves a large number of unknown parameters, obtaining dynamic responses for whole structure with considerable number of DOFs can be incredibly time consuming. The substructure method (Koh et al., 2003a) was proposed to focus on a part of the structure we are interested in, which significantly reduces the number of unknown parameters and DOFs. The equation of motion for a substructure extracted from Eq. (2.1) yields

$$\begin{bmatrix} M_{rj} & M_{rr} \end{bmatrix} \begin{Bmatrix} \ddot{u}_j \\ \ddot{u}_r \end{Bmatrix} + \begin{bmatrix} C_{rj} & C_{rr} \end{bmatrix} \begin{Bmatrix} \dot{u}_j \\ \dot{u}_r \end{Bmatrix} + \begin{bmatrix} K_{rj} & K_{rr} \end{bmatrix} \begin{Bmatrix} u_j \\ u_r \end{Bmatrix} = P_r \tag{2.2}$$

where subscripts *r* and *j* denote internal and interface DOFs of the substructure. Treating interface responses as 'input' for the substructure concerned, Eq. (2.2) can be rearranged as

$$[M_{rr}]\{\ddot{u}_r\} + [C_{rr}]\{\dot{u}_r\} + [K_{rr}]\{u_r\} = \{P_r\} - [M_{rj}]\{\ddot{u}_j\} - [C_{rj}]\{\dot{u}_j\} - [K_{rj}]\{u_j\} \tag{2.3}$$

The concept of "quasi-static displacement" vector is adopted to eliminate the requirement of time signals of displacement and velocity since the acceleration measurement is preferred over displacement and velocity in practice (Koh et al., 2003b). The displacements at internal DOFs are expressed as the sum of quasi-static displacements $\{u_r^s\}$ and relative dynamic displacements $\{u_r^*\}$

$$\{u_r\} = \{u_r^s\} + \{u_r^*\} \tag{2.4}$$

Quasi-static displacements can be obtained by solving Eq. (2.3) while ignoring the applied force, inertia effect and damping effect (all time-derivative terms set to zero).

$$[K_{rr}]\{u_r^s(t)\} = -[K_{rj}]\{u_j\} \tag{2.5}$$

or

$$\{u_r^s\} = -[K_{rr}]^{-1}[K_{rj}]\{u_j\} = [r]\{u_j\} \tag{2.6}$$

where $[r]$ is called the influence coefficient matrix which relates internal DOFs to interface DOFs under the quasi-static condition. Based on the quasi-static concept, we have

$$\{\dot{u}_r^s\} = -[K_{rr}]^{-1}[K_{rj}]\{\dot{u}_j\} = [r]\{\dot{u}_j\} \tag{2.7}$$

$$\{\ddot{u}_r^s\} = -[K_{rr}]^{-1}[K_{rj}]\{\ddot{u}_j\} = [r]\{\ddot{u}_j\} \tag{2.8}$$

Substituting Eq. (2.7) and Eq. (2.8) into Eq. (2.3) leads to

$$[M_{rr}]\{\ddot{u}_r^*\} + [C_{rr}]\{\dot{u}_r^*\} + [K_{rr}]\{u^*{}_r\} = \{P_r\} - \left([M_{rj}] + [M_{rr}][r]\right)\{\ddot{u}_j\} - \left([C_{rj}] + [C_{rr}][r]\right)\{\dot{u}_j\} \tag{2.9}$$

where $\{\ddot{u}_r^*\}$, $\{\dot{u}_r^*\}$ and $\{u^*{}_r\}$ are responses with applied forces located within the substructure, inertial and damping effects into consideration. Since damping force is usually small compared to inertia force in typical civil engineering structures, the velocity dependent part in the interface forces is assumed to be negligible. Thus Eq. (2.9) can be rearranged as

$$[M_{rr}]\{\ddot{u}_r^*\} + [C_{rr}]\{\dot{u}_r^*\} + [K_{rr}]\{u^*{}_r\} = \{P_r\} - \left([M_{rj}] + [M_{rr}][r]\right)\{\ddot{u}_j\} \tag{2.10}$$

If there is no force applied within the substructures, $\{P_r\}$ vanishes and the response of internal DOFs are determined solely by the interface forces. Equation (2.10) can be written as

$$[M_{rr}]\{\ddot{u}_r^*\}+[C_{rr}]\{\dot{u}_r^*\}+[K_{rr}]\{u^*{}_r\}=-\left([M_{rj}]+[M_{rr}][r]\right)\{\ddot{u}_j\} \tag{2.11}$$

Only accelerations (no displacements or velocities) at interface DOFs are required to compute the interface forces.

## 2.2 Angular acceleration recovery method

The angular acceleration recovery method is based on the derived strain-to-displacement relation by Reich and Park (2001) to determine nodal rotational displacements with strains. Within an element, the displacement $\{u\}$ can be divided into deformation $\{d\}$ and rigid body motion $\{r\}$ as follows

$$\{u\}=\{d\}+\{r\} \tag{2.12}$$

The rigid body motion can be written as

$$\{r\}=[\Phi_\alpha]\{\alpha\} \tag{2.13}$$

where $[\Phi_\alpha]$ and $\{\alpha\}$ are the elemental rigid body modes and associated rigid body motion amplitude. Within an element, the displacement-strain relation is

$$\{s\}=[S]\{u\} \tag{2.14}$$

Since the rigid body motion does not induce any strain, substitute Eq. (2.12) into Eq. (2.14)

$$\{s\} = [S]\{u\} = [S](\{d\} + \{r\}) = [S]\{d\} \tag{2.15}$$

From Eq. (2.15), the deformation can be obtained by taking pseudo inverse operation on the rank-deficient matrix $[s]$

$$\{d\} = [\Phi_s]\{s\} = \left[[S]^T[S]\right]^{-1}[S]^T\{s\} \tag{2.16}$$

Hence, the displacement within an element can be expressed as

$$\{u\} = [\Phi_s]\{s\} + [\Phi_\alpha]\{\alpha\} \tag{2.17}$$

where $[\Phi_s]\{s\}$ and $[\Phi_\alpha]\{\alpha\}$ represent the deformation and rigid body motion within an element in Eq. (2.12). For a beam, plate or shell element, the displacement $\{u\}$ involves translational displacement $\{u_w\}$ and angular displacement $\{u_\theta\}$. Equation (2.17) is partitioned into translational and angular groups, giving

$$\begin{Bmatrix} u_w \\ u_\theta \end{Bmatrix} = \begin{bmatrix} \Phi_{sw} \\ \Phi_{s\theta} \end{bmatrix}\{s\} + \begin{bmatrix} \Phi_{\alpha w} \\ \Phi_{\alpha\theta} \end{bmatrix}\{\alpha\} \tag{2.18}$$

With the measured translational motion and strain, the unknown angular displacement $\{u_\theta\}$ and rigid body motion amplitude $\{\alpha\}$ can be obtained by solving Eq. (2.18) as follows

$$\begin{Bmatrix} \alpha \\ u_\theta \end{Bmatrix} = \begin{bmatrix} -\Phi_{\alpha w} & 0 \\ -\Phi_{\alpha\theta} & I \end{bmatrix}^{-1} \left\{ \begin{bmatrix} \Phi_{sw} \\ \Phi_{s\theta} \end{bmatrix}\{s\} - \begin{bmatrix} I \\ 0 \end{bmatrix}\{u_w\} \right\} \tag{2.19}$$

From Eq. (2.19), it is obvious that the angular displacement $\{u_\theta\}$ and rigid body motion amplitude $\{\alpha\}$ can be uniquely determined by the measured strain and translational displacement within an element. Reich and Park (2001) adopted this approach and successfully obtained unknown angular displacements by use of strain and translational displacement measurements in numerical examples of a cantilever beam and a cantilever plate. In practice, however, the acceleration measurement is preferred over displacement since displacement transducers are difficult or expensive to install, compared with accelerometers. Furthermore, from Eq. (2.10), instead of interface angular displacements, interface angular accelerations are involved as a part of complete interface acceleration measurements, which are indispensable for forward analysis of substructures. Differentiating Eq. (2.19) twice with respect to time yields

$$\begin{Bmatrix} \ddot{\alpha} \\ \ddot{u}_\theta \end{Bmatrix} = \begin{bmatrix} -\Phi_{\alpha w} & 0 \\ -\Phi_{\alpha\theta} & I \end{bmatrix}^{-1} \left\{ \begin{bmatrix} \Phi_{sw} \\ \Phi_{s\theta} \end{bmatrix} \{\ddot{s}\} - \begin{bmatrix} I \\ 0 \end{bmatrix} \{\ddot{u}_w\} \right\} \tag{2.20}$$

From Eq. (2.20), it is clear that the translational acceleration $\{\ddot{u}_w\}$ can be measured directly with accelerometers and $\{\ddot{s}\}$ can be obtained by differentiating the measured strain. Then the angular acceleration $\{\ddot{u}_\theta\}$ can be solved with measured $\{\ddot{u}_w\}$ and computed $\{\ddot{s}\}$ with Eq. (2.20).

## 2.3 Search space reduction method

The convergence rate and accuracy of GA highly depend on the size of the search space. Search space reduction method (SSRM), proposed by Koh and Perry (2006,

2010), yields more accurate solutions with improved efficiency by adaptively reducing the search space limits for unknown parameters in GA. The essential idea of SSRM is simple: reduce the time spent on looking far outside the area where the optimal solution lies in, and let the search space for those parameters reduce quickly. These are achieved by carrying out several runs of the improved GA based on migration and artificial selection (iGAMAS), followed by the computation of the mean and standard deviation of the identified parameters. The standard deviation indicates the uncertainty of the parameter. Small value of standard deviation implies converged identified parameter. When some parameters converge almost exactly, the SSRM effectively reduces the number of unknown parameters and those remaining can be identified more efficiently. The flowchart of SSRM is illustrated in Fig. 2.1.

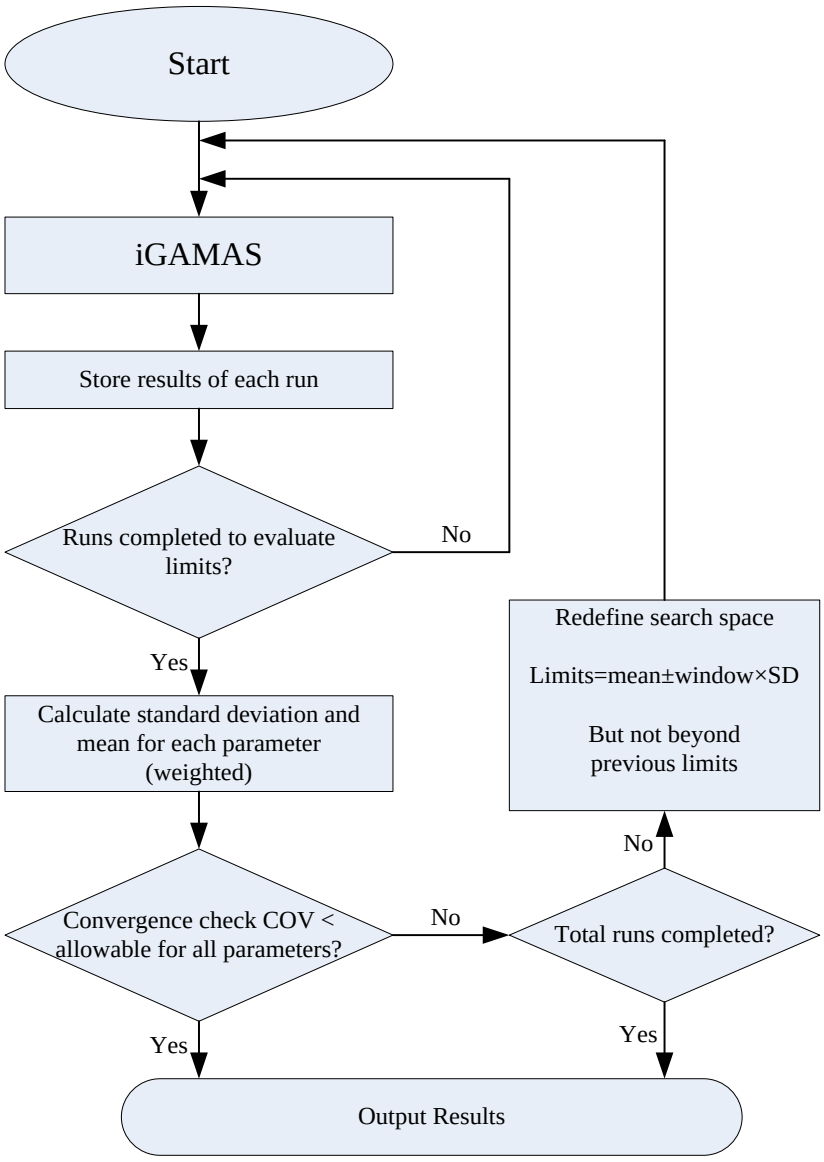


Figure 2.1 Flowchart of SSRM

The basic parameters defined in SSRM are the number of runs for evaluation of search limits, the width of the reduced search space window and the total number of runs. The number of runs is used for evaluating the search space, hence the value of the number of runs should be selected moderately so that it is sufficient to get a good estimation of the mean of the parameters, but not so large that it includes very old results that would slow down the convergence. In general, more runs will make the

system identification more robust at the price of increase in total computational time. The new search space is defined as

Search space = Mean ± Window × Standard deviation

The new search space is usually not wider than the original limits. In SSRM, the mean values of parameters are calculated using weighted results and the more recent runs are given a higher weight. A small standard deviation implies the mean is very likely close to the optimal parameter value and the search limits can be reduced since normally the value of width of window is unchanged. It is important to choose a window sufficiently small to achieve convergence but adequately wide to confine the actual solution within the new search space. In practice, a value of window width of about 4 has been found to be efficient. The total number of runs is decided by accuracy requirement. The mean values and standard deviation of parameters can be obtained from results of the previous runs. Then the updated search limits can be calculated to narrow down the search space. Generally, the results will be increasingly accurate when the search space reduces after each run. However, accuracy will be limited due to factors such as noise and it is possible that there is no further improvement after a time. Therefore in general, more total runs lead to more accurate results; but the computational time increases rapidly.

The heart of SSRM is the improved GA based on migration and artificial selection, whose important features distinguishing iGAMAS (Perry et al., 2006; Koh and Perry, 2010) from ‘normal’ GA are inclusion of multiple species, artificial selection,

regeneration and variable data length procedure. The flowchart of iGAMAS is shown in Fig. 2.2.

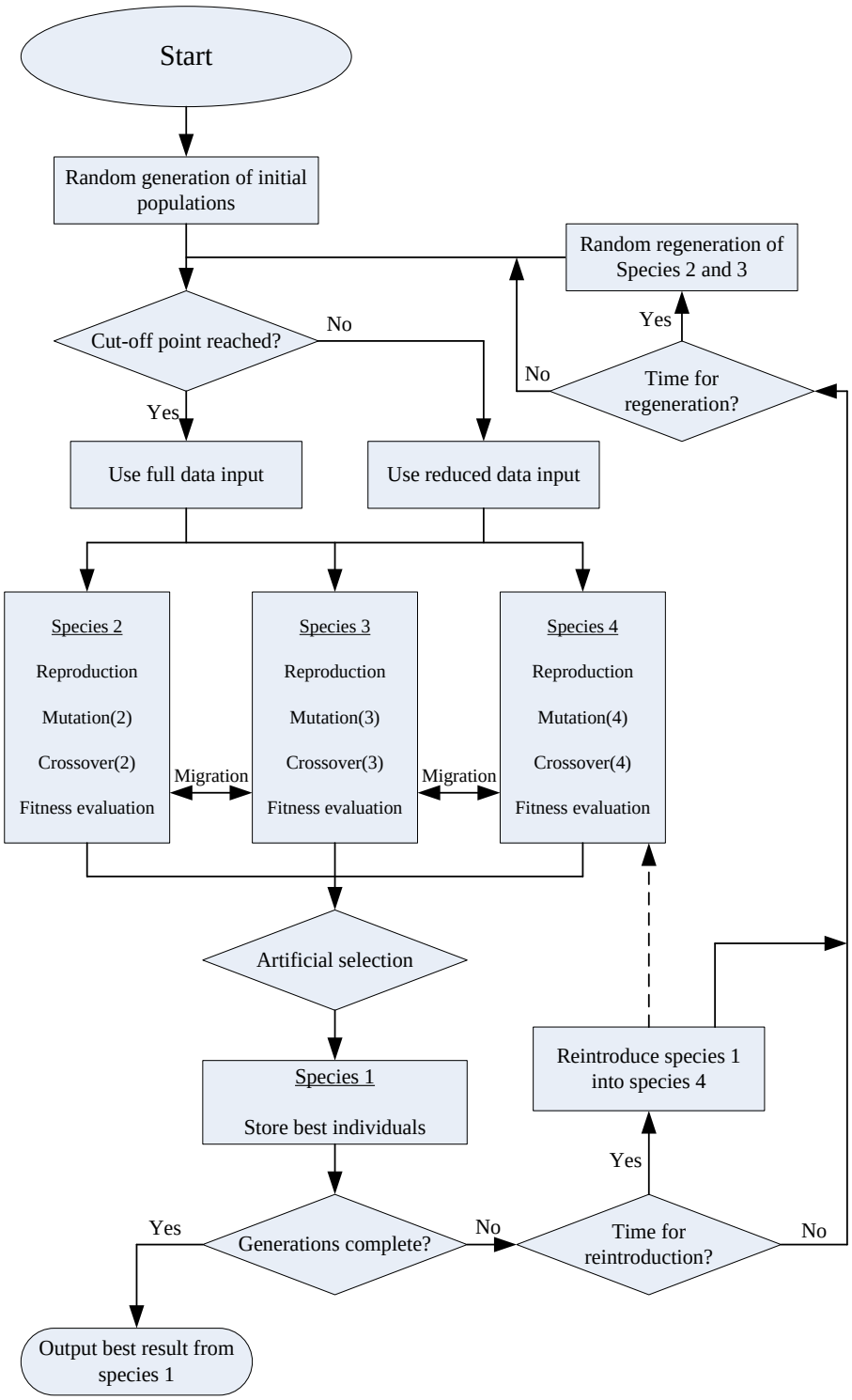


Figure 2.2 Flowchart of iGAMAS

The real power of the iGAMAS strategy lies in division of the population into different species. In GA, it is difficult to find a balance between utilizing the information from previous good solutions (exploitation), and maintaining a broad search capacity (exploration). With multiple species, this problem is greatly settled since as one species searches broadly another searches locally around the best solutions. Four species have been adopted in iGAMAS. Species 1 is used to store the best results and species 2-4 conduct the search from a very broad random search to a more refined local search.

The solutions with GA easily converge to local optima and it is difficult to find the global optimal solution. Regeneration involves the complete random replacement of a species. In iGAMAS, only species 2 and 3 are regenerated, which allows species 4 to focus on refining the previously generated solutions and species 2 and 3 search for new possibilities. A reintroduction is introduced to ensure that species 4 operates on a set of good solutions, by inserting individuals from species 1 into species 4 at a prescribed interval. Migration allows exchanging information between species, which help share important information among different species by exchanging randomly selected individuals. Artificial selection ensures that the fittest individuals are stored in species 1 for future refinement. If any individuals are better, they will replace the worst individuals in species 1 so that species 1 always contains the best solutions.

## 2.4 Substructural identification strategy

It is generally difficult or expensive to measure the complete angular accelerations at the interface of beam and plate types of substructures due to the difficulty or expense to accurately measure angular accelerations in practice. In contrast, measurements of strains and translational acceleration can be readily and economically obtained with strain gauges and translational accelerometers, which are widely applied in experiments and industry. Therefore, it is beneficial to compute interface angular accelerations by incorporating strain and translational acceleration measurements. In this study, by adopting angular acceleration recovery method as discussed in Section 2.2, the interface and some internal angular accelerations will be firstly computed by use of the strain and translational acceleration measurements. The complete interface acceleration measurements are obtained to ensure substructural forward analysis. The flowchart of substructural identification is shown in Fig. 2.3.

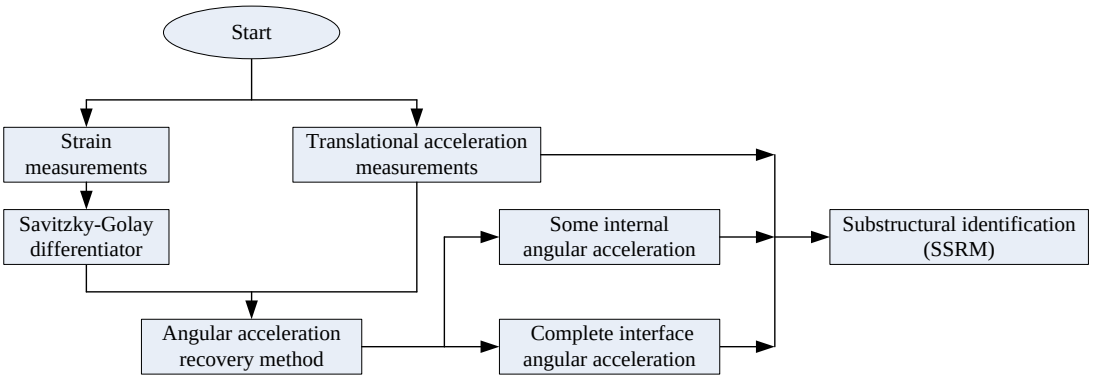


Figure 2.3 Flowchart of substructural identification strategy using measurements of strains and translational accelerations

As briefed in Section 2.3, SSRM achieves significant enhancement in terms of accuracy and efficiency compared to a standard GA, by narrowing the search space adaptively based on the statistics of results obtained. In this study, SSRM is adopted as the search engine to identify unknown substructural parameters by minimizing the difference between the simulated and measured internal accelerations in the substructure through a fitness function. The fitness function in GA is defined as

$$f = \frac{1}{c + \sum_{i=1}^{M} \sum_{j=1}^{L} \frac{\left| \ddot{u}_m(i,j) - \ddot{u}_e(i,j) \right|^2}{E\left( \ddot{u}_m{}^2(i) \right)}} \tag{2.21}$$

where subscripts $m$ and $e$ denote measured and estimated quantities, respectively; $L$ is the number of time steps and $M$ is the number of measurement sensors used. $E\left( \ddot{u}_m{}^2(i) \right) = \sum_{n=1}^{L} \ddot{u}_m{}^2(i,j) / L$ represents the mean squared value of $i$th measured accelerations. Constant $c$ is chosen to have the same order of normalized summed square error which is the second term in the denominator of the fitness function. In this study, an appropriate value for the constant $c$ is predefined as 0.001, with the same magnitude of the summed square error in the following two numerical examples. In general, more reliable identification results will be obtained with more measurements. Therefore, the measurements in the fitness function include not only the directly measured translational accelerations but also some recovered angular accelerations at internal DOFs.

## 2.5 Numerical examples

The performance of the proposed substructural identification strategy is demonstrated for the application of damage detection and structural identification through two numerical examples of a simply supported beam and a cantilever plate. The mass parameter for each element is assumed to be known in both examples. The unknown parameters include the flexural rigidity in the beam example and Young's modulus in the plate example in the respective substructures, as well as the two damping coefficients. A fairly broad search range of these parameters is defined as half to double of their exact values. For the simply supported beam example, the damage in the substructure is quantified by comparing the values of the flexural rigidity for each element before and after damage occurrence. For the cantilever plate, the substructure health status can be evaluated based on the computed elemental stiffness from the identified Young's modulus.

The simulated responses of all DOFs of beam and plate numerical models are first computed in terms of displacement, velocity and acceleration with Newmark's constant acceleration method. Damping effect is considered by assuming 5% critical damping for the first two modes. The uncontaminated strains at the selected measurement points are computed with these simulated responses accordingly. In practice, measurements are inevitably contaminated by noise which may affect the accuracy of identification results. Thus the noise effects should be considered in the numerical study. To simulate noise polluted measurements, a noise contaminated signal $X$ is represented by adding noise to a clean signal $X_{clean}$ as follows

$$X = X_{clean} + Noise \times Noise\ Level \times RMS\ (X_{clean}) \tag{2.22}$$

where '*Noise*' is randomly generated noise vector of Gaussian distribution with zero mean and unit standard deviation. '*Noise Level*' is the given noise level. $RMS\ (X_{clean})$ is the root-mean-square of the clean measurement. The effect of measurement noise is considered by introducing three levels of noise, 0%, 5% and 10%. To consider the stability of random search of GA based on its nature of stochastic search, the substructural identification results in this chapter are averaged from 5 tests with different simulated measurement data.

### 2.5.1 Substructural damage identification on a simply supported beam

A simply supported beam of 960 mm length, 50 mm width and 3 mm height is modeled by 16 identical elements connected to 17 nodes as shown in Fig. 2.4. There are two DOFs, i.e., a vertical translation and a rotation on each intermediate node, while only the rotation is considered for the two supporting nodes. The Young's modulus and density of the beam are $2.1\times10^{11}$N/m$^2$ and 7,862 kg/m$^3$, respectively. Euler beam model is applied with negligible shear strain due to the large length to height ratio.

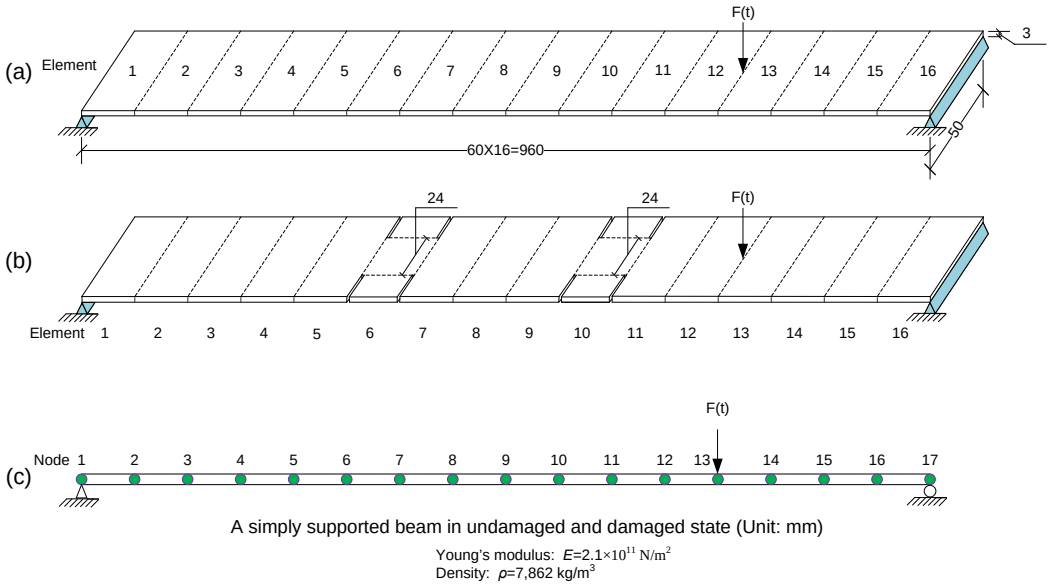


Figure 2.4 A simply supported beam (a) Without damage, (b) With damage and (c) Its numerical model

Damage in the simply supported beam is simulated as decrease in flexural rigidity by cutting the beam transversely as indicated in Fig. 2.4, in which the effective beam width in element 6 and 10 is reduced from 50 mm to 24 mm. A random excitation acts on node 13. Structural response subjected to this excitation is computed for 0.4 s with a sampling rate of 5,000. To quantify the damages in this simply supported beam, the measurements in undamaged and damaged states are required, which serve to identify the flexural rigidity of substructure before and after damage occurrence. In this study, the extent of the damage is defined as the percentage of flexural rigidity loss to the undamaged flexural rigidity

$$D_i = \frac{EI_{i\_u} - EI_{i\_d}}{EI_{i\_u}} \times 100\% \tag{2.23}$$

where $D_i$ is the damage extent for element $i$, $EI_{i\_u}$ and $EI_{i\_d}$ are the flexural rigidity of the undamaged and damaged element $i$. With known exact structural parameters in

undamaged and damaged states, the flexural rigidity is 23.625 $N \cdot m^2$ and 11.34 $N \cdot m^2$ for undamaged and damaged element, respectively. Therefore, the damage extent in element 6 and 10 is 52% due to the reduction of element width. In this study, the absolute identification error in the identified stiffness is defined as the ratio of absolute error in the identified value to the exact value.

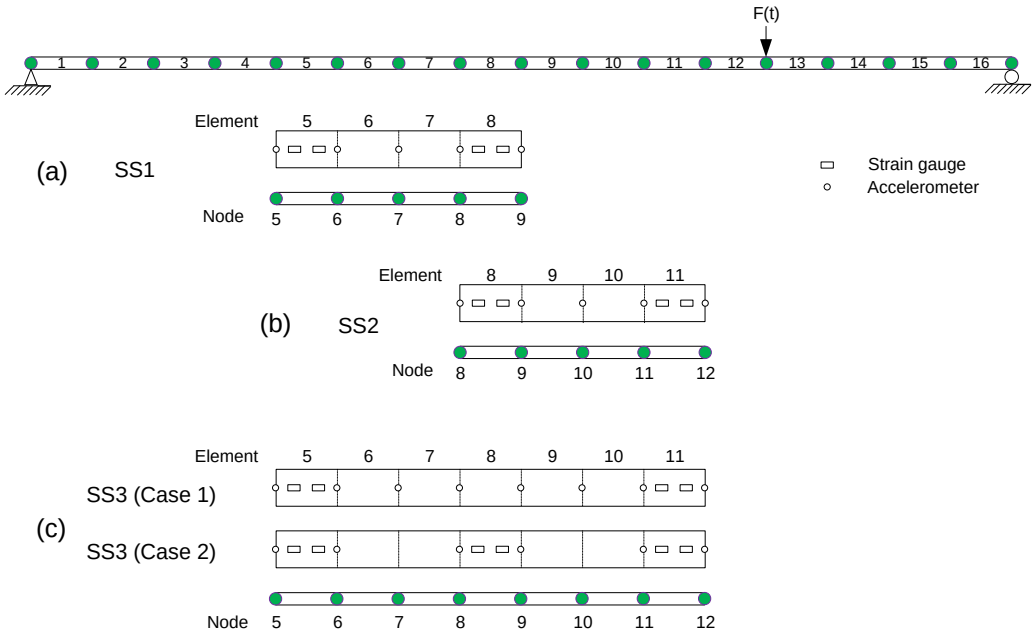


Figure 2.5 Three different substructures with sensor placements (a) SS1, (b) SS2 and (c) SS3

Three different substructures are investigated, respectively denoted as SS1, SS2 and SS3 for convenience shown in Fig. 2.5. SS1, SS2 and SS3 contain elements 5-8, elements 8-11 and elements 5-11, respectively. The strain information from installed strain gauges at the top surface of beam in these three substructures is obtained. The translational (linear) accelerations from instrumented accelerometers are measured at the selected locations illustrated in Fig. 2.5. To recover interface angular accelerations of SS1, SS2 and SS3, the strains are assumed to be measured in elements 5 and 8, elements 8 and 11, elements 5 and 11 or elements 5, 8 and 11,

respectively. For SS1, the translational accelerations are assumed to be available at 5 nodes, namely, the $5^{th}$, $6^{th}$, $7^{th}$, $8^{th}$ and $9^{th}$ node. For SS2, the translational accelerations are assumed to be measured at nodes 8, 9, 10, 11 and 12. In the identification, two damping parameters are also taken as unknowns resulting in 6, 6 and 9 unknown parameters for SS1, SS2 and SS3, respectively. The GA parameters used for identification of SS1, SS2 and SS3 are presented in Table 2.1.

Table 2.1 GA parameters used for identification of SS1, SS2 and SS3

| | SS1 and SS2 | SS3 |
|---|---|---|
| Number of unknown parameters | 6 | 9 |
| Population size | 30 × 3 | 50 × 3 |
| Runs | 4/10 | 4/10 |
| Generations | 100 | 100 |
| Crossover rate | 0.4 | 0.4 |
| Mutation rate | 0.2 | 0.2 |
| Window width | 4.0 | 4.0 |
| Migration | 0.05 | 0.05 |
| Regeneration | 3 | 3 |
| Reintroduction | 30 | 30 |

To improve the accuracy of identification results, not only the measured internal translational accelerations but also some recovered internal angular accelerations are accounted in evaluation of the fitness function. The recovered angular accelerations at nodes 6 and 8 of SS1 are involved in the fitness function evaluation. In SS2, the recovered angular accelerations at nodes 9 and 11 are treated as measurements and used in evaluation of the fitness function. The damage identification results for SS1 and SS2 are shown in Fig. 2.6 and Fig. 2.7. The substructural identification errors for SS1 and SS2 in pre-damaged and post-damaged states are listed in Table 2.2.

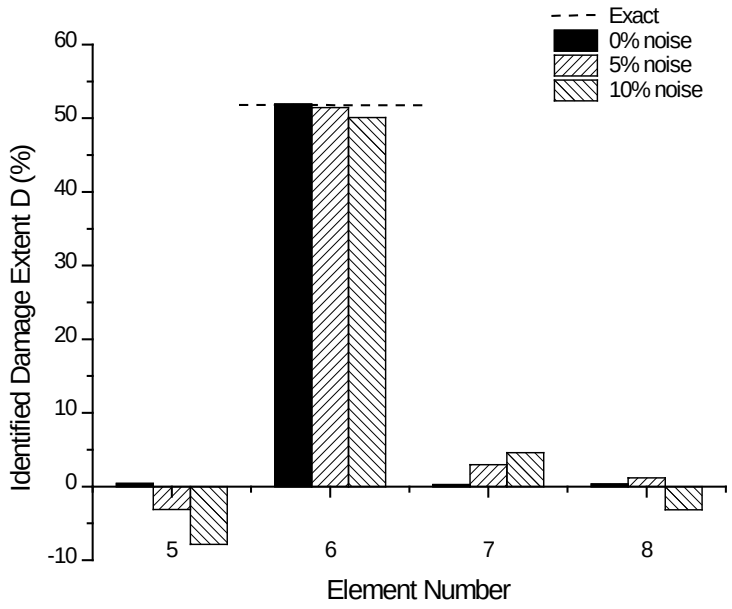


Figure 2.6 Identified damage extent of SS1

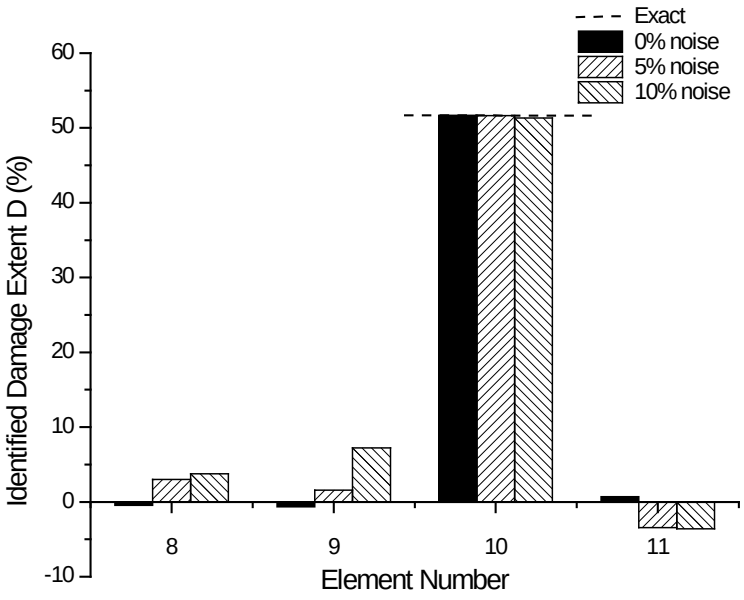


Figure 2.7 Identified damage extent of SS2

Table 2.2 Absolute identification errors of SS1 and SS2 in undamaged and damaged states

| Beam state | Noise level | SS1 | | SS2 | |
|---|---|---|---|---|---|
| | | Mean error (%) | Max error (%) | Mean error (%) | Max error (%) |
| Undamaged | 0% | 1.56 | 2.97 | 2.27 | 3.59 |
| | 5% | 3.60 | 5.96 | 5.24 | 7.87 |
| | 10% | 5.51 | 11.87 | 6.75 | 11.67 |
| Damaged | 0% | 1.39 | 2.54 | 1.91 | 2.64 |
| | 5% | 4.42 | 6.48 | 2.03 | 4.09 |
| | 10% | 6.48 | 9.10 | 7.03 | 9.26 |

The identified results in Fig. 2.6 and Fig. 2.7 show that the proposed method gives reliable identification results of the locations and extents of damage in element 6 and 10. When the measurements contain 10% noise, the extents of the damage in element 6 of SS1 and element 10 of SS2 are identified as 50.11% and 51.32% reduction in flexural rigidity, which are very close to the exact 52% flexural rigidity degradation. In the worst case, the maximum false damage identified is 7.85% and 7.21% in element 5 of SS1 and element 9 of SS2 when the strains and translational measurements are contaminated by 10% noise. In addition, the substructural identification errors in Table 2.2 show that the flexural rigidities for undamaged and damaged substructures are successfully identified with the proposed identification strategy even when the measurements are polluted by 10% noise.

Two different sensor placement schemes are applied to identify SS3, as shown in Fig 2.5, denoted as Case 1 and Case 2. Twelve sensors are employed for both cases: four strain gauges and eight accelerometers in Case 1 while six strain gauges and six accelerometers in Case 2. In Case 1, the strain measurements are collected in element 5 and 11, and the translational accelerations are available at nodes 5-12. In

Case 2, the strains in elements 5, 8 and 11, the translational accelerations at nodes 5, 6, 8, 9, 11 and 12 are measured. In Case 1, the recovered angular accelerations at node 6 and 11 as well as the directly measured translational accelerations at node 6, 7, 8, 9 10 and 11 are used in the fitness function. In Case 2, the recovered angular accelerations as well as the measured translational accelerations at node 6, 8, 9 and 11 are employed to compute the fitness function in GA. The damage identification results of Case 1 and Case 2 for SS3 are shown in Fig. 2.8 and Fig. 2.9. The substructural identification errors of both cases in undamaged and damaged states are listed in Table 2.3.

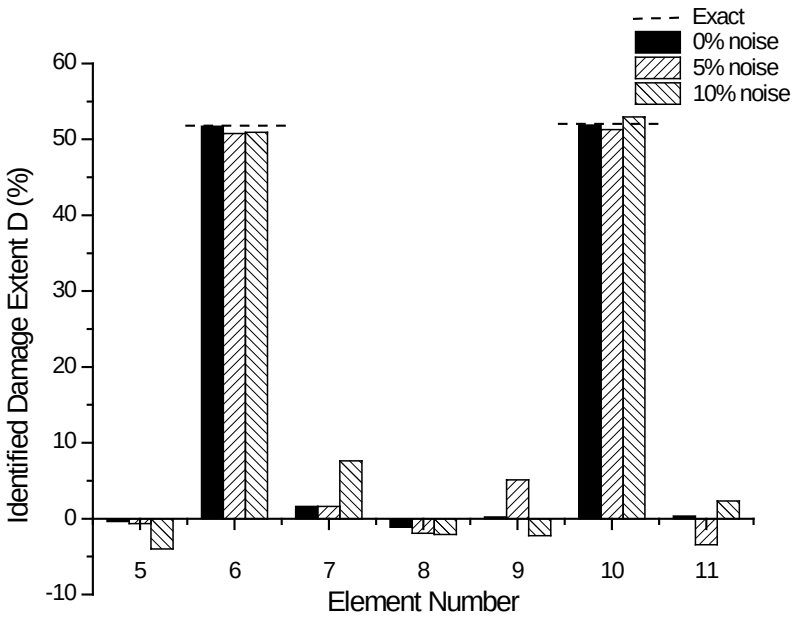


Figure 2.8 Identified damage extent of SS3 (Case 1)

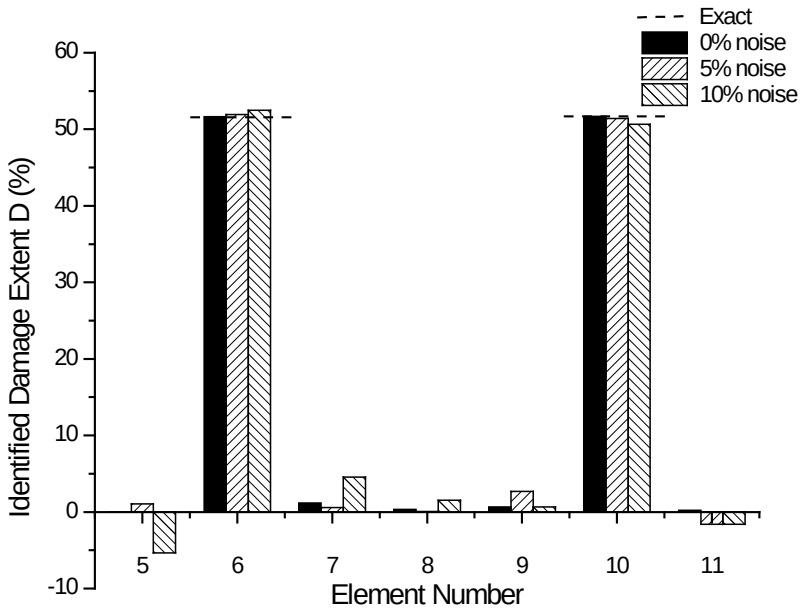


Figure 2.9 Identified damage extent of SS3 (Case 2)

Table 2.3 Absolute identification errors for Case 1 and Case 2 of SS3 in undamaged and damaged states

| Beam state | Noise level | SS3 | | | |
|---|---|---|---|---|---|
| | | Case 1 | | Case 2 | |
| | | Mean error (%) | Max error (%) | Mean error (%) | Max error (%) |
| Undamaged | 0% | 1.17 | 2.38 | 1.91 | 2.92 |
| | 5% | 3.92 | 6.38 | 2.42 | 3.35 |
| | 10% | 6.97 | 11.95 | 4.48 | 7.07 |
| Damaged | 0% | 0.87 | 2.08 | 1.72 | 3.16 |
| | 5% | 3.48 | 6.05 | 2.52 | 3.67 |
| | 10% | 6.09 | 10.68 | 3.93 | 6.35 |

Damage identification results in Fig. 2.8 and Fig. 2.9 show that the identified damages in element 6 and 10 are quite close to the exact values. The maximum false identified damage is less than 8% in element 7 of SS3 (Case 1) and around 5% in element 5 of SS3 (Case 2) when 10% noise is introduced into the measurements. These results, including the maximum error 11.95% for Case 1 and 7.07% for Case

2, as listed in Table 2.3, indicate that the location and severity of damaged in SS3 are successfully identified with both sensor placement schemes even if the measurements are contaminated by 10% noise.

From the damage identification results in Fig. 2.8 and Fig. 2.9, the advantage of the sensor placement scheme of Case 2 over that of Case 1 is not remarkable. In both cases, the damages in SS3 can be successfully identified and the maximum false identification errors around 8% for Case 1 and 5% for Case 2 are comparable. Nevertheless, the substructural identification errors in Table 2.3 provide clear evidence that more accurate identification results are obtained in Case 2 than Case 1, especially when relatively high noise level is introduced. The maximum identification error for the undamaged SS3 decreases to 7.07 % of Case 2 from 11.95% of Case 1 and 6.85% of Case 2 from 10.68% of Case 1 for the damaged SS3. Compared with Case 1, the sensor placement scheme in Case 2 show its advantages in terms of accuracy of identification results due to more number of angular accelerations at internal DOFs used in fitness function evaluation. The sensitivity study indicates that internal angular accelerations are more sensitive to substructural parameters than translational accelerations at internal DOFs. A more detailed discussion is given in Section 2.6.2.

### 2.5.2 Substructural identification on a cantilever plate

A 2 m long, 2 m wide and 0.04 m thick cantilever plate shown in Fig. 2.10 is modeled by 8 × 8 thin plate elements, in which the out-of-plane shear strain is negligible due to small ratio of plate thickness to its length or width. There are three DOFs at each node, one translation and two rotations except for the nodes at the

fixed edge. The Young's modulus and density of the plate are $2.1\times10^{11}$ N/m$^2$ and 7,862 kg/m$^3$, respectively. A random excitation is applied at one corner of the free edge, shown in Fig. 2.10. Subjected to this excitation, structural response is computed for 0.4 s with a sampling rate of 5,000.

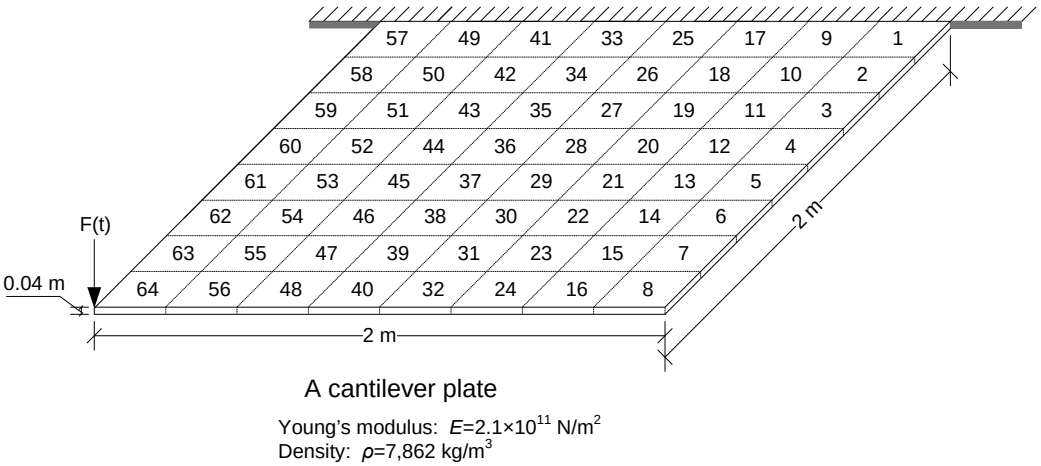


Figure 2.10 A cantilever plate model with excitation at a corner

In this cantilever plate, two different substructures SS1 and SS2 are considered, shown in Fig. 2.11. SS1 contains 16 elements, i.e., elements 19, 20, 21, 22, 27, 28, 29, 30, 35, 36, 37, 38, 43, 44, 45 and 46. There are 24 elements in SS2, i.e., elements 6, 7, 8, 14, 15, 16, 22, 23, 24, 30, 31, 32, 38, 39, 40, 46, 47, 48, 54, 55, 56, 62, 63 and 64.

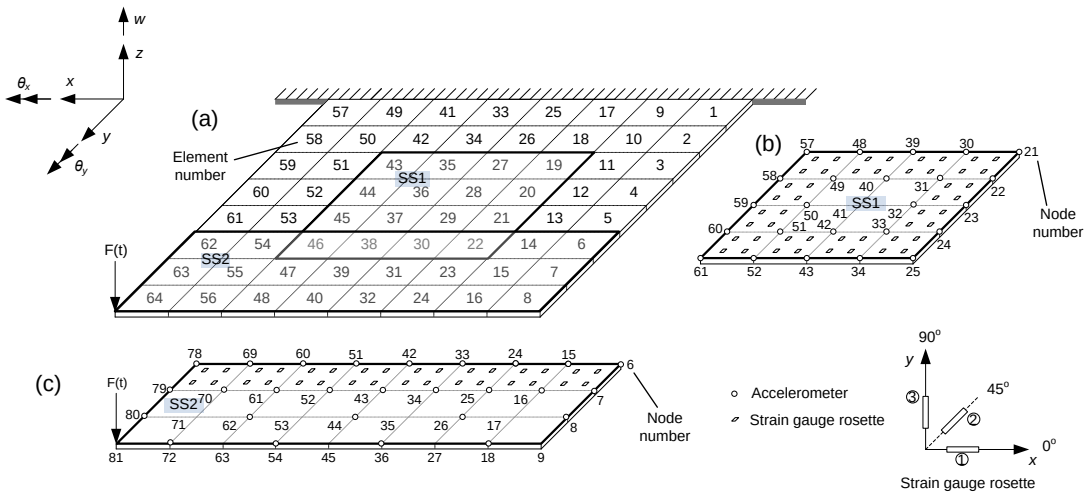


Figure 2.11 (a) A cantilever plate, (b) SS1 and (c) SS2

To obtain complete interface acceleration measurements, translational accelerometers and strain gauge rosettes are installed at the interface of SS1 and SS2. In total, 24 accelerometers and 48 strain gauge rosettes are employed in SS1. There are 27 accelerometers and 32 strain gauge rosettes installed in SS2. The strain gauge rosettes in Fig. 2.11 measure three in-plane strains $\{\varepsilon_x \quad \varepsilon_y \quad \gamma_{xy}\}$ and the accelerometers record the translational acceleration signals on selected locations. In SS1, the internal measurements includes the directly measured translational accelerations and recovered angular accelerations at nodes 31, 32, 33, 40, 42, 49, 50 and 51, thus there are 24 number of internal responses involved for fitness function evaluation in GA. In SS2, 36 internal responses are used to guide GA to search for the optimal solution, including the directly measured translational accelerations at 18 nodes 7, 8, 16, 18, 25, 26, 34, 36, 43, 44, 52, 54, 61, 62, 70, 72, 79 and 80 as well as the recovered angular accelerations at nodes 7, 16, 25, 34, 43, 52, 61, 70 and 79. In substructural identification, the unknown stiffness for each element and two unknown damping coefficients result in 18 and 26 unknown parameters for SS1 and

SS2, respectively. The GA parameters used for identification of SS1and SS2 are listed in Table 2.4.

Table 2.4 GA parameters used for identification of SS1 and SS2

| | SS1 | SS2 |
|---|---|---|
| Number of unknown parameters | 18 | 26 |
| Population size | 50 × 3 | 90 × 3 |
| Runs | 4/20 | 4/20 |
| Generations | 200 | 200 |
| Crossover rate | 0.4 | 0.4 |
| Mutation rate | 0.2 | 0.2 |
| Window width | 4.0 | 4.0 |
| Migration | 0.05 | 0.05 |
| Regeneration | 3 | 3 |
| Reintroduction | 30 | 30 |

Figures 2.12 and 2.13 present the stiffness identification results of SS1 and SS2 with 0%, 5% and 10% noise polluted measurements. The mean and maximum identification errors of SS1 and SS2 are summarized in Table 2.5.

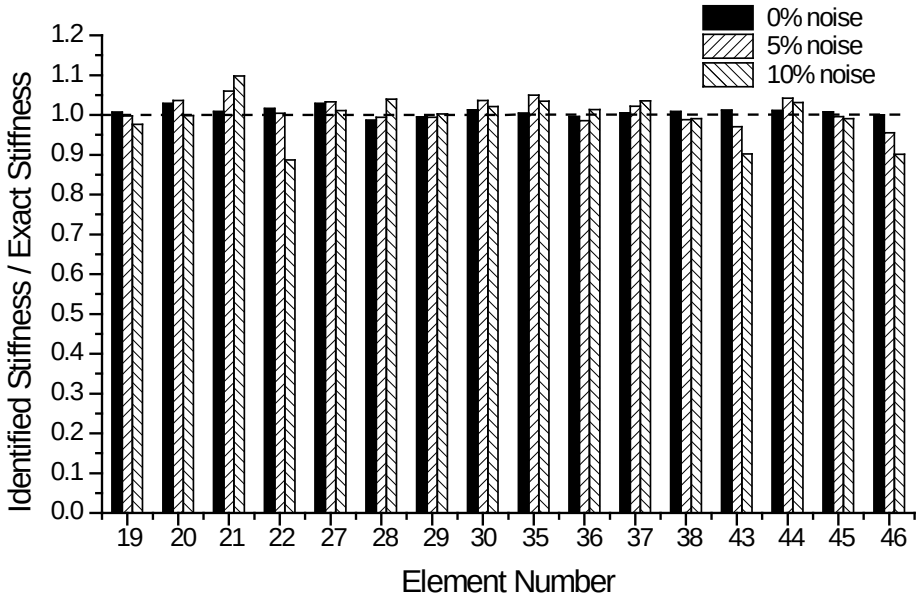


Figure 2.12 Stiffness identification results of SS1

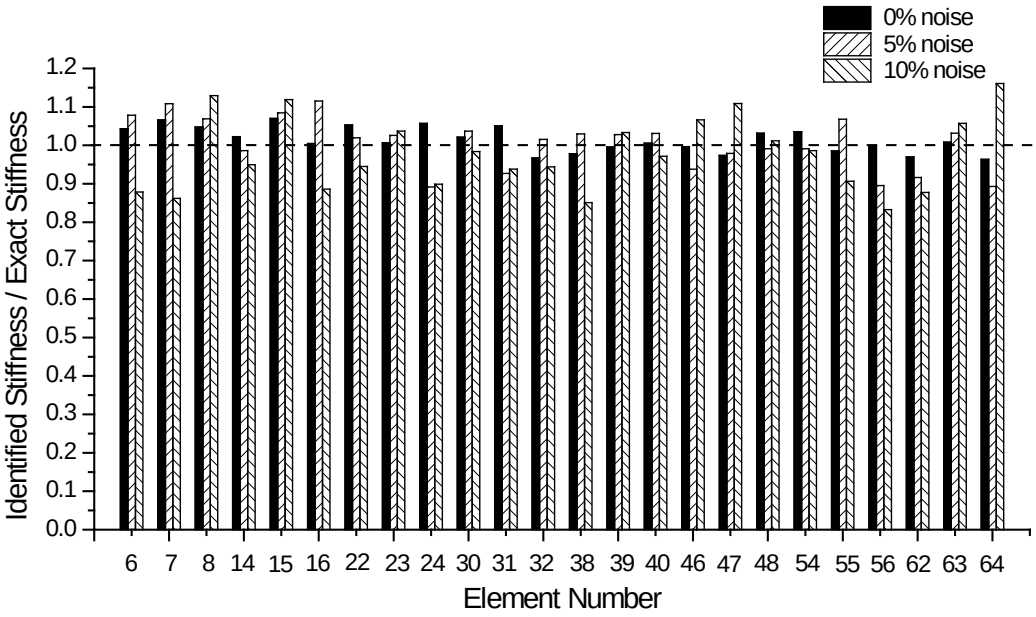


Figure 2.13 Stiffness identification results of SS2

Table 2.5 Absolute identification errors of SS1 and SS2

| Noise level | SS1 | | SS2 | |
|---|---|---|---|---|
| | Mean error (%) | Max error (%) | Mean error (%) | Max error (%) |
| 0% | 1.08 | 2.91 | 2.87 | 6.98 |
| 5% | 3.55 | 6.26 | 5.55 | 11.54 |
| 10% | 6.38 | 11.30 | 8.39 | 16.67 |

The identification results of SS1 and SS2 in Figs. 2.12-2.13 indicate that the stiffness can be reasonably identified even with noisy measurements. The proposed strategy is effective to deal with complex interfaces where a considerable number of angular acceleration measurements are required for substructural identification. Since GA yields a good solution but not the exact solution based on its heuristic search nature, it is difficult to identify unknown parameters exactly even with clean signals, as indicated in Table 2.5 for 0% noise case. It is also observed that the optimal solution in GA search domain shifts due to the noise in the measurements

(Zhang, 2009), which would definitely affect the identified results. The two factors both contribute to the identification error in each identified parameter. Therefore, quality of the identified results is evaluated by the mean error of all unknown parameters in a statistical sense. As seen in Table 2.5, the mean and maximum identification errors of 1.08% and 2.91% in SS1 for unpolluted measurement indicate that the values of identified stiffness are quite close to the exact solution. The mean and maximum error of 6.38% and 11.30% in SS1 show that the identification results in SS1 are quite excellent even when the measurements are contaminated by 10% noise. In comparison with the identification results of SS1, the identified stiffness in SS2 deviates from the exact solution to some extent, but still acceptable from practical point of view. As indicated in Table 2.4, there are 18 and 26 unknown parameters involved in SS1 and SS2, respectively. The main reason of more accurate identification results achieved for SS1 is that there is less number of unknown parameters involved in SS1 compared with that in SS2. The other reason is that more accurate angular accelerations at internal nodes are recovered in SS1 with average values from surrounding different elements. In Fig. 2.11, the recovered angular accelerations at nodes 31, 33, 49 and 51 in SS1 are the average values from three adjacent elements, while the other angular accelerations are averaged from two adjoining elements. Generally, more accurate values are obtained by the averaging technique which can reduce the effect of noise. However, in SS2, although the angular acceleration at nodes 16, 25, 34, 43, 52, 61, 70 and 79 are averaged from two adjacent elements, larger errors exist in the recovered angular accelerations at the two corner nodes 7 and 79 since they are computed from only one element with the recovery method in Section 2.2.

## 2.6 Discussion

### 2.6.1 Differentiation error

From Eq. (2.20), the second order derivatives of the measured strains are needed to compute the angular accelerations. Therefore, it is a critical issue to select an appropriate differentiation algorithm in this identification strategy, since the accuracy of recovered angular acceleration is largely dependent on it. In practice, measurements are inevitably contaminated by noise, and inappropriate differentiation operation will substantially amplify the noise effect in the results. In this regard, Savitzky-Golay differentiation algorithm is adopted in this study in view of its several advantages (Luo et al., 2005). Savitzky-Golay differentiation algorithm is based on a simple idea of the least-squares polynomial fitting by a moving window. Furthermore, the differentiation coefficients can be easily obtained from a well-established table (Savitzky et al., 1964). Moreover, Savitzky-Golay differentiation algorithm can be tailored with arbitrary length and polynomial order for versatile applications. Savitzky-Golay differentiation algorithm provides a good numerical derivative estimation of signal, especially those containing noise.

Although Savitzky-Golay algorithm is potentially accurate for differentiation, it suffers from a major drawback that it is unable to accurately compute the derivatives at two ends of the signal due to reduced number of measurement data involved for derivatives estimation. In this regard, large errors exist at the two ends of the estimated second derivatives of the strain measurements. In addition, it is very difficult to obtain accurate second derivatives of the transient responses due to the

large fluctuation in the measurements, especially when the applied force starts from a relatively high magnitude. Therefore, large differentiation errors will be induced in the recovered interface angular acceleration at the initial part, due to the drawback of Savitzky-Golay differentiation algorithm and the difficulty of acquiring accurate derivatives of violently fluctuating measurements. For instance, the exact and recovered angular acceleration at node 8 in SS3 in Fig. 2.5 with the unpolluted translational acceleration and strain measurements for the first 200 data points are plotted in Fig. 2.14 when the applied force starts from a high amplitude.

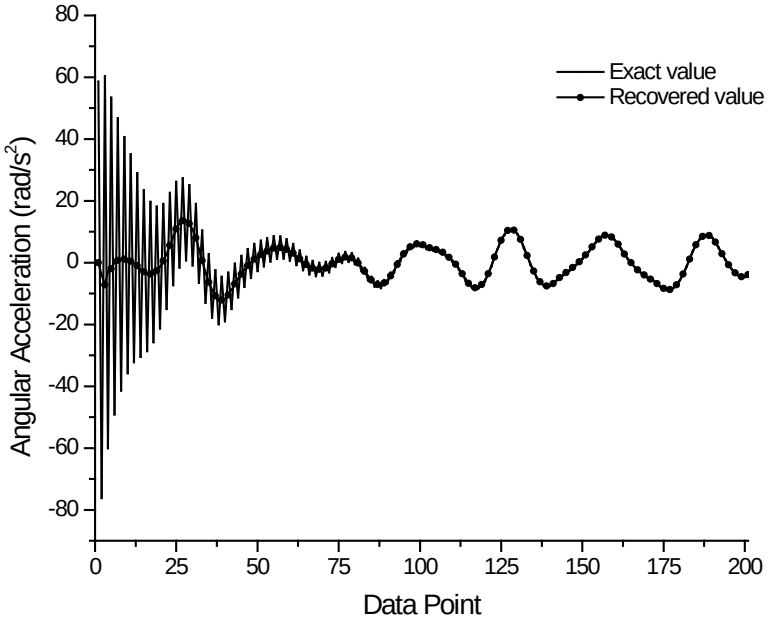


Figure 2.14 Exact and recovered interface angular acceleration at node 8 of SS3

Large deviations in recovered angular acceleration at the initial part shown in Fig. 2.14 will inevitably affect accuracy of the identification results. Large discrepancy is also discovered in simulated acceleration at internal DOFs at initial part due to inaccurate estimation of interface angular accelerations at the beginning part. Although the effect of differentiation error at the ending part of simulated responses

is not as serious as that at the beginning part, it is beneficial to exclude the comparison between the simulated response and measurements at two ends in fitness function to mitigate effects of differentiation error on the identification results. This operation will certainly cost some computational time for the first certain time steps. Fortunately, the differentiation error in the recovered angular acceleration decays fast if random forces starting from small amplitude are applied. Therefore, the additional computational time can be substantially reduced since the differentiation error only affects the simulated responses in limited initial time steps.

### 2.6.2 Sensitivity studies

The equation of motion for a substructure can be written as

$$[M_{rr}]\{\ddot{u}_r\}+[C_{rr}]\{\dot{u}_r\}+[K_{rr}]\{u_r\}=\{P_r\}-[M_{rj}]\{\ddot{u}_j\}-[C_{rj}]\{\dot{u}_j\}-[K_{rj}]\{u_j\} \tag{2.3}$$

By introducing two Rayleigh damping coefficients, the damping matrix can be expressed as $[C_{rr}]=a_0[M_{rr}]+a_1[K_{rr}]$ and $[C_{rj}]=a_0[M_{rj}]+a_1[K_{rj}]$. It is assumed that the mass matrix remains unchanged during the identification. Differentiating Eq. (2.3) with respect to elemental stiffness $K_i$, we have

$$[M_{rr}]\frac{\partial\{\ddot{u}_r\}}{\partial K_i}+[C_{rr}]\frac{\partial\{\dot{u}_r\}}{\partial K_i}+[K_{rr}]\frac{\partial\{u_r\}}{\partial K_i}=-a_1\frac{\partial[K_{rr}]}{\partial K_i}\{\dot{u}_r\}-\frac{\partial[K_{rr}]}{\partial K_i}\{u_r\}-a_1\frac{\partial[K_{rj}]}{\partial K_i}\{\dot{u}_j\}-\frac{\partial[K_{rj}]}{\partial K_i}\{u_j\} \tag{2.24}$$

In substructural identification, the two unknown damping coefficients $a_0$ and $a_1$ are treated as the unknown structural parameters needed to be identified. Thus it is necessary to discuss the response sensitivity with respect to these two unknown damping coefficients. Differentiating Eq. (2.3) with respect to $a_0$ and $a_1$, we obtain

$$\begin{aligned}
&[M_{rr}]\frac{\partial\{\ddot{u}_r\}}{\partial a_0}+[C_{rr}]\frac{\partial\{\dot{u}_r\}}{\partial a_0}+[K_{rr}]\frac{\partial\{u_r\}}{\partial a_0}=-[M_{rr}]\{\dot{u}_r\}-[M_{rj}]\{\dot{u}_j\}\\
&[M_{rr}]\frac{\partial\{\ddot{u}_r\}}{\partial a_1}+[C_{rr}]\frac{\partial\{\dot{u}_r\}}{\partial a_1}+[K_{rr}]\frac{\partial\{u_r\}}{\partial a_1}=-[K_{rr}]\{\dot{u}_r\}-[K_{rj}]\{\dot{u}_j\}
\end{aligned} \tag{2.25}$$

Therefore, through Eq. (2.24) and Eq. (2.25), the internal response sensitivity with respect to structural parameters can be computed.

In the numerical example of substructural damage identification of a simply supported beam, two different sensor placements are settled for SS3 as shown in Fig. 2.15.

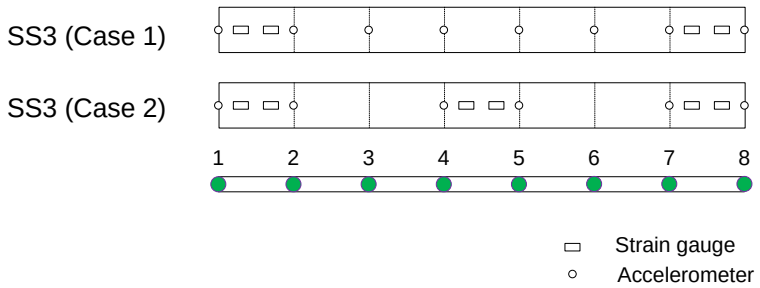


Figure 2.15 Two different sensor placements for damage identification of SS3

The same number of sensors is employed as well as the same number of internal measurements used in fitness function evaluation for Case1 and Case 2. The only difference between these two cases is that more internal translational accelerations are involved in Case 1 and more angular accelerations are involved in Case 2. For instance, translational accelerations at node 3 are exclusively involved in Case 1 and angular accelerations at node 4 are only involved in Case 2. The sensitivity of these two response in 1 s with respect to element stiffness $K_1$, $K_3$, $K_5$ and $K_7$ are computed.

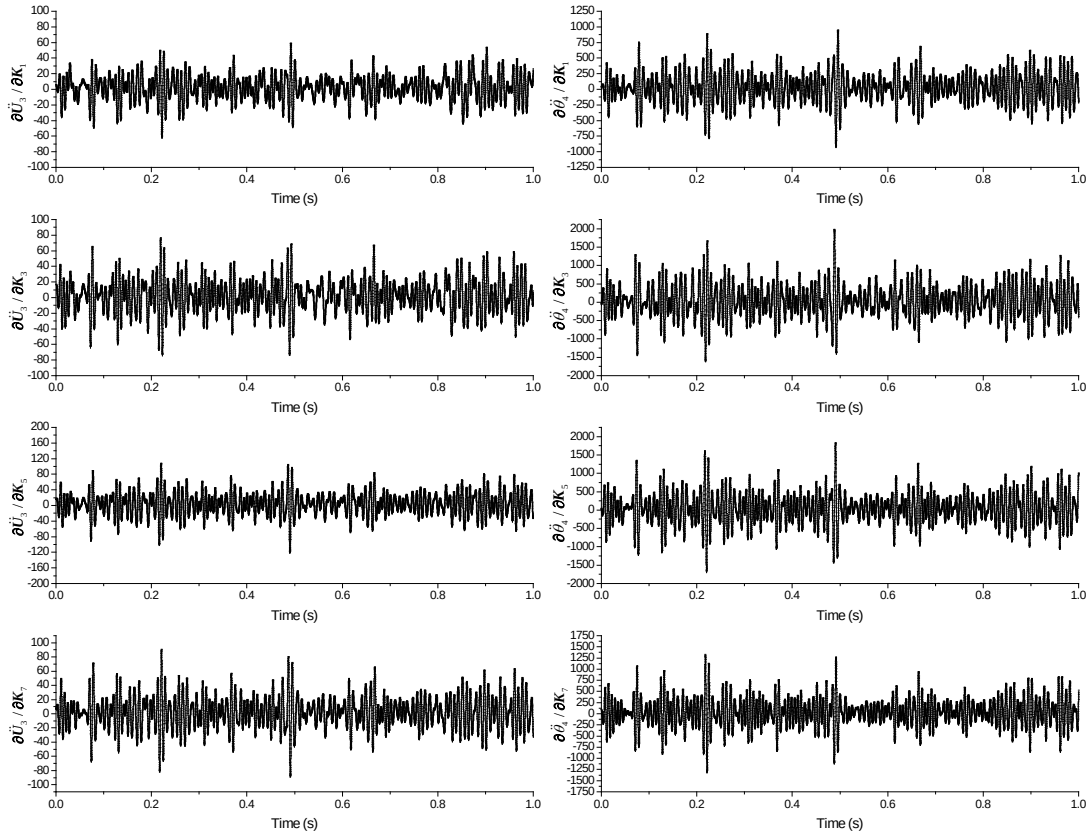


Figure 2.16 Sensitivity of translation acceleration at node 3 and angular acceleration at node 4 to elemental stiffness K1, K3, K5 and K7 of SS3

In Fig. 2.16, sensitivities for the angular acceleration at node 4 are at least one order larger than those of the translational acceleration at node 3, which implies that the angular acceleration at node 4 is significantly more sensitive to the change of stiffness than the translational acceleration at node 3. The sensitivity study is also applied to other internal responses in SS3. It is found that angular acceleration is more sensitive to the change of stiffness values than translational acceleration at internal DOFs. As more angular acceleration at internal DOFs are used in the fitness function, the measurement scheme in Case 2 achieves better performance than Case 1 in terms of accuracy of the identification results shown in Table 2.3. With measured strains and translational accelerations, not only the angular accelerations at interface but also some angular accelerations at internal DOFs are recovered by the

proposed recovery method. The accuracy of identification results can be significantly improved by employing these recovered internal angular accelerations in evaluation of the fitness function. In this regard, it is worthwhile to recover more number of angular accelerations at internal DOFs by judiciously measuring strains and translational accelerations at the interior of substructures for the purpose of improving the accuracy of identification results.

## 2.7 Summary

In this chapter, a substructural identification strategy with angular acceleration recovery method and SSRM is proposed to identify unknown substructural parameters. In substructural identification, due to the requirement of angular acceleration measurements at the interface of beam and plate substructures as well as the difficulty or expense to measure them, a recovery method is developed to compute the interface angular accelerations by use of the translational accelerations and strain measurements. Incorporating the recovery method, SSRM is employed to identify unknown physical parameters for substructural systems due to its excellent global and local search ability. The proposed identification strategy is validated through two numerical simulations, i.e., substructural damage detection in a simply supported beam and substructural identification in a cantilever plate. The results show that the locations and severities of damages in the simply supported beam are successfully identified, and the elemental stiffness in a cantilever plate is determined to be close to the exact values. In addition, the effectiveness of the proposed strategy is investigated by introducing different levels of noise into the measurements.

The existence of large differentiation errors at the two ends of the computed angular acceleration time histories inevitably affects the accuracy of identification results. While the differentiation error attenuates rapidly in the initial part of recovered angular responses, its effect on the identification results can be largely alleviated by excluding the comparison between the affected simulated responses and measurements in fitness function. The sensitivity studies show that the angular accelerations are more sensitive to the change of stiffness than translational accelerations at internal DOFs. Therefore, to improve the accuracy of the identification results, it is beneficial to use more number of internal angular accelerations for evaluation of the fitness function by extending the measurements scheme of strain and translational acceleration into the interior of substructures.

# Chapter 3. Global Structural Identification with Unknown Input

Generally, force measurements are required in structural identification since they are treated as input information. Nevertheless, in some situations, it is difficult to acquire force measurement data. For instance, external excitations such as wind loads or earthquake loads are difficult to be accurately measured in practice. As reviewed in Section 1.4, although many structural identification methods have been proposed to address the absence of excitation measurements, most of them are only applicable to ambiently excited structures due to Gaussian noise approximation for the excitations. Generally, the performance of these methods may not be satisfactory with noisy measurements. In this chapter, an iterative identification strategy is proposed for global structural identification without measurements of excitation forces. The locations of applied forces in the structure are assumed known in the process of identification. The strategy is a synergy of Tikhonov regularization method and SSRM, which are employed for force identification and structural parameter identification, respectively.

To facilitate force identification with Tikhonov regularization method, the discrete time state space form is developed for global structures. After Tikhonov regularization method for force identification is briefly reviewed, the

implementation of the proposed identification strategy is described, followed by numerical and experimental studies.

## 3.1 Discrete time state space form for global structure

A multi-DOF dynamic system can be described as

$$[M]\{\ddot{u}(t)\}+[C]\{\dot{u}(t)\}+[K]\{u(t)\}=\{P(t)\} \tag{3.1}$$

where $[M]$, $[C]$ and $[K]$ are mass matrix, damping matrix and stiffness matrix of the structural system, respectively. $\{\ddot{u}(t)\}$, $\{\dot{u}(t)\}$ and $\{u(t)\}$ represent the acceleration, velocity and displacement responses. $\{P(t)\}$ is the excitation forces applied to the structural system. Newmark method of constant acceleration is adopted herein to compute dynamic responses of the structural system for each time step.

$$\begin{cases} \{\dot{u}\}_{k+1}=\{\dot{u}\}_k+\Delta t\left[(1-\delta)\{\ddot{u}\}_k+\delta\{\ddot{u}\}_{k+1}\right] \\ \{u\}_{k+1}=\{u\}_k+\Delta t\{\dot{u}\}_k+\frac{\Delta t^2}{2}\left[(1-2\alpha)\{\ddot{u}\}_k+2\alpha\{\ddot{u}\}_{k+1}\right] \end{cases} \tag{3.2}$$

where $\alpha$ and $\delta$ are the Newmark constants ($\alpha=1/4$, $\delta=1/2$), and $k$ and $\Delta t$ are the time step and time interval. Substituting Eq. (3.2) into Eq. (3.1), equation of motion for the structural system can be expressed in two consecutive time steps as

$$\{U\}_{k+1}=[A]\{P\}_{k+1}+[B]\{U\}_k \tag{3.3}$$

where $\{U\}=\{\{u\}\ \ \{\dot{u}\}\ \ \{\ddot{u}\}\}^T$, consisting of dynamic displacement, velocity and acceleration responses. The matrices $[A]$ and $[B]$ are

$$[A]=\begin{bmatrix}\Delta t^2\alpha[I] & \Delta t\delta[I] & [I]\end{bmatrix}^T\left[M^*\right]^{-1} \tag{3.4}$$

$$[B]=\begin{bmatrix}[I] & \Delta t[I] & \frac{\Delta t^2}{2}(1-2\alpha)[I]\\ 0 & [I] & \Delta t(1-\delta)[I]\\ 0 & 0 & 0\end{bmatrix}-[A]\begin{bmatrix}[K] & [C]+\Delta t[K] & \Delta t(1-\delta)[C]+\frac{\Delta t^2}{2}(1-2\alpha)[K]\end{bmatrix} \tag{3.5}$$

where $\left[M^*\right]=[M]+\Delta t\delta[C]+\Delta t^2\alpha[K]$. In practice, the measurements $\{y\}$ only contain a limited number of structural responses. Herein, mapping matrix $[R]$ is established to relate the measurements $\{y\}$ to the structural dynamic response $\{U\}$. Then the measurements $\{y\}$ at time step $k+1$ can be expressed as

$$\{y\}_{k+1}=[R]\{U\}_{k+1} \tag{3.6}$$

In this study, it is assumed that the structure starts to respond from at-rest state. Substituting Eq. (3.6) into Eq. (3.3) from the first to the last time step $n$, the relation between measurements $\{y\}$ and excitation forces $\{P\}$ is expressed as

$$\begin{Bmatrix}\{y\}_1\\ \{y\}_2\\ \vdots\\ \{y\}_k\\ \vdots\\ \{y\}_n\end{Bmatrix}=\begin{bmatrix}[R][A_1] & 0 & \cdots & 0 & 0 & 0\\ [R][B][A_1] & [R][A] & \cdots & 0 & 0 & 0\\ \vdots & \vdots & \vdots & \vdots & \vdots & \vdots\\ [R][B]^{k-1}[A_1] & [R][B]^{k-2}[A] & \cdots & [R][A] & 0 & 0\\ \vdots & \vdots & \vdots & \vdots & \vdots & \vdots\\ [R][B]^{n-1}[A_1] & [R][B]^{n-2}[A] & \cdots & [R][B]^{n-k}[A] & \cdots & [R][A]\end{bmatrix}\begin{Bmatrix}\{P\}_1\\ \{P\}_2\\ \vdots\\ \{P\}_k\\ \vdots\\ \{P\}_n\end{Bmatrix} \tag{3.7}$$

In Eq. (3.7), $[A_1]=\begin{bmatrix}0 & 0 & [M]^{-1}\end{bmatrix}^T$ is determined by the assumed initial condition of zero displacement and velocity responses. Equation (3.7) can be represented in short form as

$$\{y\} = [H]\{P\} \tag{3.8}$$

## 3.2 Tikhonov regularization

Estimating unknown input excitations to a structural system with measurement data is an inverse dynamic problem. Generally, it is difficult to solve this problem since the matrix relating the unknown input (excitations) to the output (measurements) is ill-conditioned. For this problem, least-square method always yields unbounded solutions with contaminated measurements. To this end, Tikhonov regularization, a method of least squares minimization, was proposed to treat this problem by imposing a penalty term in the objective function (Tikhonov et al., 1995). Appropriate selection of the optimal regularization parameter, which is the coefficient for the penalty term, is the key issue in Tikhonov regularization method. Usually, discrepancy principle, generalized cross-validation (GCV) and L-curve method are adopted to compute the optimal regularization parameter. The general rule of the discrepancy principle (Phillips, 1962) is to choose the regularization parameter by setting the residual norm equal to some upper bounds of the errors in the measurements. Nevertheless, it is pointed out that a close bound of the errors in the measurements is generally difficult to estimate (Hansen and O´leary, 1993) as the major disadvantage of the discrepancy principle. The performance of GCV (Trujillo and Busby, 1989) was investigated in the inverse heat conduction problem. It works well but suffers from comparatively expensive computation for large size problems. To address this issue, with reasonable computational resources, the L-curve method was proposed (Hansen, 1992; Hansen and O´leary, 1993) to choose the regularization parameter at the characteristic L-shaped ‘corner’ in the graph of

the norm of regularized solution versus the norm of the corresponding residual. Therefore, in this study, L-curve method is adopted to determine the regularization parameter since it does not require the information of close bound of noise in measurements, which is difficult to estimate in practice and it shows higher computational efficiency compared with GCV.

Moving forces on a bridge, modeled as Euler-Bernoulli beam and Timoshenko beam (Law and Zhu, 2000), were identified using the Tikhonov regularization method embedded with L-curve method to determine the optimal regularization parameter. In their study, the identified forces are significantly improved especially at the beginning and end of the time history with the regularization procedure. Later on, they extended their research into identifying vehicles axles load and moving forces on a bridge modeled as an orthotropic rectangular plate (Zhu and Law, 2000, 2001). In addition, the prestress force in a prestressed concrete beam (Law and Lu, 2005) was identified in time domain by a system identification approach and Tikhonov regularization technique with measured displacements and strains. Furthermore, inverse programming and Tikhonov regularization incorporated into the moving force identification algorithm were applied to a theoretical bridge model to derive the optimal force solution (Gonz´alez et al., 2008). In this study, considering its favourable performance in the field of force identification, Tikhonov regularization is employed to identify unknown excitations imposed on structural systems.

## 3.3 Iterative global structural identification strategy

In this chapter, an iterative strategy is proposed to identify the unmeasured excitation forces and the unknown structural parameters. It is assumed that the locations of applied forces in the structure are known. The flowchart of the identification strategy is shown in Fig. 3.1.

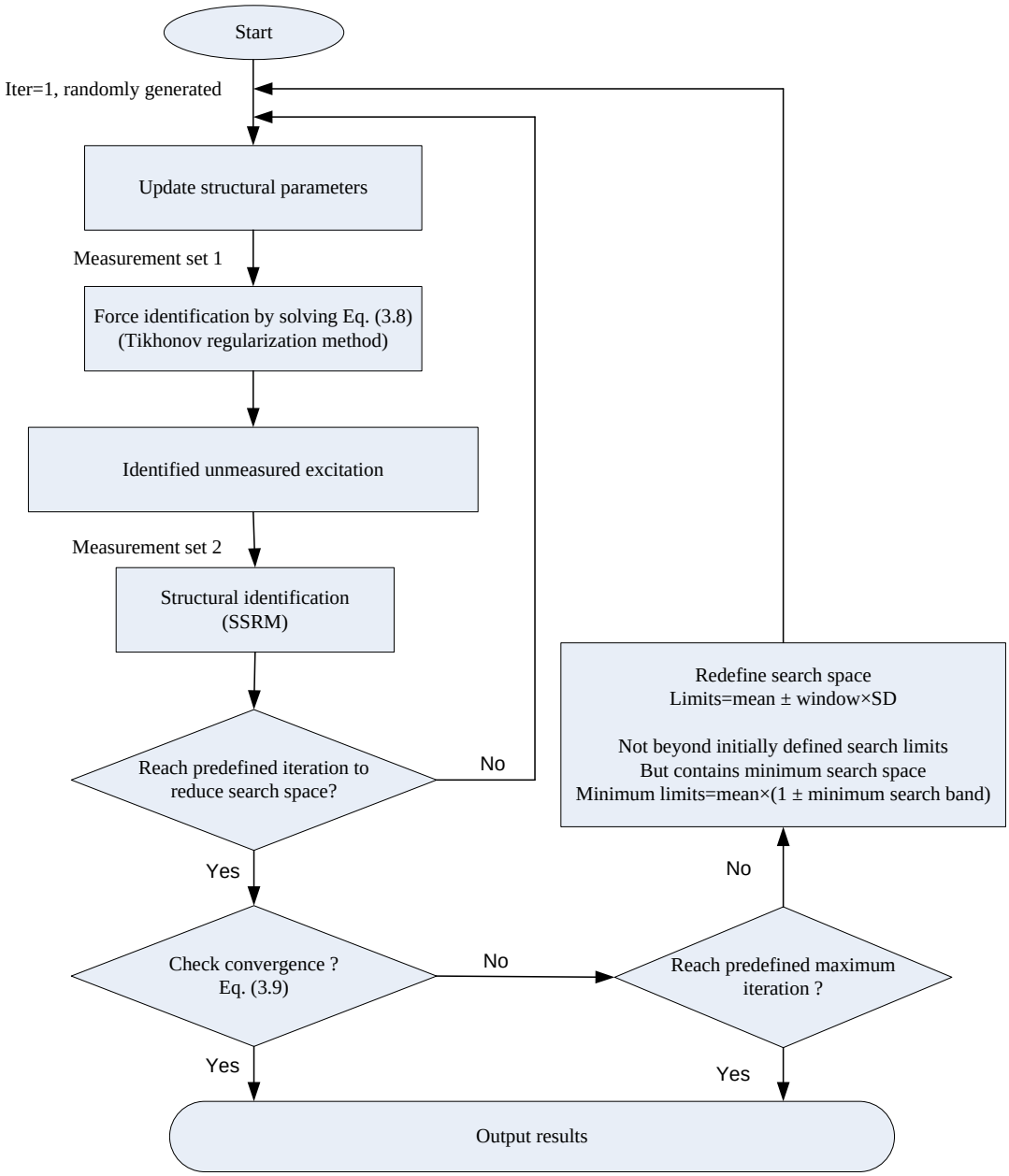


Figure 3.1 Flowchart of global structural identification strategy with unknown input

Prior to structural identification, the measurements are grouped into two sets, denoted as measurement set 1 and set 2. As shown in Fig. 3.1, measurement set 1 is used for force identification with Tikhonov regularization method while set 2 is employed for parameter identification with SSRM. The number of measurements in set 1 should be equal to or larger than that of unknown forces applied to the structure. Set 1 and set 2 may share some but not all of the measurements. Equation (3.7), used for force identification, is derived into state space based on Eq. (3.1), used for parameter identification. Shown in different form, these two equations are actually equivalent with different purposes. Equation (3.7) is employed for force computation and Eq. (3.1) is solved repeatedly to estimate the structural parameters. Set 1 and set 2 must contain different measurements with the purpose of updating excitation forces and structural parameters iteratively. The procedure for global structural identification with the proposed strategy is explained as follows:

Step 1: Start with an initial guess of the structural parameters by random generation from their search space.

Step 2: Compute $[H]$ in Eq. (3.8) for the structure according to the locations of measurements in set 1 with the values of structural parameters.

Step 3: Identify the unknown excitation forces by solving Eq. (3.8) with Tikhonov regularization method based on knowledge of locations of the applied forces.

Step 4: Identify structural parameters with SSRM by minimizing the difference between the simulated responses and the measurement set 2 based on identified excitations from step 3 as input.

Step 5: Update structural parameters with the identification results from step 4, and then go to step 2.

Step 5: Repeat the identification procedure from step 2 to step 5 until the convergence criterion in Eq. (3.9) is satisfied or the predefined maximum iteration number is reached.

The convergence criterion is that the mean absolute error after *iter* iterations $err_{mean}^{iter}$ should be not greater than the prescribed tolerance *tol* in Eq. (3.9).

$$err_{mean}^{iter} = \frac{\sum_{i=1}^{N} \frac{\left| K_i^{iter} - K_i^{iter-1} \right|}{K_i^{iter}}}{N} \le tol \tag{3.9}$$

where $N$ is the number of unknowns involved in structural identification. $K_i^{iter-1}$ and $K_i^{iter}$ are the identified $i$th parameter after *iter*-1 and *iter* iterations, respectively. In this study, the two unknown damping coefficients are excluded in computation of $err_{mean}^{iter}$ in Eq. (3.9) since unknown structural stiffness values are the key parameters of interest. The algorithm of the strategy is as follows.

*Initialization:* $\{x\}_{initial} = \{a\}_{initial} + U(0,1) \times (\{b\}_{initial} - \{a\}_{initial})$

$\{y\} \rightarrow \{y\}_{set\,1}$ *and* $\{y\}_{set\,2}$

**For** *iter* = 1 to predefined maximum iteration number

  **If** *iter* = 1

    $\{x\}_{iter} = \{x\}_{initial}$

  **Else**

    $\{x\}_{iter} = \{x\}_{iter\text{-}1}$

  **End**

$[H]_{iter} \leftarrow \{x\}_{iter}$ (Eq. (3.8))

Force identification (Tikhonov regularization method) by solving

$\{y\}_{set\ 1} = [H]_{iter}\{P\}_{iter} \quad \rightarrow \quad \{P\}_{iter}$

**If** *iter* $\leq$ predefined iteration to reduce search space

$\{a\}_{iter} \leftarrow \{a\}_{initial}$ and $\{b\}_{iter} \leftarrow \{b\}_{initial}$

**Else**

$\{a\}_{iter} = mean - window \times standard\ deviation$

$\{b\}_{iter} = mean + window \times standard\ deviation$

$\{a\}_{minimum} = mean \times (1 - minimum\ search\ band)$

$\{b\}_{minimum} = mean \times (1 + minimum\ search\ band)$

$\{a\}_{iter} \leftarrow min(\ max(\{a\}_{initial}, \{a\}_{iter}), \{a\}_{minimum})$

$\{b\}_{iter} \leftarrow max(\ min(\{b\}_{initial}, \{b\}_{iter}), \{b\}_{minimum})$

**End**

Parameter identification (SSRM):

Input: $\{P\}_{iter}$ and $(\{a\}_{iter}, \{b\}_{iter}) \rightarrow \{x\}_{iter}$

Check convergence with Eq. (3.9)

**End**

Figure 3.2 Algorithm of global structural identification with unknown input

In the algorithm presented in Fig. 3.2, $U(0,1)$ stands for uniform probability distribution. With the predefined initial search limits ($\{a\}_{initial}$, $\{b\}_{initial}$) for the unknown parameters, the initial estimated structural parameters $\{x\}_{initial}$ are randomly generated in their search limits. The measurements $\{y\}$ are grouped to measurement set 1 $\{y\}_{set\ 1}$ and measurement set 2 $\{y\}_{set\ 2}$, which are employed to identify unmeasured excitation forces and unknown structural parameters, respectively.

To improve convergence rate of identification, four parameters are employed to redefine the search space for each parameter, including predefined iteration to

reduce search space, predefined iteration for evaluating the search limits, the width of window for search space reduction and predefined minimum search band. Before the predefined iteration to reduce search space reached, a large search space for each parameter is employed for sufficient exploration since the estimated parameters deviate severely from their exactness at the beginning. Subsequently, it is beneficial to improve convergence rate by reducing search space based on a coarse estimation of structural parameters from previous iterations. It is found that 5 iterations are sufficient for a large exploration to achieve a coarse estimation of each parameter. Therefore, for the first 5 iterations, a large exploration space [0.5, 2] for each parameter is defined in SSRM, and then the search space is evaluated and updated from the $6^{th}$ iteration. The new search space is determined by the number of iterations for evaluating the search limits, the width of the reduced search space window and the defined minimum search band. The results of previous 5 iterations have been sufficient for evaluating the new search space. A window width of about 4 has been found to be efficient to redefine the new search space based on its weighted average value and standard deviation. Furthermore, a suitable value of 0.1 for the minimum search band is defined to prevent premature searching induced by overly constrained search space.

## 3.4 Numerical examples

To test the performance of the proposed strategy for global structural identification, a simply supported beam and a cantilever plate subjected to unknown excitation forces are taken as numerical examples with the aim of identifying the stiffness of each element and the two Rayleigh damping coefficients. The simply supported

beam in Fig. 3.3 and the cantilever plate in Fig. 3.8 are both meshed by 16 elements, which results in 18 unknown parameters in GA for both examples. The initial search space for each unknown parameter is defined as [0.5, 2] of their exact values. The GA parameters for each of the two examples are shown in Table 3.1.

Table 3.1 GA parameters used for global beam and plate identification

| | Beam and Plate |
|---|---|
| Number of unknown parameters | 18 |
| Population size | 90 × 3 |
| Runs | 4/20 |
| Generations | 200 |
| Crossover rate | 0.4 |
| Mutation rate | 0.2 |
| Window width | 4.0 |
| Migration | 0.05 |
| Regeneration | 3 |
| Reintroduction | 30 |

In both numerical examples, 0.02 and 20 are adopted as the tolerance in Eq. (3.9) and the maximum number of iterations, respectively. Signals of 0.4 s are recorded from the accelerometers installed on the beam and plate with a sampling rate of 5,000. Furthermore, noise effect is investigated by introducing 0%, 5% and 10% noise in the measurement data.

### 3.4.1 Damage identification on a simply supported beam

The same simply supported beam in Fig. 2.4 is taken as the first numerical example to verify the performance of the proposed identification strategy. It is assumed that the unknown random force is applied at node 13 while 10 accelerometers at nodes 2, 3, 4, 6, 8, 10, 12, 14, 15 and 16 are instrumented to record translational acceleration signals shown in Fig. 3.3.

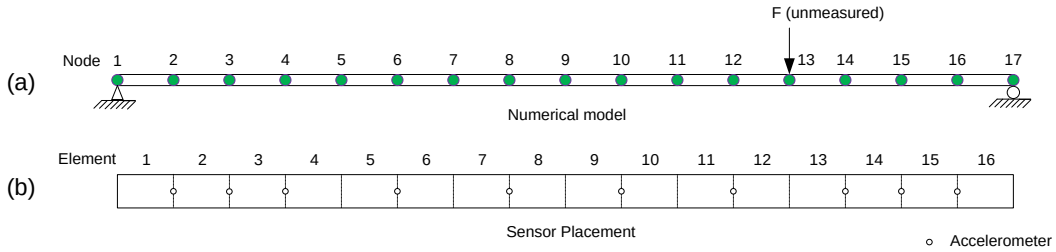


Figure 3.3 The simply supported beam (a) Numerical model and (b) Sensor placement

In this study, the acceleration measurements at nodes 2, 3, 6, 8, 10, 12 and 15, denoted as set 1 are used to identify unknown input forces with Tikhonov regularization method. The measurements at nodes 2, 4, 6, 8, 10, 14 and 16, denoted as set 2 for fitness function evaluation with Eq. (2.21) to identify the 18 unknown structural parameters, including flexural rigidities of 16 elements and 2 damping coefficients. After 20 iterations, the identified damage extents in the 16 elements for 0%, 5% and 10% noise cases are presented in Fig. 3.4.

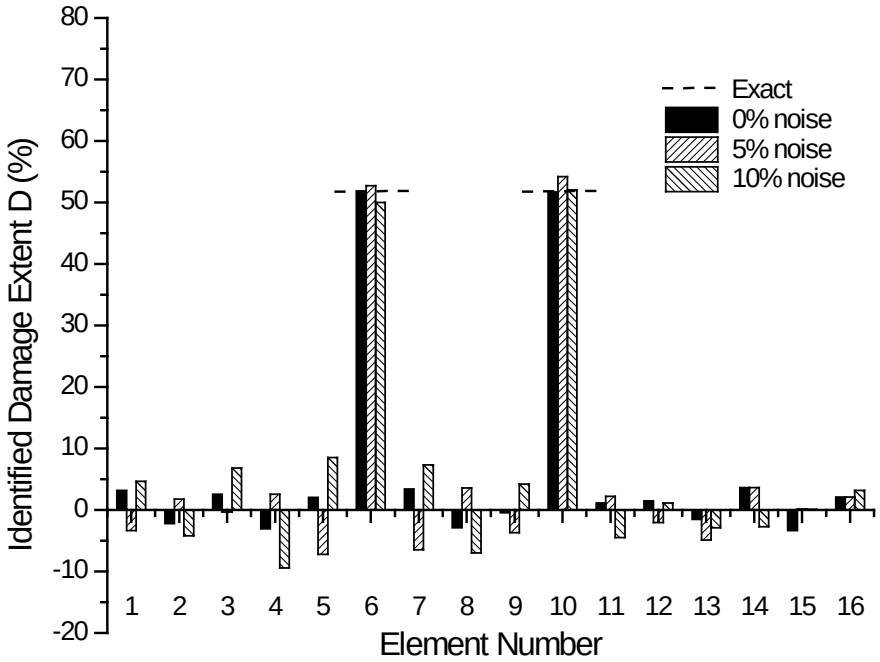


Figure 3.4 Identified damage extent of the simply supported beam

As seen in Fig. 3.4, with 0%, 5% and 10% noise contaminated measurements, the damage extents in element 6 are detected as 51.6%, 52.7% and 50.0%. For 0%, 5% and 10% noise cases, 51.7%, 54.2% and 52.1% reduction of flexural rigidity are identified in element 10. These identified damages in elements 6 and 10 are very close to the exact value 52%. The maximum falsely identified damages are less than 10% for the 10% noise case. These excellent damage identification results indicate that the proposed strategy is able to accurately locate and quantify the damages in the beam even with noisy measurements. The identification errors for undamaged and damaged beam after $1^{st}$, $5^{th}$, $10^{th}$and $20^{th}$ iteration are tabulated in Table 3.2. After 20 iterations, the optimal regularization parameter $\lambda$ is determined by L-curve method as 0.0065, 0.2113 and 0.2812 for 0%, 5% and 10% noise cases. A large value of regularization parameter also indicates that there is a large residual error in the identified results.

Table 3.2 Absolute identification errors with respect to noise level and iteration number

| Noise level | Iteration number | Undamaged state | | Damaged state | |
|---|---|---|---|---|---|
| | | Mean error (%) | Maximum error (%) | Mean error (%) | Maximum error (%) |
| Noise free | 1 | 50.94 | 92.47 | 39.87 | 76.32 |
| | 5 | 6.30 | 22.35 | 5.12 | 16.24 |
| | 10 | 2.86 | 5.70 | 2.13 | 6.74 |
| | 20 | 0.76 | 1.95 | 1.08 | 2.74 |
| 5% noise | 1 | 33.97 | 93.79 | 37.91 | 70.26 |
| | 5 | 12.03 | 39.21 | 15.62 | 36.20 |
| | 10 | 5.97 | 12.49 | 7.67 | 16.51 |
| | 20 | 3.99 | 6.54 | 3.34 | 6.88 |
| 10% noise | 1 | 40.42 | 87.62 | 35.17 | 82.07 |
| | 5 | 16.31 | 35.59 | 15.02 | 30.08 |
| | 10 | 8.44 | 22.21 | 8.20 | 20.76 |
| | 20 | 5.06 | 10.67 | 6.55 | 11.28 |

In Table 3.2, the identification errors are quite large for the $1^{st}$ iteration since the unknown parameters are generated in a random way within the search space. Then

the identification errors start to reduce rapidly. After 20 iterations, acceptable identification results are achieved with less than 7% and 12% of mean and maximum errors for undamaged and damaged beam based on 10 % noise contaminated measurements. The identification results for the undamaged beam with unpolluted measurements for the 20 iterations are plotted in Fig. 3.5 and Fig. 3.6.

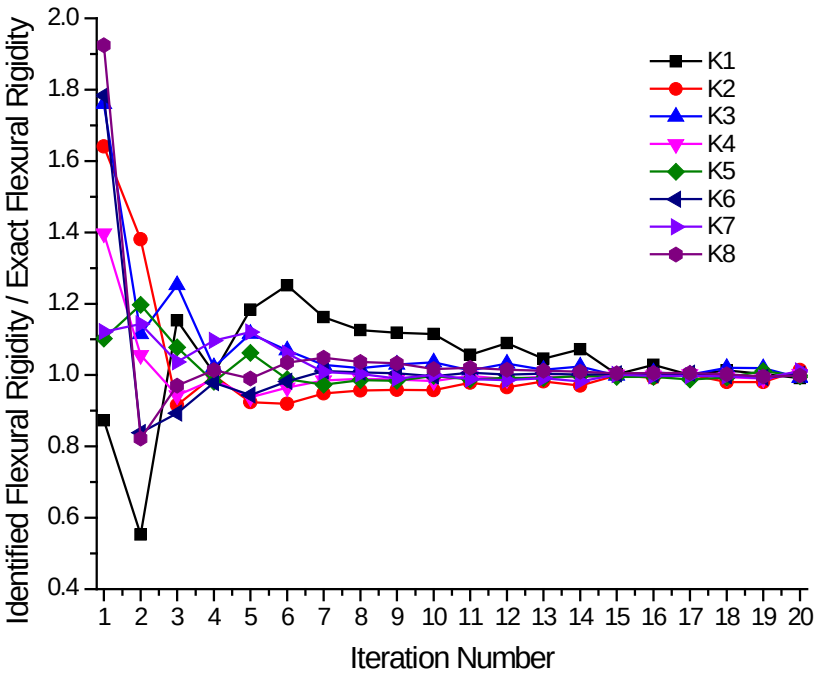


Figure 3.5 Identification results of elements 1-8 in undamaged beam, 0% noise

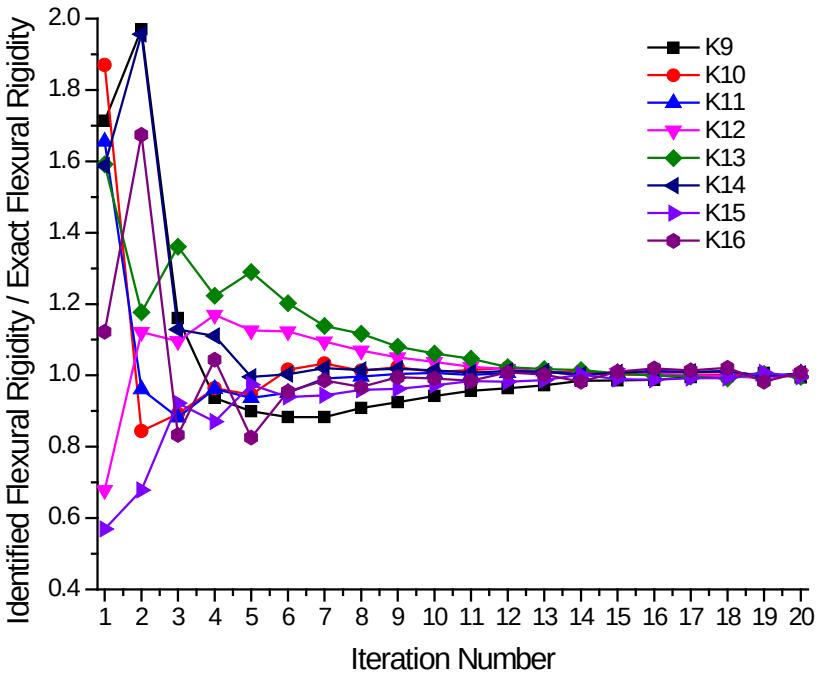


Figure 3.6 Identification results of elements 9-16 in undamaged beam, 0% noise

As demonstrated in Fig. 3.5 and Fig. 3.6, in the 1st iteration, the randomly estimated flexural rigidities of 16 elements from their corresponding search spaces yield largely deviated results with considerable maximum and mean errors of 92.5% and 50.9%. But the subsequent iterations, the identified flexural rigidities converge fast to their exact values. Excellent results with less than 2% and 1% for the maximum and mean errors after 20 iterations are achieved. Moreover, fluctuated identification results are present in the first 5 iterations due to the broad search space [0.5, 2] for each parameter. In the subsequent iterations, gradually converged identified values of flexural rigidities are achieved after the implementation of evaluating and updating their search spaces. For instance, the identified values of flexural rigidity in element 8 and the corresponding search space for 20 iterations are plotted in Fig. 3.7.

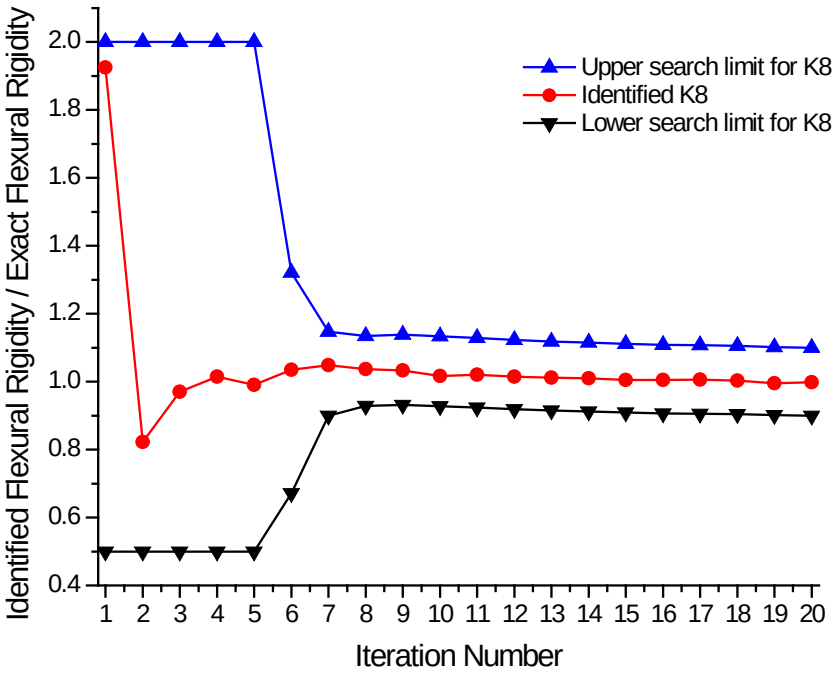


Figure 3.7 Identified flexural rigidity and its search space of element 8, 0% noise

With implementation of the search space updating method illustrated by the algorithm in Fig. 3.2, the results in Fig. 3.7 demonstrate that a broad search limit [0.5, 2] is predefined for the unknown parameters for the first 5 iterations. Then from the 6$^{th}$ iteration, the new search limit is redefined by the computed mean values and standard deviation based on the identification results from the previous 5 iterations. A minimum search limit [0.9, 1.1] is also defined herein to prevent premature local optima, especially when insensitive parameters are involved. The new updated and reduced search space for each parameter after 5 iterations is effective to improve the convergence rate by spending more computational time on evaluation of the candidates close to the global optima.

### 3.4.2 Structural identification on a cantilever plate

A cantilever plate, with length, width and thickness of 2 m, 2 m and 0.04 m, shown in Fig. 3.8 is taken as the second numerical example to validate the performance of the proposed strategy. The cantilever plate is modeled by 4 × 4 thin plate elements with negligible out-of-plane shear strains due to large ratio of in-plane dimensions to its thickness. At each node, there are three DOFs, one translation and two rotations except for the nodes at the fixed edge. The Young's modulus and density of the plate in this numerical simulation are $2.1\times10^{11}$ N/m$^2$ and 7,862 kg/m$^3$, respectively. A random excitation is applied at one corner of the free edge, shown in Fig. 3.8. Structural responses are computed for 0.4 s with a sampling rate of 5,000.

There are 18 unknown structural parameters, including 16 stiffness and 2 damping coefficients. The translational acceleration signals are recorded at nodes 2, 4, 8, 10, 12, 14, 18, 20, 22 and 24, thus 10 accelerometers are installed. The measurements at nodes 2, 4, 8, 12, 20 and 24, denoted as set 1 and the measurement data at nodes 2, 4, 10, 14, 18, 20, 22 and 24 denoted as set 2 are employed to identify the excitation force and structural parameters, respectively.

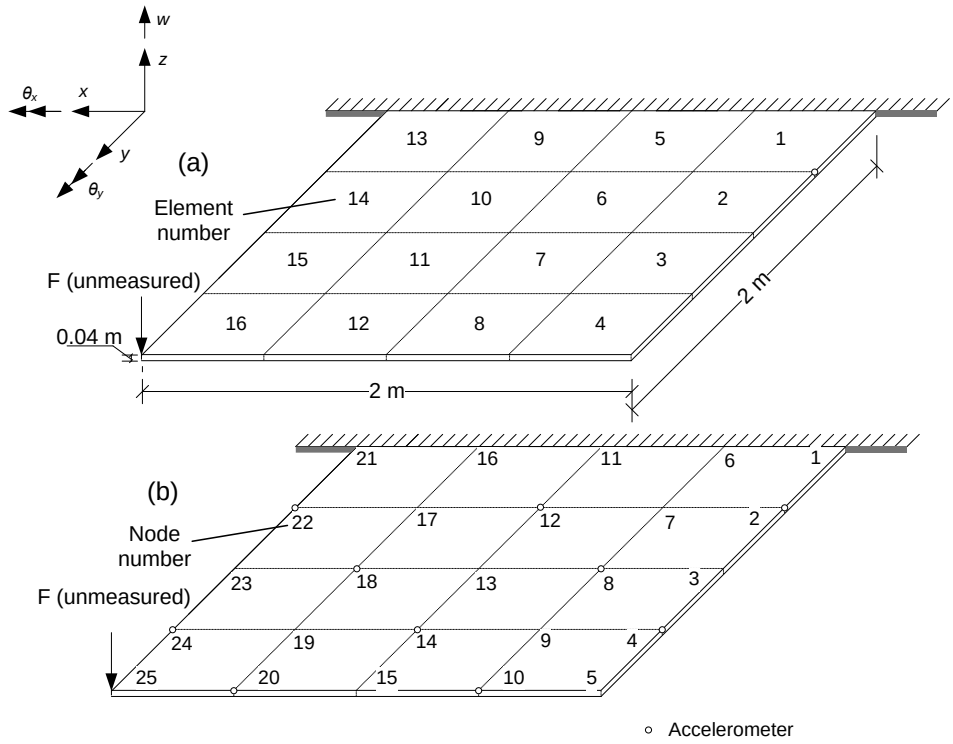


Figure 3.8 (a) Numerical model of a cantilever plate and (b) Sensor placement

The identification results after 20 iterations with 0%, 5% and 10% noise contaminated measurements are presented in Fig. 3.9 while the maximum and mean identification errors are listed in Table 3.3.

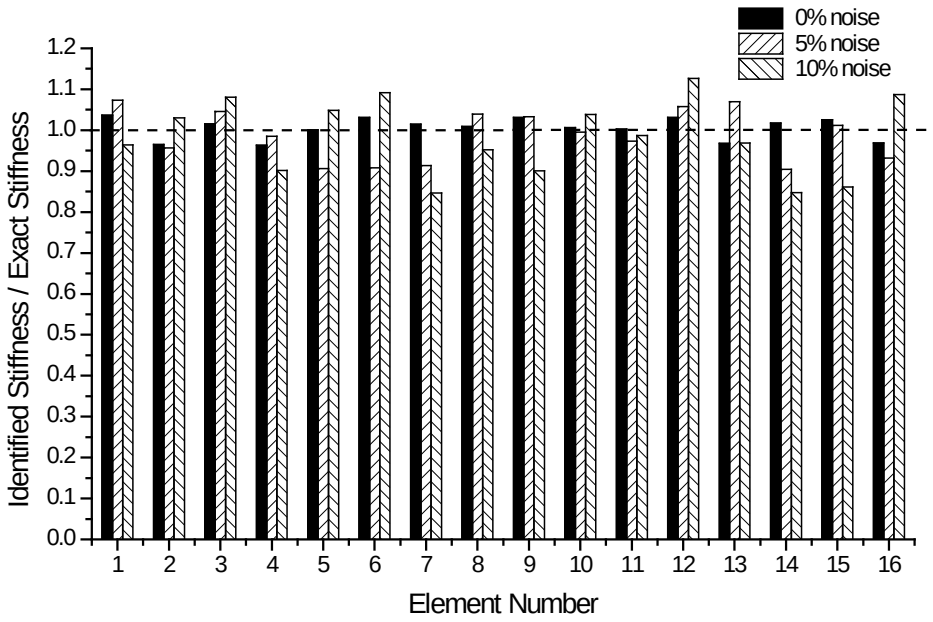


Figure 3.9 Stiffness identification results of the cantilever plate

Table 3.3 Absolute identification errors with respect to noise level

| Noise level | Plate | |
|---|---|---|
| | Mean error (%) | Maximum error (%) |
| 0% | 2.01 | 3.70 |
| 5% | 5.34 | 9.55 |
| 10% | 8.09 | 15.35 |

The identified stiffness of each element illustrated in Fig. 3.9 is in good agreement with the exact value for 0%, 5% and 10% noise cases based on only 10 acceleration measurements. Satisfactory identification results with mean error of 8.09% and maximum error of 15.35% are achieved for the 10% noise case. The results show that the proposed strategy is capable of accurately identifying unknown structural parameters without excitation measurements.

## 3.5 Experimental study

To further verify the effectiveness of the proposed strategy for global structural identification, an experimental study on a 10-storey steel frame in Fig. 3.10, which was fabricated by Trinh T. N. (2010), is conducted.

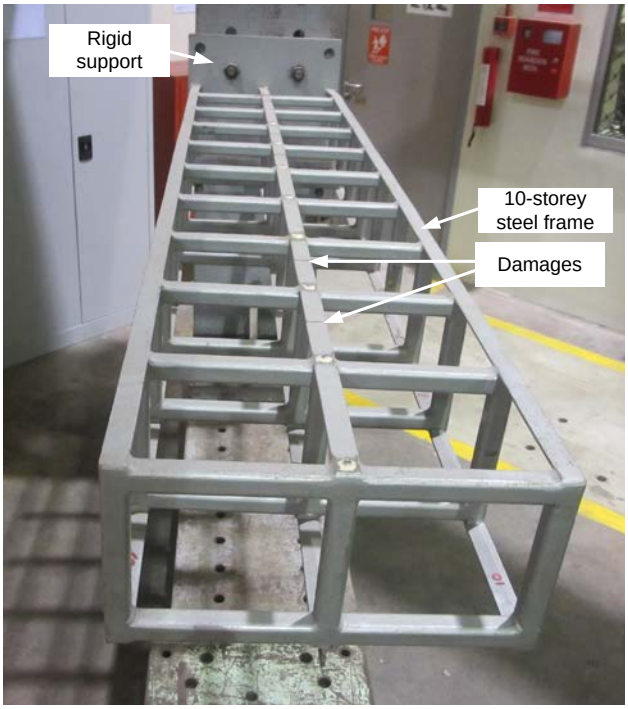


Figure 3.10 The 10-storey steel frame

The frame, total height of 2.0 m and a plan of 0.2×0.4 m, consists of 6 flexible columns (rectangular section of 0.0046×0.025 m) and relatively stiff beams (square hollow sections of 0.025×0.025 m). According to measured mass and volume of a piece of sample, the density of the steel used in the experiment is determined as approximately 7,540 kg/m$^3$. A lumped mass numerical model, shown in Fig. 3.11, is built to represent this frame which behaves as a 2D shear building due to the symmetry of structure and loading as well as significantly heavy beam system at each level compared with the columns. The lumped mass of each level is approximately calculated from the member sizes and steel density. The mass is 3.25 kg for levels 1-9 and 3.00 kg for level 10.

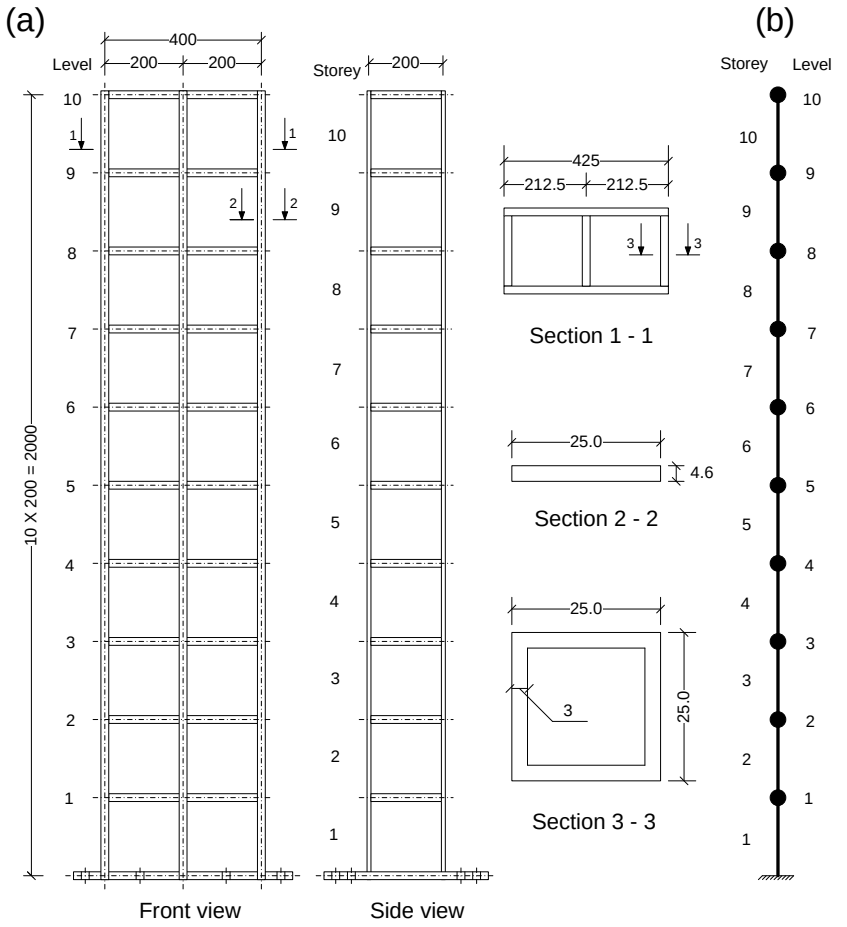


Figure 3.11 (a) Illustration of a 10-storey steel frame and (b) The lumped-mass model

### 3.5.1 Stiffness measurements

A static test is conducted herein to estimate the stiffness of each frame level. The frame is mounted horizontally to a rigid vertical support and force is applied by hanging a weight with hooks at different level in the frame. The displacement at each level is recorded using displacement transducers and a data acquisition system. From Eq. (3.10), the stiffness of each storey can be computed as applied force divided by the displacement difference between adjacent levels. To mitigate the effect of possible frame torsion, two displacement transducers are symmetrically

installed at each level to give the average displacement measurement for computation of stiffness.

$$K_i = \frac{W}{\Delta x_i} \tag{3.10}$$

where $K_i$ is the stiffness at storey $i$; $W$ is the applied weight at level $i$ and $\Delta x_i$ is the displacement difference between level $i$ and $i-1$.

In the experiment, to reduce noise effect on measurement signals, sufficiently heavy weights of 25, 30 and 35 kg are sequentially applied at each level. First the weight was applied at level 10 and the displacements are measured at levels 9 and 10. This procedure is repeated for the remaining storeys by shifting the whole system of applied weights and transducers inwards up to level 1 by applying the weight at level 1 and measuring the displacement at level 1. The instrumentation for static test is shown in Fig. 3.12.

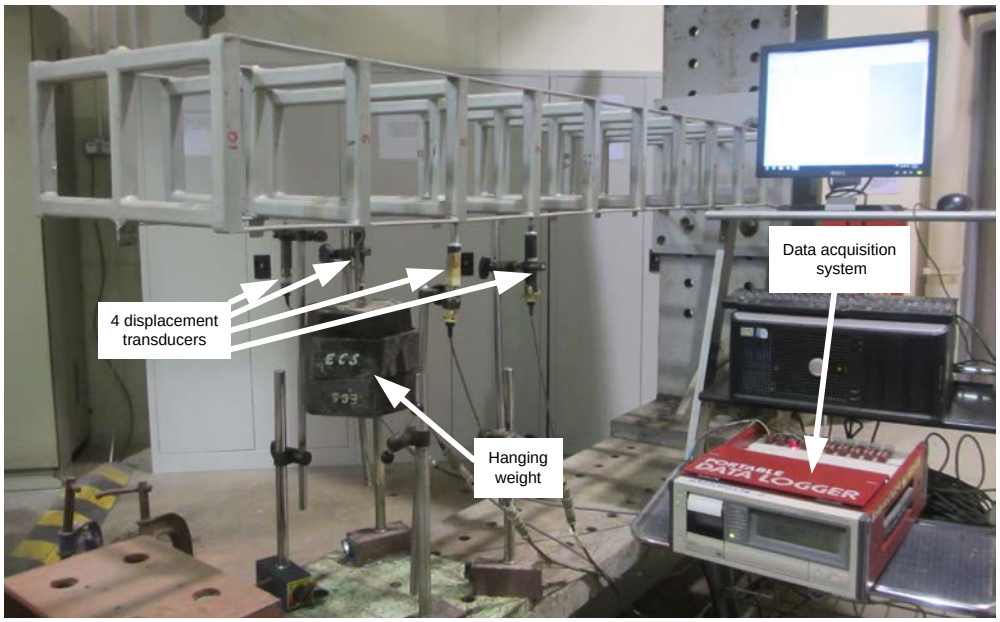


Figure 3.12 Instrumentation of the static test

Three heavy weights 25, 30 and 35 kg are sequentially applied to the frame from level 10 to level 1. For each applied weight, the stiffness of each storey is computed with Eq. (3.10) based on the corresponding displacement measurement data. With the three computed stiffness values under different applied weights, the least-square method is employed for estimating stiffness of each storey. The measured stiffness of each storey by static test is shown in Table 3.4.

Table 3.4 Measured stiffness by static test

| Storey | Measured stiffness (kN/m) |
|---|---|
| 1 | 475.96 |
| 2 | 277.42 |
| 3 | 430.88 |
| 4 | 283.41 |
| 5 | 267.68 |
| 6 | 396.09 |
| 7 | 378.09 |
| 8 | 263.91 |
| 9 | 252.09 |
| 10 | 362.55 |

The stiffness value of different storey shown in Table 3.4 is quite different since there are some damages existed in the frame, indicated in Fig. 3.10. Based on the measured stiffness values of each storey listed in Table 3.4, and with estimated mass 3.25 kg for levels 1-9 and 3.00 kg for level 10 based on known steel density and dimension of member size of the frame, the natural frequencies of the frame are computed and shown in Table 3.5.

Table 3.5 Natural frequencies computed from measured stiffness by static test

| Mode number | Natural frequency (Hz) |
|---|---|
| 1 | 7.71 |
| 2 | 22.66 |
| 3 | 35.82 |
| 4 | 52.36 |
| 5 | 64.54 |
| 6 | 75.89 |
| 7 | 82.28 |
| 8 | 88.78 |

| | |
|---|---|
| 9 | 99.00 |
| 10 | 101.81 |

Subsequently, the stiffness of each storey is validated by an impact test. The frame is hammered at level 10 and the accelerometers, installed at every level, collect the measurement data using a 16-channel digital oscilloscope with 2,000 samples/s. The natural frequencies of this frame are obtained from the power spectra of 3 s measurement data in frequency domain via Fast Fourier transform (FFT). The FFT results from the impact test with frequency ranging from 0 to 100 Hz are shown in Fig. 3.13.

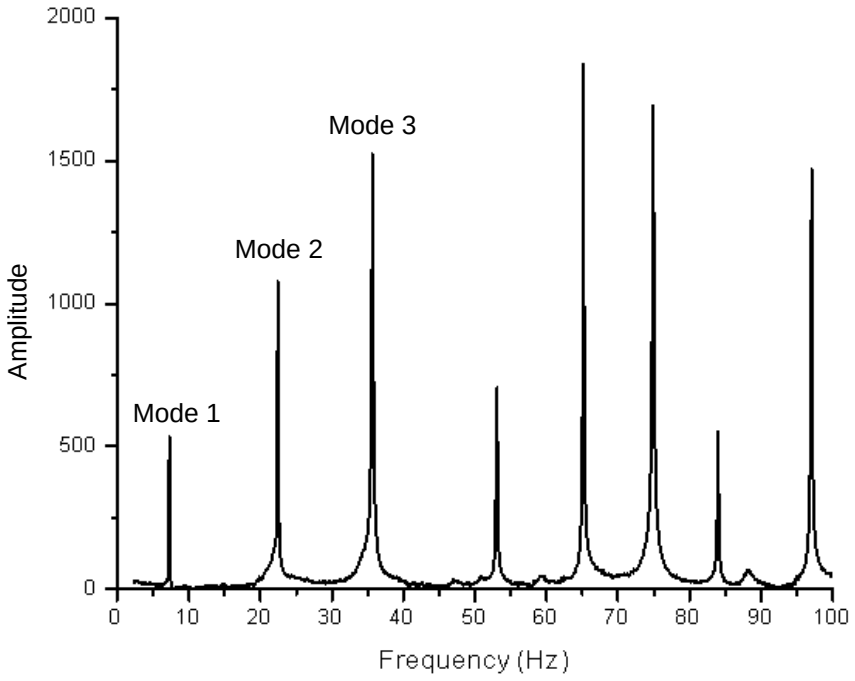


Figure 3.13 Natural frequencies of the frame

From Fig. 3.13, the first eight natural frequencies from the impact test are 7.4, 23.0 37.2, 53.0, 65.5, 76.8, 84.0 and 97.5 Hz. They are merely 4.0%, 1.5%, 3.9% 1.22%, 1.49%, 1.17%, 2.09% and 9.82% different from the results by static test in Table

3.5. It shows that the first seven natural frequencies from the impact test are in excellent agreement with those from the static test. It validates the correctness of the measured frame stiffness from static test and verifies the accurateness of the assumed lumped mass numerical model in representing the frame behaviour.

### 3.5.2 Dynamic test

In this study, an excitation force is generated by a shaker acting vertically on the frame through a connection rod at level 10, as shown in Fig. 3.14. The signal of excitation forces generated by NI software (LabView SignalExpress) is passed through a power amplifier (Labworks PA-141) to produce sufficient power for the electromagnetic shaker (Labworks ET-126B). The signal from accelerometers is collected by data acquisition unit (Yokogawa SL1000), shown in Fig. 3.14.

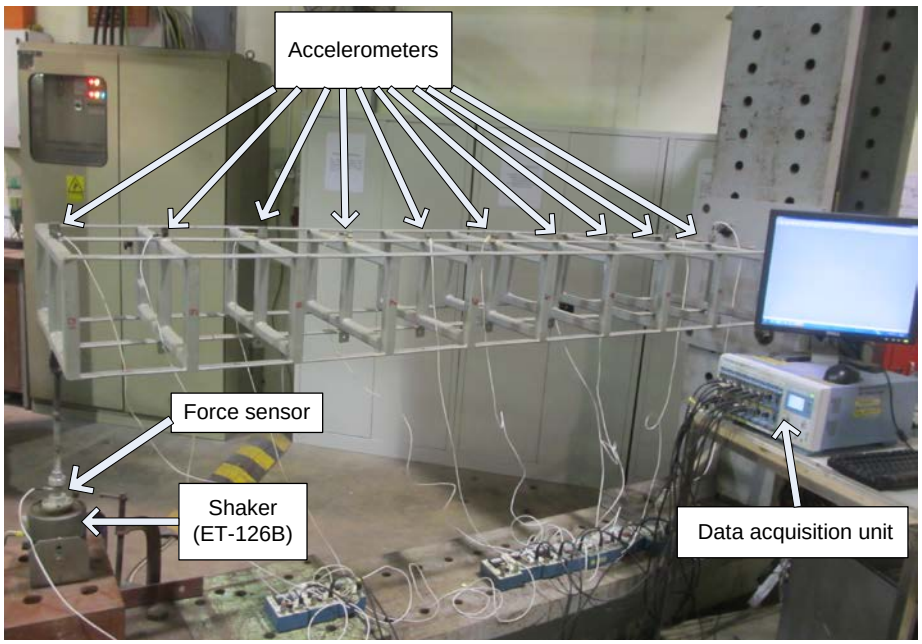


Figure 3.14 Instrumentation of the dynamic test

Ten accelerometers are mounted on top of each level of the frame, as shown in Fig. 3.14 and Fig. 3.15, and the specifications for these accelerometers are listed in Table 3.6. An ICP (Integrated Circuit Piezoelectric) force sensor (PCB-208C02) with a sensitivity of 49.59 mV/lbf is installed between the shaker and the connection rod to measure the applied force, shown in Fig. 3.14.

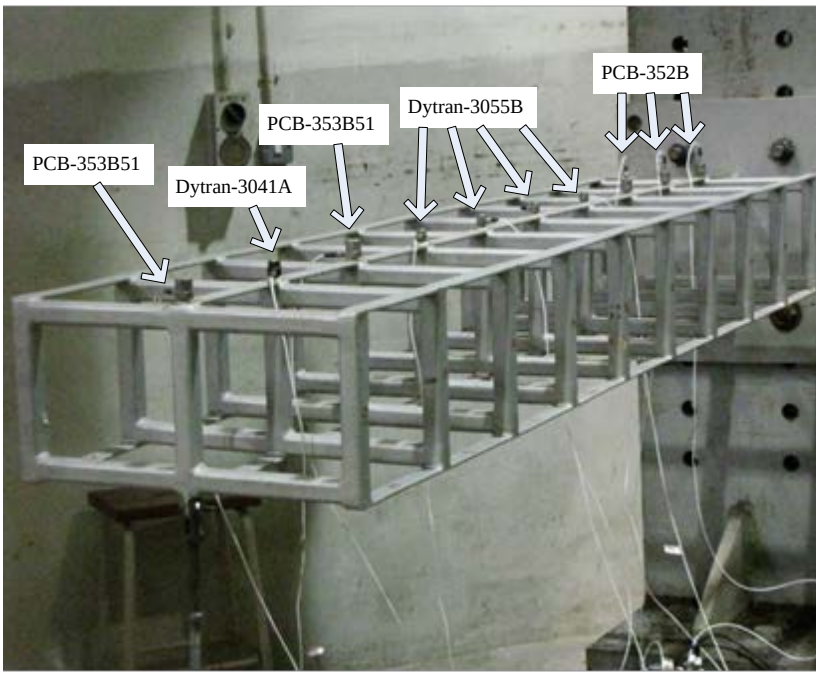


Figure 3.15 Installed accelerometers on the frame

Table 3.6 Specifications of the accelerometers installed on the frame

| level | Accelerometer model | Sensitivity (mV/g) | Measurement range | Frequency range (Hz) |
|---|---|---|---|---|
| 1 | PCB-352B | 1,021 | ±5g | 2 – 10,000 |
| 2 | PCB-352B | 1,021 | ±5g | 2 – 10,000 |
| 3 | PCB-352B | 1,017 | ±5g | 2 – 10,000 |
| 4 | Dytran-3055B | 505.5 | ±10g | 1 – 10,000 |
| 5 | Dytran-3055B | 513.4 | ±10g | 1 – 10,000 |
| 6 | Dytran-3055B | 494 | ±10g | 1 – 10,000 |
| 7 | Dytran-3055B | 520.3 | ±10g | 1 – 10,000 |
| 8 | PCB-353B51 | 522 | ±10g | 1 – 2,000 |
| 9 | Dytran-3041A | 530.2 | ±10g | 1 – 3,000 |
| 10 | PCB-353B51 | 489 | ±10g | 1 – 2,000 |

Signals from the 10 installed accelerometers are recorded at a sampling rate of 2,000. Thus 2 s of measurement time results in 4K sample points recorded from each accelerometer. Random force is generated from the shaker to excite the frame at level 10, illustrated in Fig. 3.14. There are 12 unknown parameters involved in the global frame identification, including 10 stiffness of each storey and 2 damping coefficients. The search range for the unknown stiffness is set as half to double of the measured values from the static test. And the search limits for the two damping coefficients ( $a_o$ and $a_1$ ) are set as 0-4 and 0-0.0002, respectively. The GA parameters are set the same as the numerical study of damage identification on the simply supported beam shown in Table 3.1 but with 12 unknown structural parameters.

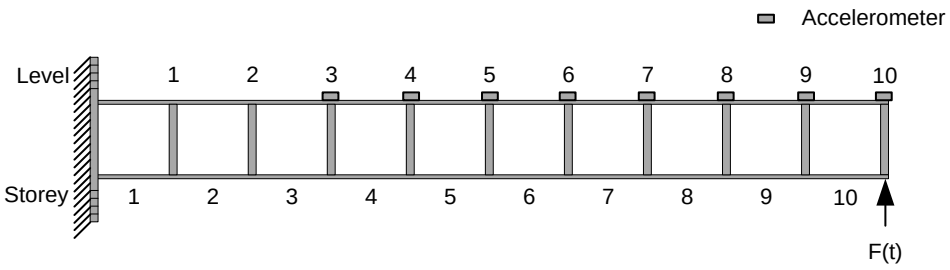


Figure 3.16 Sensor placements in the frame

As shown in Fig. 3.16, the measurements at level 1 and 2 are excluded in structural identification due to relatively low signal-to-noise ratio. A dynamic test is carried out for stiffness identification of global frame with the measurements of the forces applied at level 10 of the frame, for the purpose of comparison of the stiffness identification without excitation measurements. Eight acceleration measurements at levels 3-10 are employed to evaluate the fitness function in GA for global frame identification with 3 different random forces applied to the frame, shown in Fig.

3.17. Figure 3.18 demonstrates that the corresponding identification results compared with the measured stiffness by the static test when the frame is excited by different random forces. The average of identified stiffness of each storey based on these three different forces is listed in Table 3.7.

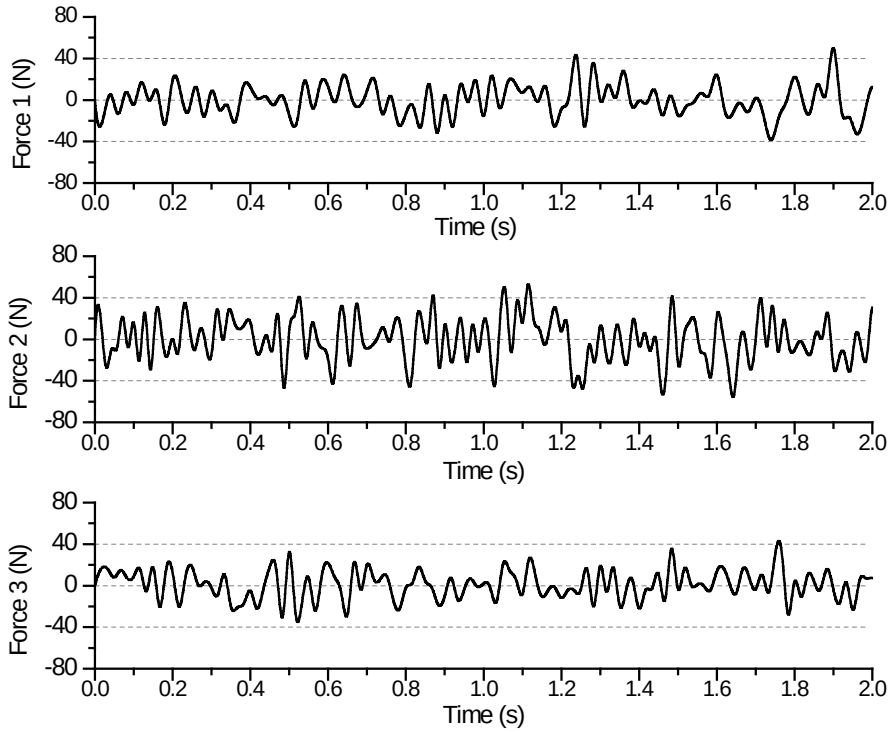


Figure 3.17 Three random forces applied to the frame at level 10

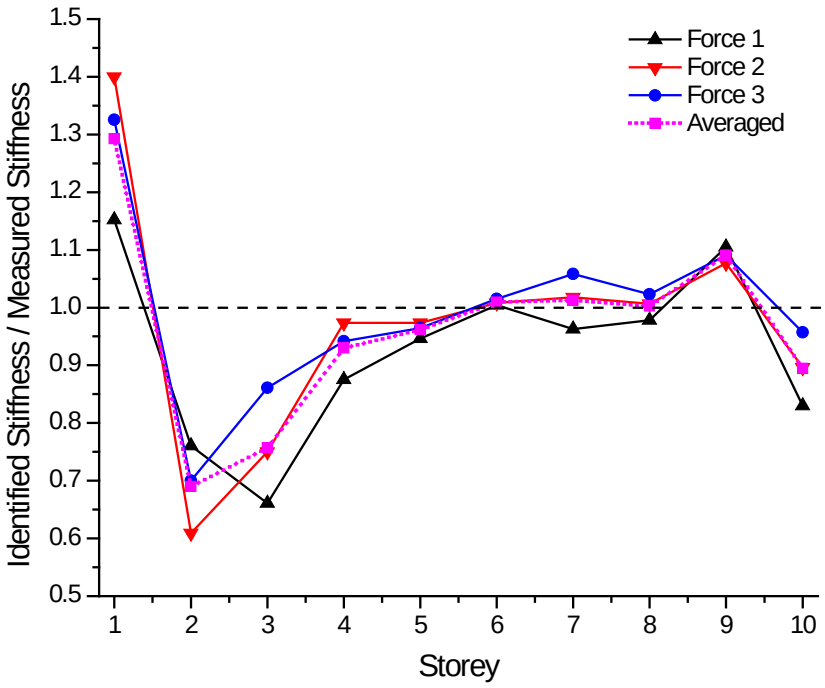


Figure 3.18 Identified stiffness of the frame with force measurements

Table 3.7 Identification results of the frame with force measurements

| Storey | Stiffness (kN/m) (static test) | Stiffness (kN/m) (dynamic test) | Error (%) |
|---|---|---|---|
| 1 | 475.96 | 615.17 | +29.25 |
| 2 | 277.42 | 191.37 | -31.02 |
| 3 | 430.88 | 326.25 | -24.28 |
| 4 | 283.41 | 263.59 | -6.99 |
| 5 | 267.68 | 257.39 | -3.85 |
| 6 | 396.09 | 399.70 | +0.91 |
| 7 | 378.09 | 383.02 | +1.30 |
| 8 | 263.91 | 264.59 | +0.26 |
| 9 | 252.09 | 275.00 | +9.09 |
| 10 | 362.55 | 324.35 | -10.54 |

From Fig. 3.18, with different forces applied to the frame, the identified stiffness is in good agreement with the measured stiffness by static test except at storeys 1-3. The noise level in the acceleration measurements at levels 1-10 is about 12.1%, 10.2%, 7.2%, 4.6%, 5.8%, 3.2%, 2.9%, 3.1%, 4.9% and 3.5% which is evaluated by the root-mean-square ratio of the noise signals to measurements. The significant difference between the measured and identified stiffness for storeys 1-3 is mainly

caused by the noisy measurements near the support. Due to high ratio of noise-to-signal for the acceleration measurements at levels 1 and 2, these two measurements are excluded in evaluating the fitness function. Therefore, it is extremely difficult to accurately identify the stiffness of these levels close to the support since no measurements near the support are involved in fitness function evaluation. Good agreement between measured and identified stiffness at levels 4-10 is achieved for static and dynamic test, with the maximum error of 10.54% at level 10, illustrated in Table 3.7.

### 3.5.3 Global frame identification with unknown input force

Subsequently, the proposed strategy is implemented to identify the frame without the force measurements as shown in Fig. 3.19.

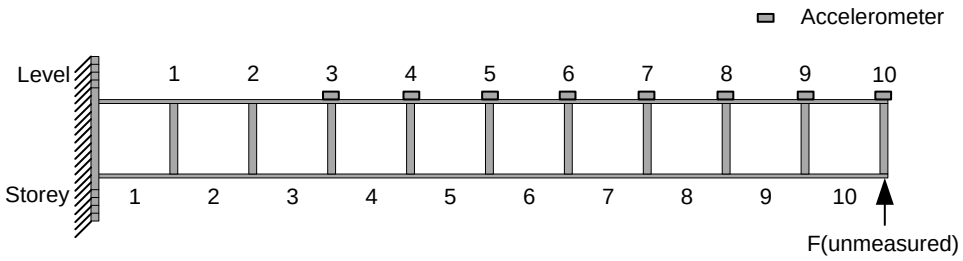


Figure 3.19 Sensor placements for frame identification without force measurements

The acceleration responses are measured at levels 3-10 under the same set of 3 different random forces as in the dynamic test, shown in Fig. 3.19. The acceleration measurements at levels 3, 5, 7 and 9 are grouped as set 1 to identify the unmeasured force applied at level 10. Measurements at levels 4, 6, 8 and 10 are grouped as set 2 to identify 12 unknown structural parameters of the frame, including the stiffness of each storey and two unknown damping coefficients. The initial search limits for the stiffness values are set as 0.5-2.0 times of their measured values in Table 3.4. The

search space for the two damping parameters is set as 0-4 and 0-0.0002, respectively. The same GA parameters in the dynamic test are selected herein. The maximum iteration number 20 and the tolerance 0.02 are predefined in the identification. The identification results compared with measured stiffness from the static test as well as the averaged results based on 3 different forces are presented in Fig. 3.20. The averaged identified stiffness for each storey based on these 3 different forces is summarized in Table 3.8.

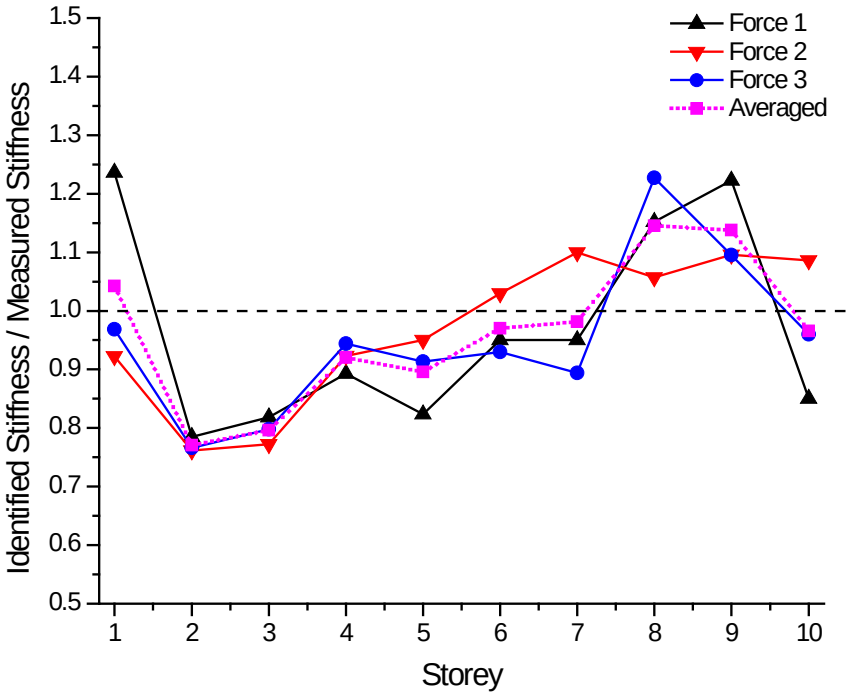


Figure 3.20 Identified stiffness of the frame without force measurements

Table 3.8 Identification results of the frame without force measurements

| Storey | Stiffness (kN/m) (static test) | Stiffness (kN/m) (dynamic test) | Stiffness (kN/m) Identified | Error (%) Compared with static test | Error (%) Compared with dynamic test |
|---|---|---|---|---|---|
| 1 | 475.96 | 615.17 | 496.17 | +4.25 | -19.34 |
| 2 | 277.42 | 191.37 | 213.84 | -22.92 | +11.74 |
| 3 | 430.88 | 326.25 | 342.99 | -20.40 | +5.13 |
| 4 | 283.41 | 263.59 | 260.74 | -8.00 | -1.08 |
| 5 | 267.68 | 257.39 | 239.76 | -10.43 | -6.85 |
| 6 | 396.09 | 399.70 | 384.21 | -3.00 | -3.88 |
| 7 | 378.09 | 383.02 | 371.02 | -1.87 | -3.13 |
| 8 | 263.91 | 264.59 | 302.30 | +14.55 | +14.25 |

| | | | | | |
|---|---|---|---|---|---|
| 9 | 252.09 | 275.00 | 286.84 | +13.78 | +4.31 |
| 10 | 362.55 | 324.35 | 350.01 | -3.46 | +7.91 |

From Fig. 3.20 and Table 3.8, there is a significant discrepancy between the identified stiffness and measured stiffness from static test and dynamic test on storeys 1-3 with identification errors up to 22.92% and 19.34%. The main reason accounting for this discrepancy is due to the low ratio of signal to noise measurements close to the support. Excluding the measurements at levels 1 and 2 also introduces huge difficulty to accurately identify stiffness of the storeys close to the support due to no nearby measurements involved in the computation of fitness function.

The identified stiffness values of the levels close to the free end of the frame also relatively severely deviate from the measured values mainly due to only 4 acceleration measurements involved in stiffness parameter identification. The accuracy of identified stiffness of mid-levels of the frame, shown in Fig. 3.20, cannot catch up with the results from the dynamic test, demonstrated in Fig. 3.18. The main reason is that there are 8 acceleration measurements involved in evaluation of fitness function in the dynamic test.

In this experiment, the accuracy of identification results suffers from the inevitable modeling errors, including the imprecise lump-mass numerical model to represent the frame, coarse estimation of the mass on each level and the approximate fixed boundary condition. Furthermore, the measurement noise inevitably affects the identification results, leading to inaccurate identified stiffness for storeys 1-3. The limited number of measurements used for stiffness parameter identification also

degrades the accuracy of identification results especially near the free end of the frame. Despite these adverse factors in the experiment, the proposed strategy is able to reasonably identify the stiffness values at levels 4-10 of the frame with maximum errors of 14.55% and 14.25% compared with those from static and dynamic tests without force measurements.

## 3.6 Estimation of force

The proposed strategy yields not only identified structural parameters but also, as a by-product, identified time history of excitation. For instance, the identified random force applied at node 13 of the undamaged simply supported beam for the first 0.4 s in Fig. 3.3 with unpolluted measurements (i.e. 0% noise) after 1st, 5th and 20th iteration are presented in Fig. 3.21 through Fig. 3.23, respectively.

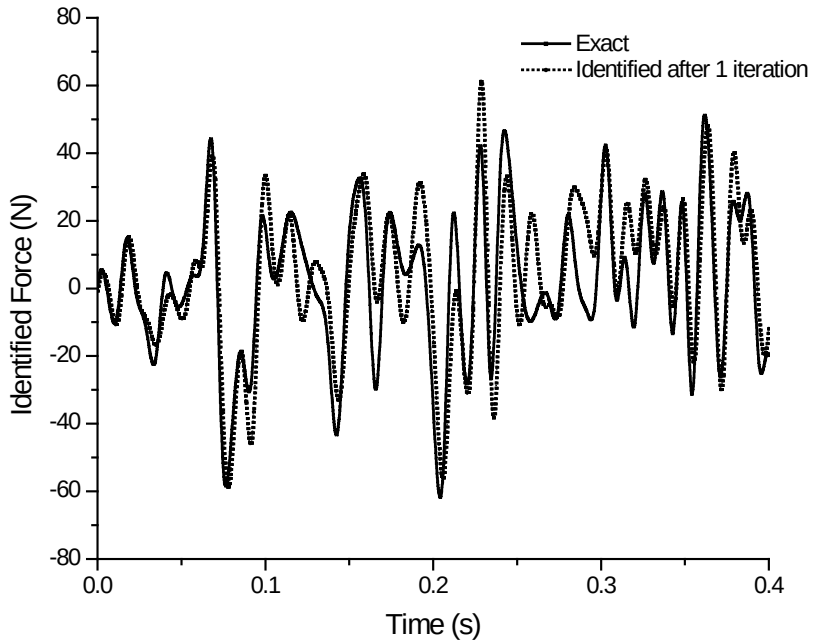


Figure 3.21 Identified force after 1 iteration, 0% noise

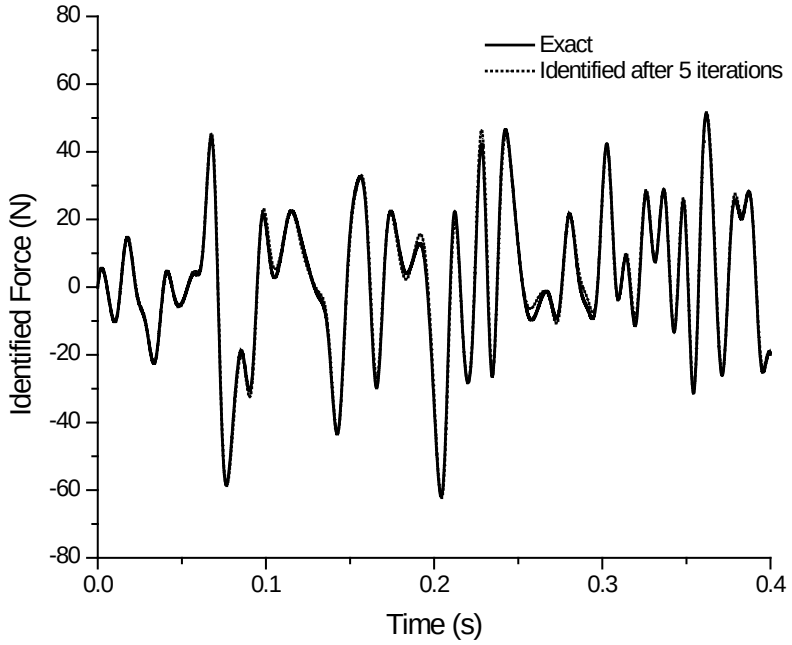


Figure 3.22 Identified force after 5 iterations, 0% noise

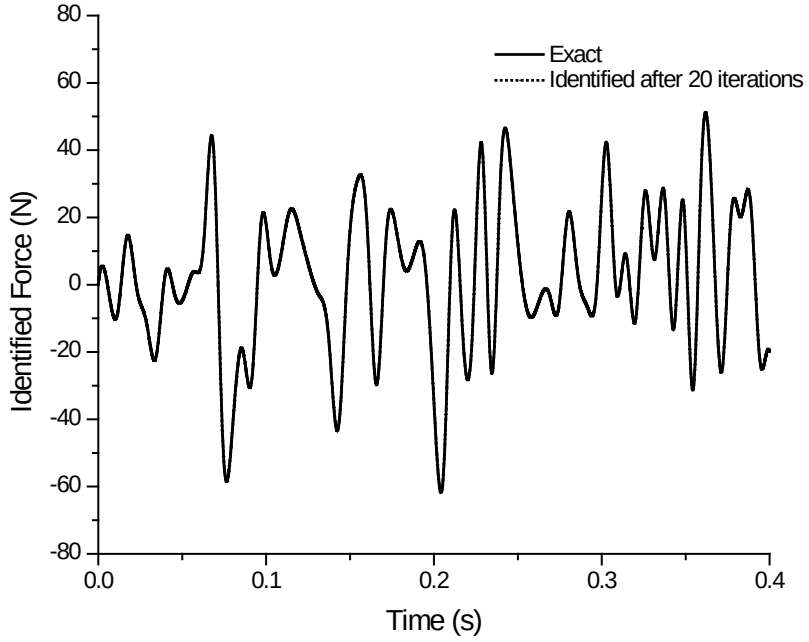


Figure 3.23 Identified force after 20 iterations, 0% noise

As seen in Fig. 3.21, there are a great difference between the identified force after the 1st iteration and the exact solution due to inaccurately estimated structural

parameters with 50.94% mean error and 92.47% maximum error, shown in Table 3.2. The difference reduces significantly after 5 iterations and the results after 20 iterations are in excellent agreement with the exact force, demonstrated in Fig. 3.23. Fast convergence in the identified force is observed from comparison among Fig. 3.21 through Fig. 3.23. The absolute error in the identified force and the mean absolute error in the identified flexural rigidities for 16 elements in each iteration are demonstrated in Fig. 3.24, indicating that the unmeasured excitations and the unknown structural parameters approach their exact values together. In Fig. 3.24, $f_{identified}$ and $f_{exact}$ represent the identified and exact force. The absolute error in the identified force is defined as the ratio of the root-mean-square (RMS) of ( $f_{identified}$ - $f_{exact}$ ) to $f_{exact}$ . The mean absolute error is computed based on the identified flexural rigidities of 16 elements in the simply supported beam.

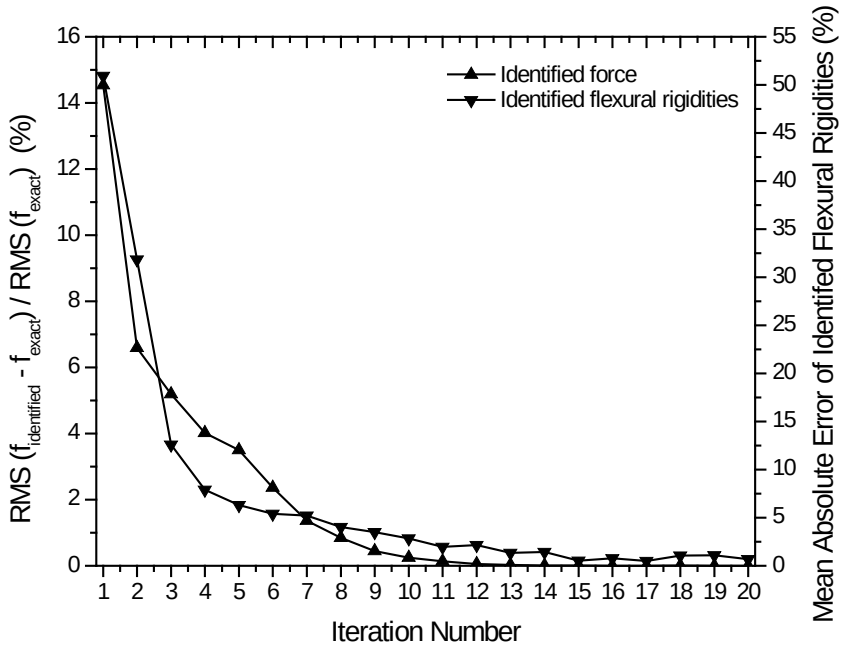


Figure 3.24 Identification errors in estimated forces and flexural rigidities, 0% noise

Furthermore, to investigate the noise effect, 1 second of the identified force time history for the 5% and 10% noise cases after 20 iterations is plotted in Fig. 3.25 and Fig. 3.26, where obvious drifts are observed in the identified force compared with its exactness. After applying FFT to the identified force and plotting power spectra of the identified force for 0-100 Hz, it is found that the drifts are only confined to low frequencies, shown in Fig. 3.27 and Fig. 3.28.

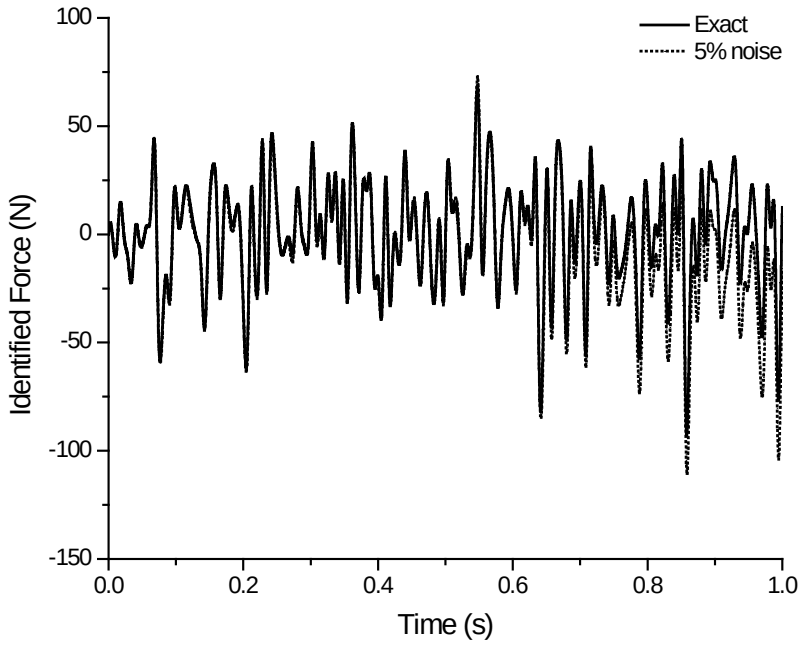


Figure 3.25 Identified force, 5% noise

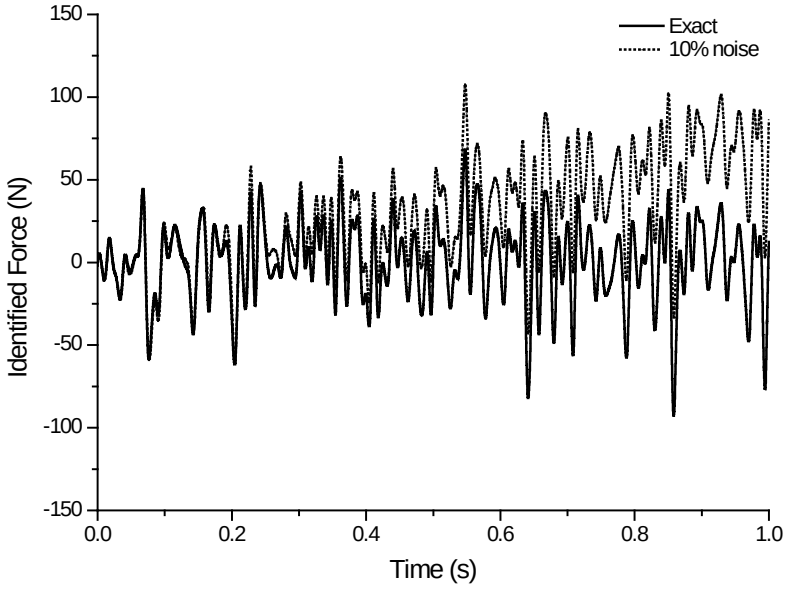


Figure 3.26 Identified force, 10% noise

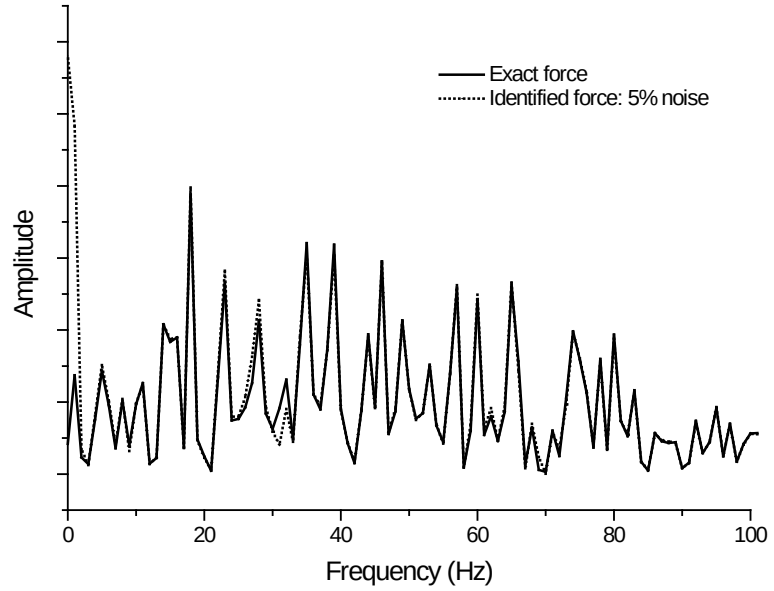


Figure 3.27 FFT results of the identified force, 5% noise

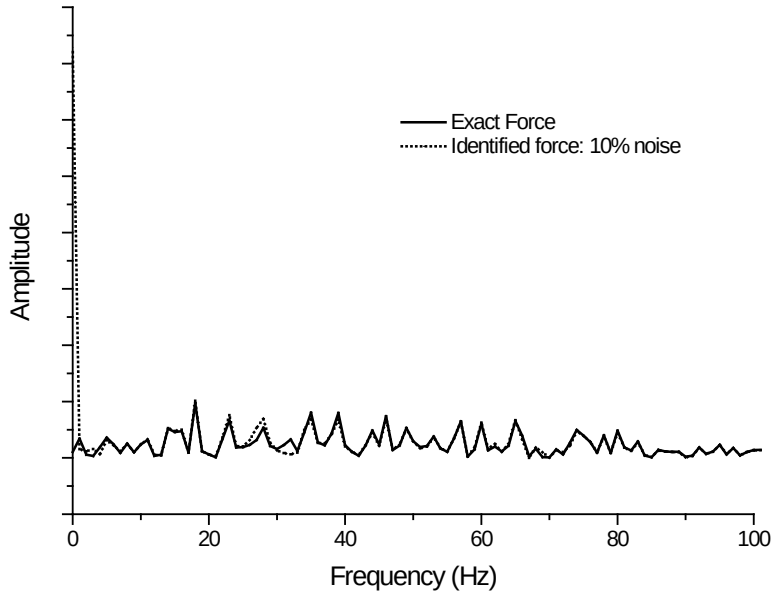


Figure 3.28 FFT results of the identified force, 10% noise

Although the time history of the identified excitation contains drift, it can be readily corrected by suppressing its low frequency components with filter methods. For 10% noise case, Fig. 3.29 demonstrates the filtered force by letting the identified force in Fig. 3.26 go through a high pass Butterworth filter with cutoff frequency of 5 Hz, which is much lower than 47.9 Hz of the first natural frequency of the simply supported beam. The filtered force is in good agreement with the exact force, implying that the proposed strategy is also capable of providing accurate estimation of the unmeasured forces.

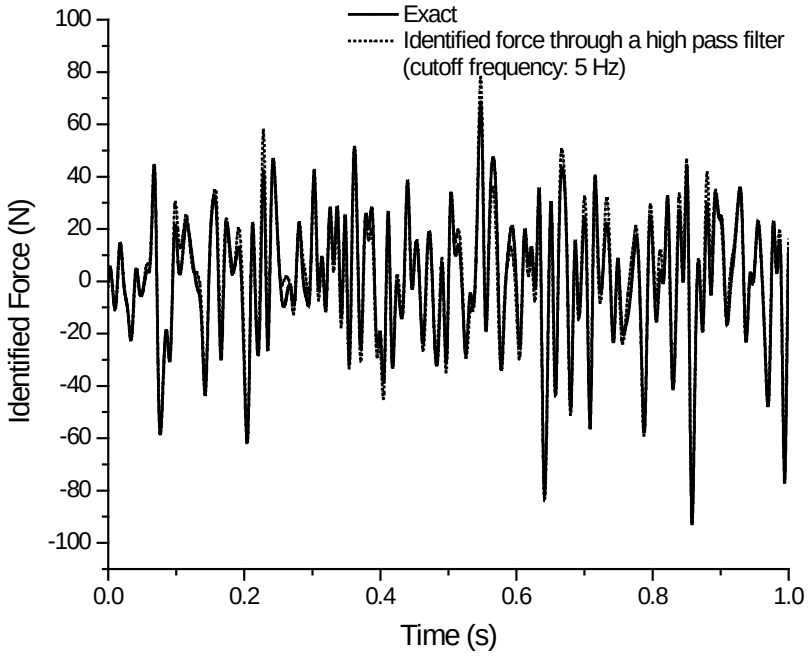


Figure 3.29 Filtered results of the identified force, 10% noise

## 3.7 Summary

In this chapter, an iterative strategy is proposed for global structural identification without force measurements. The identification strategy, a synergy of Tikhonov regularization method for force identification and SSRM for parameter identification, is developed to identify the unknown parameters of structures. Force identification and parameter identification are carried out iteratively to achieve a converged optimal solution. In this strategy, to improve the convergence rate, a technique for computation and renewal of search space is developed to save computational time on evaluating the candidates far away from the optimal solution. A minimum search space is defined for sufficient exploration to prevent premature local optima.

The proposed strategy is applied to global structural identification on a simply supported beam and a cantilever plate to examine its performance. Numerical results show that the strategy is able to accurately locate and quantify the damages in the beam as well as estimate the stiffness of the plate. The effectiveness of the strategy is demonstrated by the converged results within 20 iterations. Reasonable identification results in terms of accuracy are achieved with 0%, 5% and 10% noise contaminated measurements.

To further validate the effectiveness of the proposed strategy, global structural identification is carried out experimentally on a 10-storey frame with 3 different random excitations. Static and dynamic tests are conducted to estimate the stiffness of each storey of the frame. Good agreement is achieved between the measured stiffness through static test and identified stiffness by dynamic test except on storeys closed to the fixed support. The proposed strategy is implemented to identify the frame stiffness without force measurements. The low ratio of signal-to-noise measurements at the levels close to the support, and the exclusion of acceleration measurements at levels 1 and 2 in the evaluation of fitness function, causes accurately identifying the stiffness values for the levels near the support extremely difficult. There are only 4 acceleration measurements involved in stiffness parameter identification, which largely degrades the accuracy of identification results with limited number of measurements. Despite these limitations, the proposed strategy provides reasonably satisfactory results except storeys 1-3, compared with those from static and dynamic test.

Based on the results from the numerical and experimental studies, the proposed strategy is able to accurately identify structural parameters without force measurements.

# Chapter 4. Substructural Identification with Unknown Input

In Chapter 2, measurements of excitation forces if applied within substructures are required for substructural identification. In practice, it is not easy to acquire accurate measurement data of excitation forces and in some cases, the forces such as seismic loads and wind loads are difficult or even impossible to measure. The absence of excitation measurements poses a huge challenge in the application of many proposed substructural identification methods. To address this issue, an iterative strategy, in conjunction with Tikhonov regularization method introduced in Section 3.2 for force identification and SSRM introduced in Section 2.3 for parameter identification, is developed herein for substructural identification without the requirement of force measurements.

In this chapter, angular accelerations at the interface of substructures are acquired by measurements of strains and translational accelerations with the recovery method in Chapter 2. The accuracy of the recovered angular accelerations is affected by not only the noise but also the differentiation error. Differentiation error in the integrated displacement and velocity from acceleration will be amplified. Therefore, it is more appropriate to develop a discrete time state space form for substructures with the concept of ‘quasi-static displacement’ instead of integration techniques. After the substructure is formulated in discrete time state space form, the procedure of

implementing the strategy for substructural identification is presented. Then numerical studies are conducted for identification on beam and plate substructures, followed by experimental work on substructural identification on a 10-storey frame.

## 4.1 Discrete time state space form for substructure with concept of 'quasi-static displacement'

Based on 'quasi-static displacement', the equation of motion of a multi-DOF damped substructural system under external forces with neglected damping force is expressed as

$$[M_{rr}]\{\ddot{u}_r^*(t)\}+[C_{rr}]\{\dot{u}_r^*(t)\}+[K_{rr}]\{u^*{}_r(t)\}=\{P_r(t)\}-\left([M_{rj}]+[M_{rr}][r]\right)\{\ddot{u}_j(t)\} \tag{4.1}$$

Section 2.1 provides the details about the derivation of Eq. (4.1). $[M_{rr}]$, $[C_{rr}]$ and $[K_{rr}]$ are the mass, damping and stiffness matrices for the substructure. Subscripts $r$ and $j$ represent internal and interfacial DOFs of substructures, respectively. $\{u^*{}_r(t)\}$, $\{\dot{u}_r^*(t)\}$ and $\{\ddot{u}_r^*(t)\}$ represent the relative dynamic displacement, velocity and acceleration of the substructure, respectively. Newmark method in Eq. (3.2) is employed to compute the substructural relative dynamic responses. Then the discrete state space form of Eq. (4.1) is

$$\{U_r^*\}_{k+1}=[A_{rr}]\{P_r\}_{k+1}+[B_{rr}]\{U_r^*\}_k+[C_{rr}]\{\ddot{u}_j\}_{k+1} \tag{4.2}$$

Herein, subscript '$rr$' distinguishes the matrix for substructure from that for global structure. $\{U_r^*\}$ represents $\{\{u^*{}_r\}\ \{\dot{u}_r^*\}\ \{\ddot{u}_r^*\}\}^T$, the relative dynamic displacement,

velocity and acceleration at internal DOFs. $\{\ddot{u}_j\}$ is the acceleration responses at interface DOFs. The matrices $[A_{rr}]$, $[B_{rr}]$ and $[C_{rr}]$ for the substructure are derived as

$$[A_{rr}] = \left[\Delta t^2\alpha[I] \quad \Delta t\delta[I] \quad [I]\right]^T \left[M_{rr}^*\right]^{-1} \tag{4.3}$$

$$[B_{rr}] = \begin{bmatrix} [I] & \Delta t[I] & \frac{\Delta t^2}{2}(1-2\alpha)[I] \\ 0 & [I] & \Delta t(1-\delta)[I] \\ 0 & 0 & 0 \end{bmatrix} - [A_{rr}]\left[[K_{rr}] \quad [C_{rr}]+\Delta t[K_{rr}] \quad \Delta t(1-\delta)[C_{rr}]+\frac{\Delta t^2}{2}(1-2\alpha)[K_{rr}]\right] \tag{4.4}$$

$$[C_{rr}] = -[A_{rr}]\left(\left[M_{rj}\right]+[M_{rr}][r]\right) \tag{4.5}$$

In Eqs. (4.3) - (4.5), $\left[M_{rr}^*\right] = [M_{rr}] + \Delta t\delta[C_{rr}] + \Delta t^2\alpha[K_{rr}]$ and $[r] = -[K_{rr}]^{-1}\left[K_{rj}\right]$. If $[R_1]$ is defined as the mapping matrix relating the limited acceleration measurements to dynamic responses of the substructure, the relative dynamic acceleration measurements $\{y^*\}$ can be expressed as

$$\{y^*\}_k = [R_1]\{U_r^*\}_k \tag{4.6}$$

Substitute Eq. (4.6) into Eq. (4.2) for every time step, $\{y^*\}$ can be written in terms of excitations located within the substructure and acceleration responses at interface as follows

$$\begin{Bmatrix} \{y^*\}_1 \\ \{y^*\}_2 \\ \vdots \\ \{y^*\}_k \\ \vdots \\ \{y^*\}_n \end{Bmatrix} = \begin{bmatrix} [R_1][A_1^*] & 0 & \cdots & 0 & 0 & 0 \\ [R_1][B_{rr}][A_1^*] & [R_1][A_{rr}] & \cdots & 0 & 0 & 0 \\ \vdots & \vdots & \vdots & \vdots & \vdots & \vdots \\ [R_1][B_{rr}]^{k-1}[A_1^*] & [R_1][B_{rr}]^{k-2}[A_{rr}] & \cdots & [R_1][A_{rr}] & 0 & 0 \\ \vdots & \vdots & \vdots & \vdots & \vdots & \vdots \\ [R_1][B_{rr}]^{n-1}[A_1^*] & [R_1][B_{rr}]^{n-2}[A_{rr}] & \cdots & [R_1][B_{rr}]^{n-k}[A_{rr}] & \cdots & [R_1][A_{rr}] \end{bmatrix} \begin{Bmatrix} \{P\}_1 \\ \{P\}_2 \\ \vdots \\ \{P\}_k \\ \vdots \\ \{P\}_n \end{Bmatrix}$$

$$+ \begin{bmatrix} [R_1][C_1^*] & 0 & \cdots & 0 & 0 & 0 \\ [R_1][B_{rr}][C_1^*] & [R_1][C_{rr}] & \cdots & 0 & 0 & 0 \\ \vdots & \vdots & \vdots & \vdots & \vdots & \vdots \\ [R_1][B_{rr}]^{k-1}[C_1^*] & [R_1][B_{rr}]^{k-2}[C_{rr}] & \cdots & [R_1][C_{rr}] & 0 & 0 \\ \vdots & \vdots & \vdots & \vdots & \vdots & \vdots \\ [R_1][B_{rr}]^{n-1}[C_1^*] & [R_1][B_{rr}]^{n-2}[C_{rr}] & \cdots & [R_1][B_{rr}]^{n-k}[C_{rr}] & \cdots & [R_1][C_{rr}] \end{bmatrix} \begin{Bmatrix} \{\ddot{u}_j\}_1 \\ \{\ddot{u}_j\}_2 \\ \vdots \\ \{\ddot{u}_j\}_k \\ \vdots \\ \{\ddot{u}_j\}_n \end{Bmatrix} \tag{4.7}$$

where the matrices $[A_1^*] = \begin{bmatrix} 0 & 0 & [M_{rr}]^{-1} \end{bmatrix}^T$ and $[C_1^*] = -[A_1^*]\left([M_{rj}] + [M_{rr}][r]\right)$ are derived based on assumed initial condition of zero displacement and velocity. It is noted that the substructural response at internal DOFs consists of two components, the quasi-static response and the relative dynamic response. In this study, only the accelerations are involved in measurements $\{y\}$ due to its ease of measuring over displacement and velocity. The quasi-static acceleration at internal DOFs is derived as Eq. (2.8) in Chapter 2

$$\{\ddot{u}_r^s\}_k = [r]\{\ddot{u}_j\}_k \tag{4.8}$$

If $[R_2]$ represents the mapping matrix relating the measurements to the substructural acceleration responses, the quasi-static acceleration measurements $\{y^s\}$ are written as

$$\{y^s\}_k = [R_2]\{\ddot{u}_r^s(t)\}_k = [R_2][r]\{\ddot{u}_j(t)\}_k \tag{4.9}$$

After summing the relative dynamic acceleration measurements $\{y^*\}$ and quasi-static acceleration measurements $\{y^s\}$, the measurements $\{y\}$ can be written as

$$\begin{Bmatrix} \{y\}_1 \\ \{y\}_2 \\ \vdots \\ \{y\}_k \\ \vdots \\ \{y\}_n \end{Bmatrix} = \begin{bmatrix} [R_1][A_1^*] & 0 & \cdots & 0 & 0 & 0 \\ [R_1][B_{rr}][A_1^*] & [R_1][A_{rr}] & \cdots & 0 & 0 & 0 \\ \vdots & \vdots & \vdots & \vdots & \vdots & \vdots \\ [R_1][B_{rr}]^{k-1}[A_1^*] & [R_1][B_{rr}]^{k-2}[A_{rr}] & \cdots & [R_1][A_{rr}] & 0 & 0 \\ \vdots & \vdots & \vdots & \vdots & \vdots & \vdots \\ [R_1][B_{rr}]^{n-1}[A_1^*] & [R_1][B_{rr}]^{n-2}[A_{rr}] & \cdots & [R_1][B_{rr}]^{n-k}[A_{rr}] & \cdots & [R_1][A_{rr}] \end{bmatrix} \begin{Bmatrix} \{P\}_1 \\ \{P\}_2 \\ \vdots \\ \{P\}_k \\ \vdots \\ \{P\}_n \end{Bmatrix}$$

$$+ \begin{bmatrix} [R_1][C_1^*]+[R_2][r] & 0 & \cdots & 0 & 0 & 0 \\ [R_1][B_{rr}][C_1^*] & [R_1][C_{rr}]+[R_2][r] & \cdots & 0 & 0 & 0 \\ \vdots & \vdots & \vdots & \vdots & \vdots & \vdots \\ [R_1][B_{rr}]^{k-1}[C_1^*] & [R_1][B_{rr}]^{k-2}[C_{rr}] & \cdots & [R_1][C_{rr}]+[R_2][r] & 0 & 0 \\ \vdots & \vdots & \vdots & \vdots & \vdots & \vdots \\ [R_1][B_{rr}]^{n-1}[C_1^*] & [R_1][B_{rr}]^{n-2}[C_{rr}] & \cdots & [R_1][B_{rr}]^{n-k}[C_{rr}] & \cdots & [R_1][C_{rr}]+[R_2][r] \end{bmatrix} \begin{Bmatrix} \{\ddot{u}_j\}_1 \\ \{\ddot{u}_j\}_2 \\ \vdots \\ \{\ddot{u}_j\}_k \\ \vdots \\ \{\ddot{u}_j\}_n \end{Bmatrix} \tag{4.10}$$

or $\{y\} = [H_1]\{P\} + [H_2]\{\ddot{u}_j\}$ in short.

With complete acceleration measurements at the interface, Eq. (4.10) can be rewritten as

$$\{y\} - [H_2]\{\ddot{u}_j\} = [H_1]\{P\} \tag{4.11}$$

By employment of $\{\bar{y}\}$ representing $\{y\} - [H_2]\{\ddot{u}_j\}$, Eq. (4.11) becomes

$$\{\bar{y}\} = [H_1]\{P\} \tag{4.12}$$

## 4.2 Iterative substructural identification strategy

To apply the proposed strategy for substructural identification, as a start, the complete acceleration responses at the interface are required, including the directly

measured translational accelerations and the recovered angular accelerations by using strain and translational acceleration measurements with the recovery method in Chapter 2. All the available acceleration measurements are grouped into two sets. Set 1 and set 2 may share some but not all of the measurements. The functions of these measurements sets are shown in Fig. 4.1.

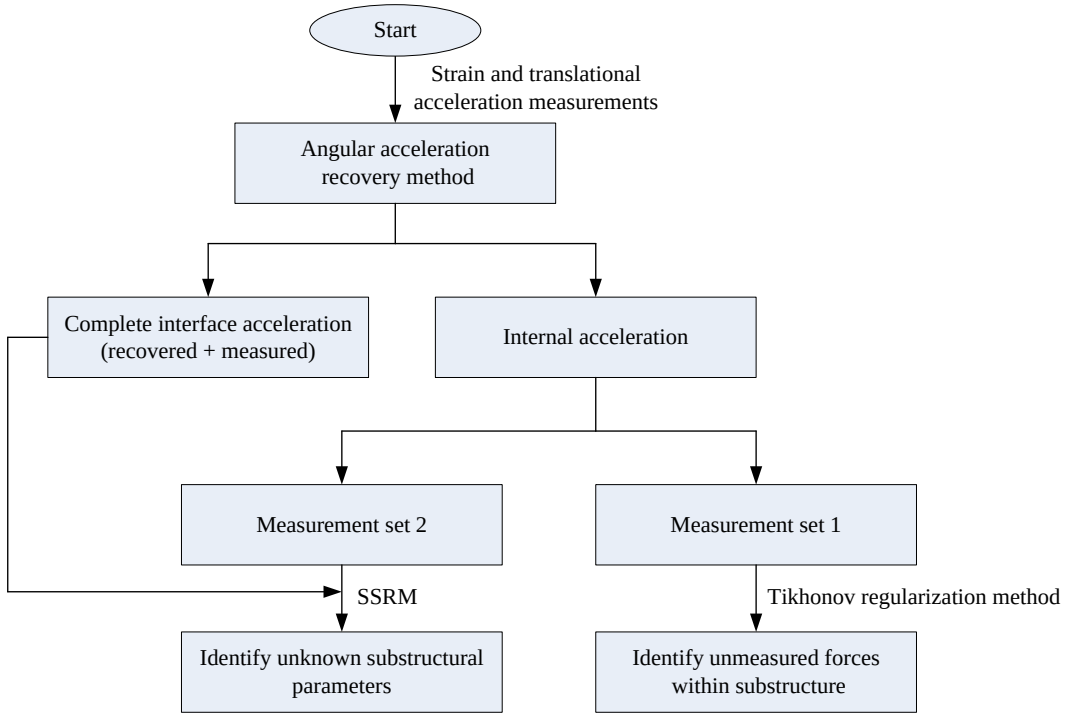


Figure 4.1 Functions of different measurement sets

As shown in Fig. 4.1, with known excitation force locations, measurement set 1 is used for force identification and set 2 is employed for substructural identification. The number of measurement set 1 should be equal to or greater than the number of the unknown forces applied within substructures. From Eq. (4.1), the responses of substructural systems are determined by two types of forces, namely the interface forces and the applied forces within substructures. The requirement of interface forces is fulfilled by acquiring complete interface measurements shown in Fig. 4.1. Finally, the proposed iterative strategy in Fig. 3.1 is implemented for substructural

identification without measurements of excitation forces. The procedure to implement the proposed strategy for substructural identification is as follows.

Step 1: Start with an initial guess of the substructural parameters, which are generated randomly from their search space.

Step 2: Compute $[H_1]$ and $[H_2]$ in Eq. (4.10) with the values of substructural parameters, according to the locations of the measurements in set 1.

Step 3: Compute $\{\bar{y}\}$ in Eq. (4.12) with available complete interface acceleration responses, including the directly measured translational accelerations as well as the recovered angular accelerations. Then the excitation forces $\{P\}$ are identified with Tikhonov regularization method by solving Eq. (4.12).

Step 4: Identify substructural parameters with SSRM based on measurement set 2 and the identified excitation forces from step 3.

Step 5: Update substructural parameters with the identification results from step 4, then go to step 2.

Step 6: Repeat the identification procedure from step 2 to step 6 until the convergence criterion in Eq. (3.9) is satisfied or the predefined maximum iteration number is reached.

## 4.3 Numerical examples

To examine the performance of the proposed strategy in the context of substructural identification, two numerical examples are studied: substructural damage detection on a simply supported beam shown in Fig. 2.4 and substructural identification on a cantilever plate shown in Fig. 2.10, both without the measurements of excitations. The same GA parameters of substructural identification of SS3 in Table 2.1 and SS2 in Table 2.4 are employed in these two examples.

In both numerical examples, 20 iterations of identification are carried out. The tolerance is set as 0.02 in the convergence criterion. The signals from the installed strain gauges or strain rosettes and accelerometers are recorded for 0.4 s with a sampling rate of 5,000. Noise effects are also investigated by considering polluted measurements with 0%, 5% and 10% noise.

### 4.3.1 Substructural damage identification on a simply supported beam

The same substructure SS3 in Fig. 2.5 located in the simply supported beam is considered in this numerical simulation. Four strain gauges are installed in element 5 and 11 at the interface and eight accelerometers are set up at nodes 5-12 in SS3, shown in Fig. 4.2. The unmeasured excitation force is applied at the $8^{th}$ node within SS3. Seven flexural rigidities for elements 5-11 in SS3 and two Rayleigh damping coefficients result in nine unknown substructural parameters to be identified. With the measured strains in elements 5 and 11 as well as translational accelerations at nodes 5, 6, 11, and 12, the angular accelerations at these four nodes are computed with the recovery method in Chapter 2. The translational acceleration measurements

at nodes 6, 8, 10 and 11 are denoted as measurements set 1. Measurements set 2 consists of the translational acceleration measurements at nodes 7 and 9 as well as the recovered angular accelerations at nodes 6 and 11.

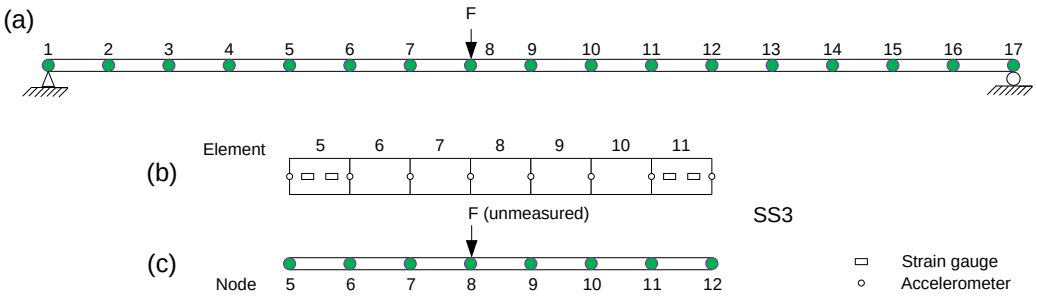


Figure 4.2 (a) The simply supported beam, (b) SS3 and the sensor placement and (c) Numerical model of SS3

The proposed strategy is implemented to identify SS3 in undamaged state and damaged state separately. The identification results of undamaged and damaged states are used to evaluate the damage extent in SS3 with Eq. (2.23). The damage identification results of SS3 are plotted in Fig. 4.3, where 0%, 5% and 10% noise contaminated measurements are considered. The mean and maximum absolute identification errors for undamaged and damaged SS3 are listed in Table 4.1.

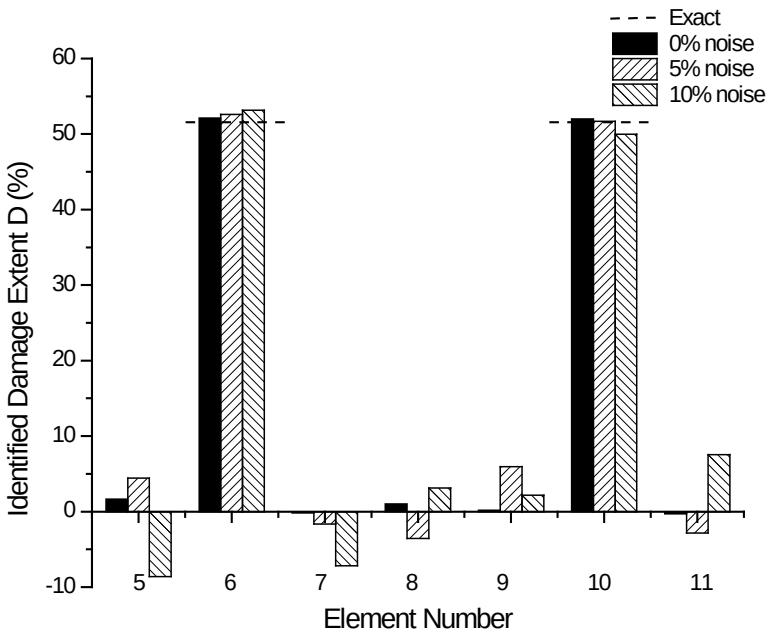


Figure 4.3 Identified damage extent of SS3

Table 4.1 Absolute identification errors of undamaged and damaged SS3 after 20 iterations

| Beam state | Noise level | Mean error (%) | Max error (%) |
|---|---|---|---|
| Undamaged | 0% | 0.65 | 1.38 |
| | 5% | 3.81 | 7.01 |
| | 10% | 7.52 | 11.56 |
| Damaged | 0% | 0.86 | 1.51 |
| | 5% | 3.55 | 8.52 |
| | 10% | 6.08 | 12.63 |

The identification results in Fig. 4.3 show that the locations and severities of damages in element 6 and 10 of SS3 are identified close to the exact values even for 10% noise case. Table 4.1 further shows the good performance of the proposed strategy with maximum error less than 13%. The identified stiffness for each element in undamaged SS3 with respect to the iteration number based on 5% noise contaminated measurements is presented in Fig. 4.4.

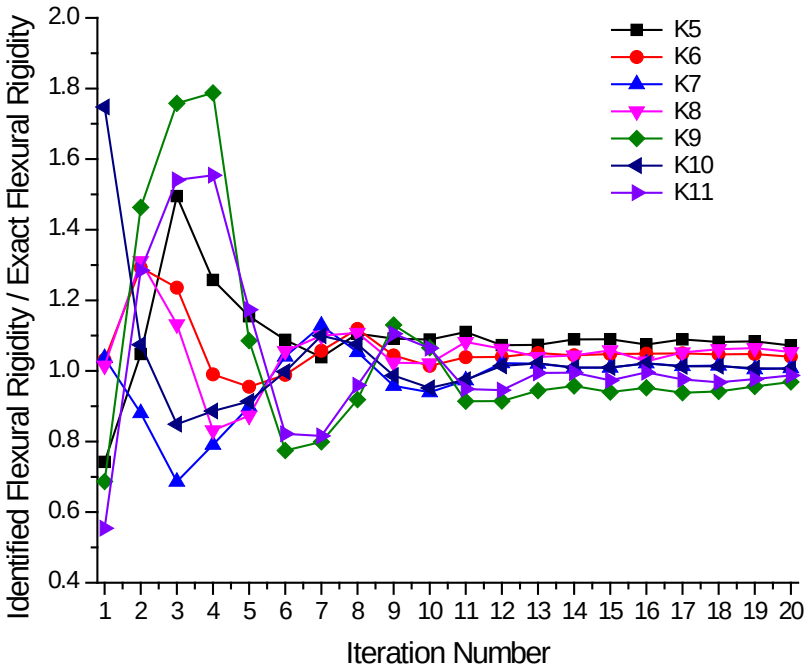


Figure 4.4 Identification results of undamaged SS3, 5% noise

Figure 4.4 indicates that the identified flexural rigidities converge rapidly to their exact values, demonstrating that the proposed strategy is effective in substructural identification without excitation force measurements. As an example of illustration, the identified flexural rigidity in element 8 with corresponding search limits in each iteration are plotted in Fig. 4.5.

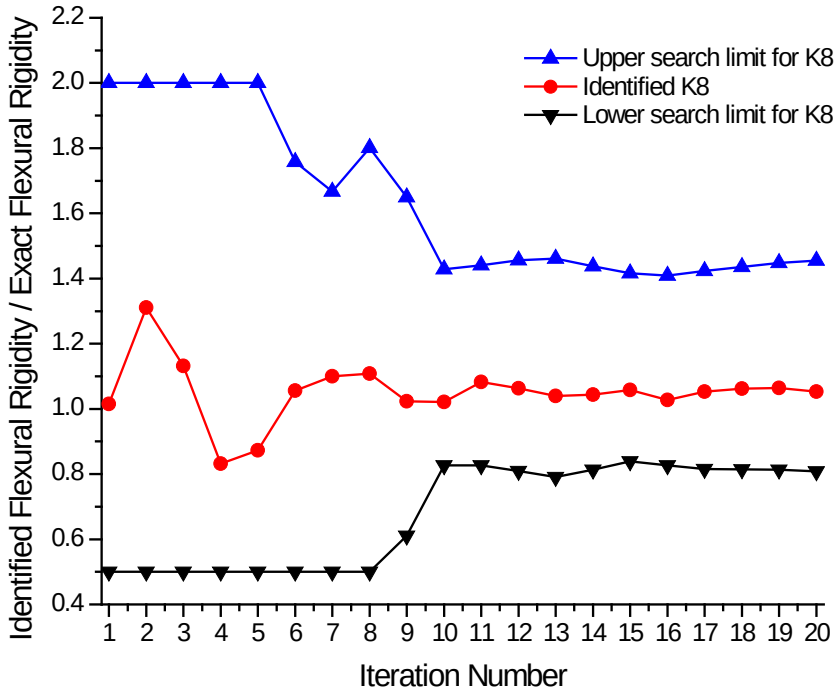


Figure 4.5 Identified flexural rigidity and its search space of element 8 in each iteration, 5% noise

In Fig. 4.5, a fairly broad search range of [0.5, 2] to its exact value is defined for each parameter in the first 5 iterations. For each parameter, from the 6$^{th}$ iteration, the search space is updated based on the identified weighted average and standard deviation of the previous 5 iterations, which enhances the computational convergence and improves the identification accuracy by devoting more computational time on evaluation of the candidates near the possible optimal solution. To prevent the searching from converging to local optima, especially for parameters insensitive to the fitness function, a minimum search space [0.9, 1.1] of the currently averaged identified values of each parameter is predefined for sufficient exploration in GA. The method in Fig. 3.2 is capable of effectively reducing the search space for the unknown parameters during converging to the global optimum.

### 4.3.2 Substructural identification on a cantilever plate

The same substructure SS2 in Fig. 2.11 located within the cantilever plate, meshed by 8 × 8 thin plate elements shown in Fig. 4.6 (a), is the second numerical example to validate the proposed identification strategy. In SS2, 32 strain gauge rosettes are installed in elements 6, 14, 22, 30, 38, 46, 54, and 64 to measure the three plane strains including two axial strains and one shear strain. The excitation force is applied at node 81, one corner at the free edge. The stiffness values of 24 elements in SS2 as well as 2 Rayleigh damping coefficients result in 26 unknown substructural parameters to be identified. Prior to substructural identification, with the proposed recovery method in Chapter 2, the angular accelerations at nodes 6, 7, 15, 16, 24, 25, 33, 34, 42, 43, 51, 52, 60, 61, 69, 70, 78 and 79 in SS2 are recovered by using the available strain and translational acceleration measurements. Measurement set 1 used for force identification and measurement set 2 used for parameter identification are listed in Table 4.2.

Table 4.2 Measurement set 1 and set 2

| | Measurement set 1 at nodes | Measurement set 2 at nodes |
|---|---|---|
| Translational acceleration $\ddot{w}$ | 7, 18, 25, 36, 43, 54, 61, 72, 79 | 8, 16, 26, 34, 44, 52, 62, 70, 80 |
| Angular acceleration $\ddot{\theta}_x$ | 16, 34, 52, 70 | 7, 25, 43, 61, 79 |
| Angular acceleration $\ddot{\theta}_y$ | 7, 25, 43, 61, 79 | 16, 34, 52, 70 |

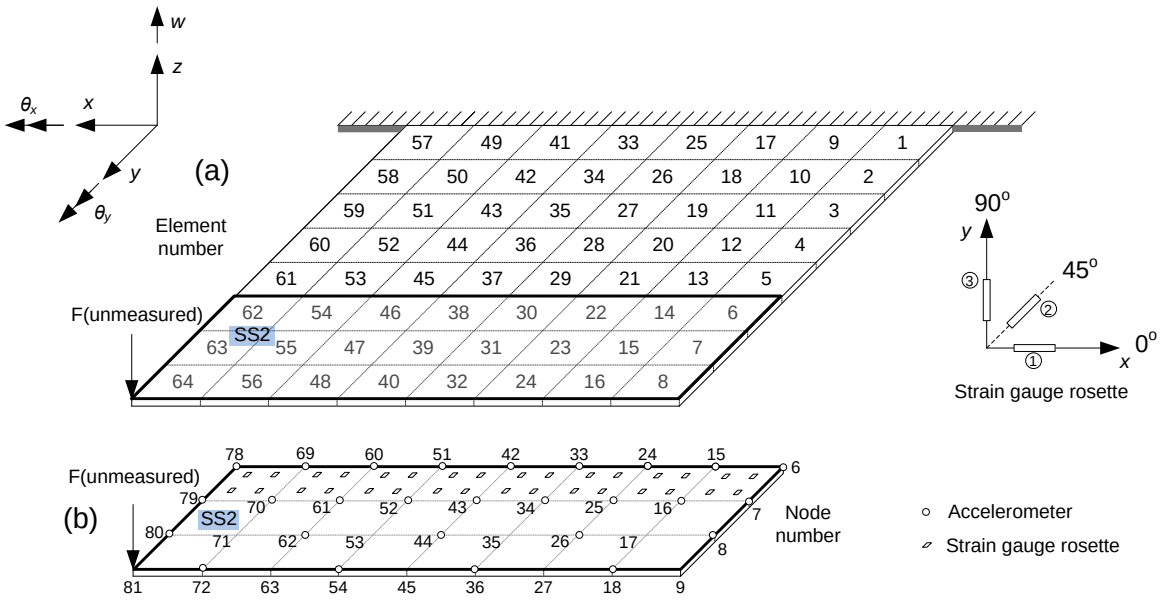


Figure 4.6 (a) The cantilever plate and (b) SS2 and the sensor placement

The identification results of SS2 after 20 iterations for the 0%, 5% and 10% noise cases are plotted in Fig. 4.7 and the identification errors are summarized in Table 4.3.

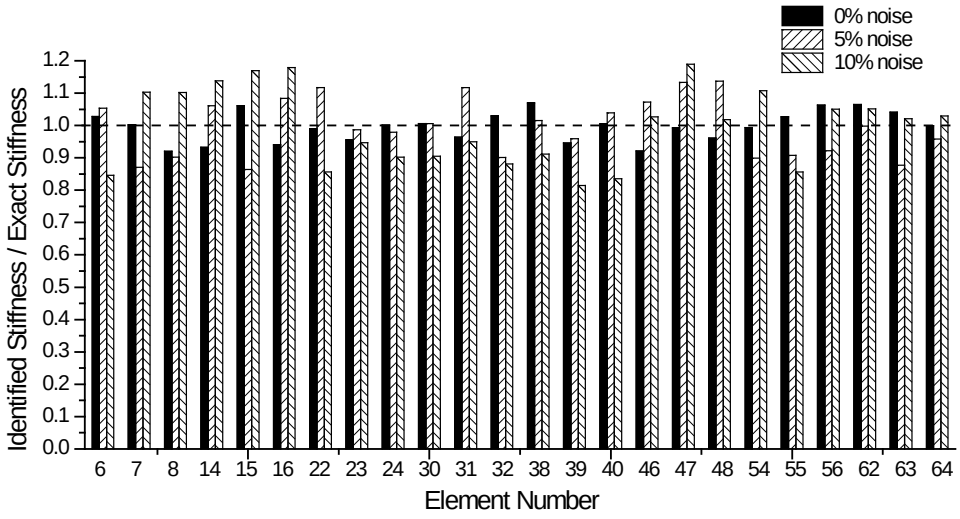


Figure 4.7 Identification results of SS2

Table 4.3 Absolute identification errors of SS2 with respect to noise level

| Noise level | SS2 in plate | |
|---|---|---|
| | Mean error (%) | Maximum error (%) |
| 0% | 3.68 | 8.00 |
| 5% | 7.54 | 13.69 |
| 10% | 10.34 | 18.95 |

From the identification results in Fig. 4.7, the 24 stiffness of SS2 are reasonably identified for 0%, 5% and 10% noise cases. In Table 4.3, in the noise-free case, certain deviations in the identification results are mainly caused by the differentiation error in the computed angular accelerations at the interface. As discussed in Section 2.6.1, the effects of differentiation error on the accuracy of identification results are largely alleviated without comparison of the initial part of simulated responses and measurements due to the difficulty to accurately compute derivatives based on insufficient measurement data at the initial part with Savitzky-Golay differentiation algorithm. Nevertheless, the accuracy in identified forces is inevitably affected by the initial part of inaccurately recovered signals since the forces are identified from the first step and measurement set 1 used for force identification involves some recovered angular accelerations. Since the unmeasured excitation forces and unknown substructural parameters are identified in an iterative way, the accuracy of identified parameters are inevitably affected by the imprecisely identified excitation forces due to the differentiation error. Although the accuracy of identified parameters suffers from the differentiation errors, acceptable identification results are still achieved from the practical point of view.

## 4.4 Experimental study

To validate the applicability of the proposed strategy to substructural identification without force measurements, parameter identification in one substructure denoted as SS1 in the 10-storey frame in Fig. 3.10 in Chapter 3, is carried out. The instrumentation of the experimental work is shown in Fig. 3.14 and Fig. 3.15. SS1 contains levels 5-10, shown in Fig. 4.8. Level 4 is the interface connecting the concerned SS1 to the remaining part of the frame. The excitation is applied at level 10 within SS1, as indicated in Fig. 4.8.

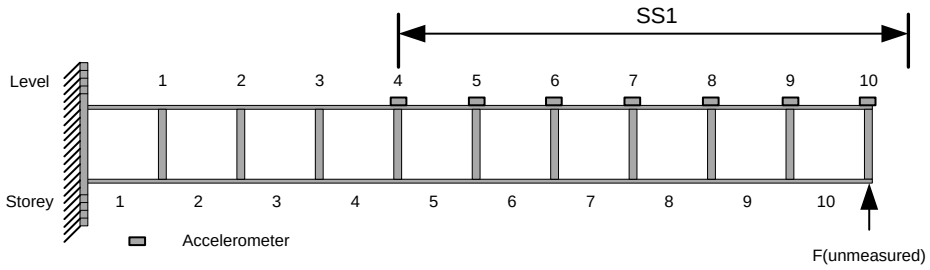


Figure 4.8 SS1 and the sensor placement

The accelerations at level 4 to level 10 are recorded for 2 seconds with a sampling rate of 2,000. Six stiffness values for the $5^{th}$ to $10^{th}$ storeys and 2 damping coefficients result in 8 unknown substructural parameters to be identified. The initially lower and upper search limits for the unknown stiffness in SS1 are set to be half and double of measured values based on the static test. The search limits for two damping coefficients ($a_o$ and $a_1$) are set as 0-4 and 0-0.0002, respectively. The same GA parameters for substructural identification in Table 3.1 but with 8 unknown parameters are selected to identify SS1. Measurement set 1 includes acceleration measurements at levels 6, 8 and 10. Acceleration signals at levels 5, 7, and 9 are

grouped as measurement set 2. 20 iterations are carried out to obtain converged identification results. The tolerance in the convergence criterion is set as 0.02. Substructural identification of SS1 is conducted with 3 different random forces, as shown in Fig. 3.16 in Chapter 3. First, substructural identification of SS1 is carried out with force measurements, donated as dynamic test, the results are presented in Fig. 4.9.

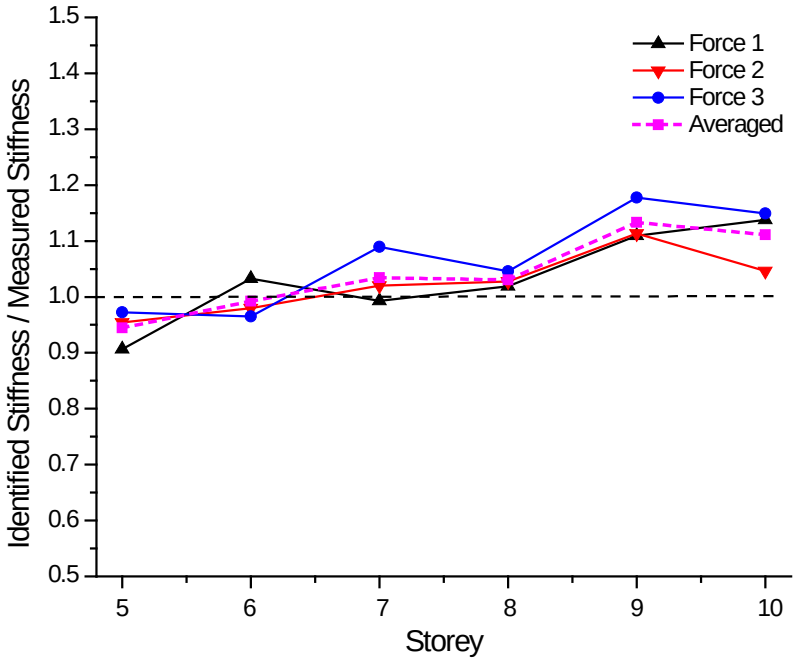


Figure 4.9 Identified stiffness of SS1 with force measurements

Table 4.4 Identification errors of SS1 with force measurements

| Storey | Stiffness (kN/m) (static test) | Stiffness (kN/m) (dynamic test ) | Error (%) |
|---|---|---|---|
| 5 | 267.68 | 252.81 | -5.56 |
| 6 | 396.09 | 393.10 | -0.75 |
| 7 | 378.09 | 391.00 | +3.41 |
| 8 | 263.91 | 271.99 | +3.06 |
| 9 | 252.09 | 285.76 | +13.36 |
| 10 | 362.55 | 402.82 | +11.11 |

From Fig. 4.9, the results based on 3 different random forces applied are in good agreement with one another. Compared with measured stiffness by static test, very good identification results are achieved with mean and maximum absolute errors of 6.21% and 13.36% shown in Table 4.4. Furthermore, with the proposed strategy, substructural identification of SS1 is carried out without measurement of force applied at level 10. Compared with measured stiffness from static test, the identification results these 3 different unknown forces are presented in Fig. 4.10. The corresponding identification errors based on the averaged results are listed in Table 4.5.

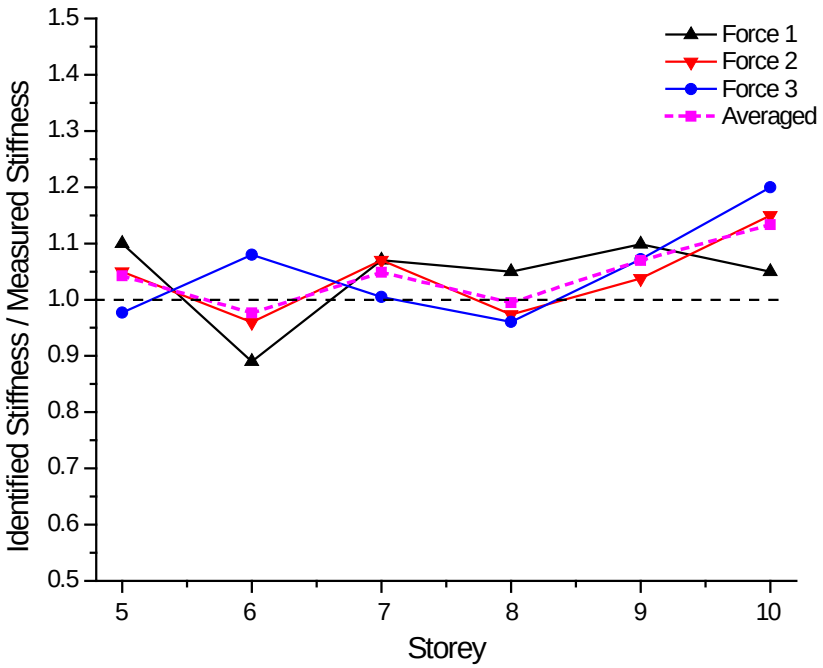


Figure 4.10 Identified stiffness of SS1 without force measurements

Table 4.5 Identification errors of SS1 without force measurements

| Storey | Stiffness (kN/m) (static test) | Stiffness (kN/m) (dynamic test) | Stiffness (kN/m) Identified | Error (%) Compared with static test | Error (%) Compared with dynamic test |
|---|---|---|---|---|---|
| 5 | 267.68 | 252.81 | 279.03 | +4.24 | +10.37 |
| 6 | 396.09 | 393.10 | 386.85 | -2.33 | -1.59 |
| 7 | 378.09 | 391.00 | 396.41 | +4.85 | +1.38 |
| 8 | 263.91 | 271.99 | 262.47 | -0.55 | -3.50 |
| 9 | 252.09 | 285.76 | 269.62 | +6.95 | -5.65 |
| 10 | 362.55 | 402.82 | 410.89 | +13.33 | +2.00 |

From Fig. 4.10 and Table 4.5, satisfactory identification results of SS1 without force measurements are achieved with mean and maximum absolute errors of 5.38% and 13.33% compared with those from the static test. The identified stiffness values of SS1 are in very good agreement with the results from the dynamic test with 4.08% mean error and 10.37% maximum error. The accuracy of identification results without force measurements in Fig. 4.10 is nothing short of the corresponding results in Fig. 4.9 with force measurements. For the case without force measurements, the unmeasured force is identified rather than measured, so that it is capable of avoiding the error in the force due to measurement noise that would pass through the simulation. All these experimental results show that the proposed strategy is applicable to substructural identification when the measurements of forces located within the substructure are difficult or even impossible to acquire.

## 4.5 Summary

In this chapter, an iterative strategy is developed for substructural identification to address the unavailability of force measurements within substructures. First, the state space form for substructures is formulated with the concept of ‘quasi-static displacement’. The angular accelerations at the interface of beam and plate

substructures are computed by means of measured strains and translational accelerations, using the recovery method in Chapter 2. In the strategy, Tikhonov regularization method is employed for force identification and SSRM is adopted for substructural parameter identification.

To test the effectiveness of the proposed strategy, two numerical examples are carried out, including damage detection in a beam substructure and stiffness identification in a plate substructure without measurements of force applied within these two substructures. The results show that the proposed strategy is able to accurately locate and quantify the damages in the beam substructure as well as identify the stiffness for the plate substructure even with 10% noise measurements. Finally, an experimental study is conducted for substructural identification on a 10-storey frame. The stiffness of the substructure is reasonably identified without excitation measurements in comparison with those from the static and dynamic tests.

# Chapter 5. Substructural Identification with Incomplete Interface Measurements

In the previous chapter, substructural parameters and unknown input excitation are identified iteratively with complete interface acceleration measurements, while the angular accelerations at interface are recovered via measurements of strains and translational accelerations. Substructural identification has advantages in terms of accuracy and efficiency, but the requirement of complete interface measurements brings considerable inconvenience, especially for angular accelerations at interface where special sensors are required.

To avoid complete interface measurements, some efforts have been endeavored on development of substructural identification methods. An approach of substructural identification in frequency domain was proposed without the need of interface measurements (Koh and Shankar, 2003). With sufficient response measurements in the substructure of concern, the unknown parameters are identified with GA by minimizing the difference between interface forces obtained using 2 different measurement sets. A Bayesian frequency domain approach (Yuen and Katafygiotis, 2006) was proposed for substructural identification without requiring any interface and excitation measurements. In their study, the interface effects on the substructure of concern were considered as additional unknown forces or support motion. In these two studies, a sufficient number of sensors are required to compute the

interface forces from two independent internal acceleration measurement sets, which is inapplicable for substructures with large number of interface DOFs. Interface forces on the substructure of concern were identified by use of damped least-square method with acceleration measurements in adjacent healthy substructures (Law et al., 2010). Subsequently, damage identification was carried out based on dynamic sensitivity analysis. The identification results on a 9-bay 3-dimensional truss structure show that the proposed method can accurately detect the location and extent of damage. However, their approach is only valid with assumption of knowing the health state of substructures around the substructure of concern.

A substructural identification method in time domain was proposed to simultaneously identify substructural parameters and input time history of the applied excitation (Sandesh and Shankar, 2009), which was validated by numerical examples of a 15-DOF shear building model, a planar truss of 55 members and a cantilever beam of 20 elements subjected to harmonic, random and impulse excitations. Although interface measurements are unnecessary, the required acceleration measurements on each interior DOF cannot be applied to substructures with a large number of internal DOFs. To overcome the need of complete internal and interface measurements, an innovative strategy, based on limited internal measurements, is proposed in this chapter for substructural identification with incomplete or even no interface measurements.

First, with an integration technique, the discrete state space form is developed for the substructure model, which facilitates Tikhonov regularization method to directly identify interface accelerations and unmeasured excitations with measurement data.

Then procedure to implement the identification strategy is presented. Two numerical examples of substructural identification and experimental works on a 10-storey frame and a small-scale jack-up in laboratory are presented to validate the identification strategy.

## 5.1 Discrete time state space form for substructure with integration technique

As mentioned in Section 2.1, the equation of motion for a substructure (without ignoring the damping forces) is

$$\begin{aligned}[M_{rr}]\{\ddot{u}_r(t)\}+[C_{rr}]\{\dot{u}_r(t)\}+[K_{rr}]\{u_r(t)\}\\ =\{P_r(t)\}-[M_{rj}]\{\ddot{u}_j(t)\}-[C_{rj}]\{\dot{u}_j(t)\}-[K_{rj}]\{u_j(t)\}\end{aligned} \tag{5.1}$$

where $[M_{rr}]$, $[C_{rr}]$ and $[K_{rr}]$ are mass, damping and stiffness matrices for the substructure. Subscripts $r$ and $j$ represent internal and interface DOFs of the substructure, respectively. From Eq. (5.1), the interface displacement, velocity and acceleration are necessary for substructural forward analysis. With trapezoidal rule, interface displacement and velocity can be obtained through integration of interface acceleration,

$$\begin{aligned}\{\dot{u}_j\}_{k+1}&=\{\dot{u}_j\}_k+\frac{\Delta t}{2}\left(\{\ddot{u}_j\}_k+\{\ddot{u}_j\}_{k+1}\right)\\ \{u_j\}_{k+1}&=\{u_j\}_k+\frac{\Delta t}{2}\left(\{\dot{u}_j\}_k+\{\dot{u}_j\}_{k+1}\right)\end{aligned} \tag{5.2}$$

where $\Delta t$ is time interval. Equation of motion for the substructure can be written in discrete state space form as

$$\{U_r\}_{k+1} = [A_{rr}]\{P_r\}_{k+1} + [B^*_{rr}]\{U_r\}_k + [C^*_{rr}]\{U_j\}_{k+1} \tag{5.3}$$

where $\{U_r\}_{k+1} = \{\{u_r\} \quad \{\dot{u}_r\} \quad \{\ddot{u}_r\}\}^T_{k+1}$ and $\{U_j\}_{k+1} = \{\{u_j\} \quad \{\dot{u}_j\} \quad \{\ddot{u}_j\}\}^T_{k+1}$ represent the displacement, velocity and acceleration for internal and interface DOFs at time step $k+1$, respectively. The matrices $[A_{rr}]$, $[B^*_{rr}]$ and $[C^*_{rr}]$ are

$$[A_{rr}] = [\Delta t^2 \alpha [I] \quad \Delta t \delta [I] \quad [I]]^T [M^*_{rr}]^{-1} \tag{5.4}$$

$$[B^*_{rr}] = \begin{bmatrix} [I] & \Delta t[I] & \frac{\Delta t^2}{2}(1-2\alpha)[I] \\ 0 & [I] & \Delta t(1-\delta)[I] \\ 0 & 0 & 0 \end{bmatrix} - [A_{rr}] \left[ [K_{rr}] \quad [C_{rr}] + \Delta t[K_{rr}] \quad \Delta t(1-\delta)[C_{rr}] + \frac{\Delta t^2}{2}(1-2\alpha)[K_{rr}] \right] \tag{5.5}$$

$$[C^*_{rr}] = -[A_{rr}][[K_{rj}] \quad [C_{rj}] \quad [M_{rj}]] \tag{5.6}$$

where $[M^*_{rr}] = [M_{rr}] + \Delta t \delta [C_{rr}] + \Delta t^2 \alpha [K_{rr}]$. In this study, zero initial conditions are assumed for the substructural displacement and velocity responses.

The mapping matrix $[R_1]$ is defined as the relation between measurements and substructural internal responses, and then measurements can be expressed in terms of interface responses and excitation forces as

$$\begin{Bmatrix} \{y\}_1 \\ \{y\}_2 \\ \vdots \\ \{y\}_k \\ \vdots \\ \{y\}_n \end{Bmatrix} = \begin{bmatrix} [R_1][A_1^*] & 0 & \cdots & 0 & 0 & 0 \\ [R_1][B_{rr}^*][A_1^*] & [R_1][A_{rr}] & \cdots & 0 & 0 & 0 \\ \vdots & \vdots & \vdots & \vdots & \vdots & \vdots \\ [R_1][B_{rr}^*]^{k-1}[A_1^*] & [R_1][B_{rr}^*]^{k-2}[A_{rr}] & \cdots & [R_1][A_{rr}] & 0 & 0 \\ \vdots & \vdots & \vdots & \vdots & \vdots & \vdots \\ [R_1][B_{rr}^*]^{n-1}[A_1^*] & [R_1][B_{rr}^*]^{n-2}[A_{rr}] & \cdots & [R_1][B_{rr}^*]^{n-k}[A_{rr}] & \cdots & [R_1][A_{rr}] \end{bmatrix} \begin{Bmatrix} \{P\}_1 \\ \{P\}_2 \\ \vdots \\ \{P\}_k \\ \vdots \\ \{P\}_n \end{Bmatrix}$$

$$+ \begin{bmatrix} [R_1][C_2^*] & 0 & \cdots & 0 & 0 & 0 \\ [R_1][B_{rr}^*][C_2^*] & [R_1][C_{rr}^*] & \cdots & 0 & 0 & 0 \\ \vdots & \vdots & \vdots & \vdots & \vdots & \vdots \\ [R_1][B_{rr}^*]^{k-1}[C_2^*] & [R_1][B_{rr}^*]^{k-2}[C_{rr}^*] & \cdots & [R_1][C_{rr}^*] & 0 & 0 \\ \vdots & \vdots & \vdots & \vdots & \vdots & \vdots \\ [R_1][B_{rr}^*]^{n-1}[C_2^*] & [R_1][B_{rr}^*]^{n-2}[C_{rr}^*] & \cdots & [R_1][B_{rr}^*]^{n-k}[C_{rr}^*] & \cdots & [R_1][C_{rr}^*] \end{bmatrix} \begin{Bmatrix} \{U_j\}_1 \\ \{U_j\}_2 \\ \vdots \\ \{U_j\}_k \\ \vdots \\ \{U_j\}_n \end{Bmatrix} \tag{5.7}$$

where the matrices $[A_1^*] = \begin{bmatrix} 0 & 0 & [M_{rr}]^{-1} \end{bmatrix}^T$ and $[C_2^*] = -[A_1^*]\begin{bmatrix} [K_{rj}] & [C_{rj}] & [M_{rj}] \end{bmatrix}$ are derived by assuming zero initial conditions for substructural displacement and velocity responses. Equation (5.7) can be expressed in short form as

$$\{y\} = [H_1]\{P\} + [H_2^*]\{U_j\} \tag{5.8}$$

Substituting Eq. (5.1) into Eq. (5.7)

$$\{y\} = [H_1]\{P\} + [H_3^*]\{\ddot{u}_j\} \tag{5.9}$$

where $[H_3^*] = [H_2^*][R^*]$ and $[R^*]$ represents the transformation matrix from acceleration to displacement, velocity and acceleration responses at interface DOFs. If some of interface accelerations are measured, $[H_3^*]$ in Eq. (5.9) is partitioned into two sub-matrices according to groups of measured and unmeasured interface accelerations.

$$\{y\} = [H_1]\{P\} + [H_3^*]_m \{\ddot{u}_j\}_m + [H_3^*]_u \{\ddot{u}_j\}_u \tag{5.10}$$

where subscripts $m$ and $u$ represent 'measured' and 'unmeasured', respectively. The unmeasured input excitations and interface accelerations are treated as unknowns, which are both identified with Tikhonov regularization method by

$$\{y\} - \left[H_3^*\right]_m \{\ddot{u}_j\}_m = \left[\left[H_1\right] \quad \left[H_3^*\right]_u\right] \begin{Bmatrix} \{P\} \\ \{\ddot{u}_j\}_u \end{Bmatrix} \tag{5.11}$$

If the excitation force is applied outside the substructure, then Eq. (5.11) can be simplified as

$$\{y\} - \left[H_3^*\right]_m \{\ddot{u}_j\}_m = \left[H_3^*\right]_u \{\ddot{u}_j\}_u \tag{5.12}$$

## 5.2 Identification strategy

In this chapter, the unknown forces and unmeasured interface accelerations are identified with Tikhonov regularization method based on the substructure model in discrete space form with integration technique. Although the substructure model with the concept of 'quasi-static displacement' has proved successful (Koh et al., 2003), the inaccuracy could result from computing relative acceleration by employing inversion of internal stiffness matrix and neglecting velocity-dependent component (damping forces) in the interface forces. To accurately estimate interface forces in terms of displacement, velocity and acceleration responses at interface DOFs, Thanh et al. (2010) proposed to directly integrate interface acceleration responses to acquire displacement and velocity. It is found that a small drift error will appear in the interface forces due to accumulated noise error upon numerical integration of contaminated acceleration measurements to obtain displacement and

velocity. Nevertheless, in a frequency domain analysis, this drift can be regarded as a low-frequency force component which has negligible effect in determining the substructural responses due to high natural frequencies of the substructure compared with the global structure (Thanh et al., 2010). The accuracy of identification results can be improved with this approach, demonstrated by numerical studies on a 20-DOF known-mass system and a 100-DOF unknown-mass system as well as experimental studies on a 10-storey frame. Therefore, in this chapter, the discrete time state space form is developed with integration technique at interface DOFs.

Prior to substructural identification, the measurements are grouped into two measurements sets, denoted as set 1 and set 2. The number of measurements in set 1 is equal to or larger than the combined number of unknown applied excitations and unmeasured interface responses. In this strategy, the unmeasured interface accelerations are treated in a similar way to the unknown input forces within substructure, which are identified with Tikhonov regularization method based on measurement set 1. It is assumed that the locations of applied excitations within substructure are known. The flowchart of the proposed strategy is presented in Fig. 5.1.

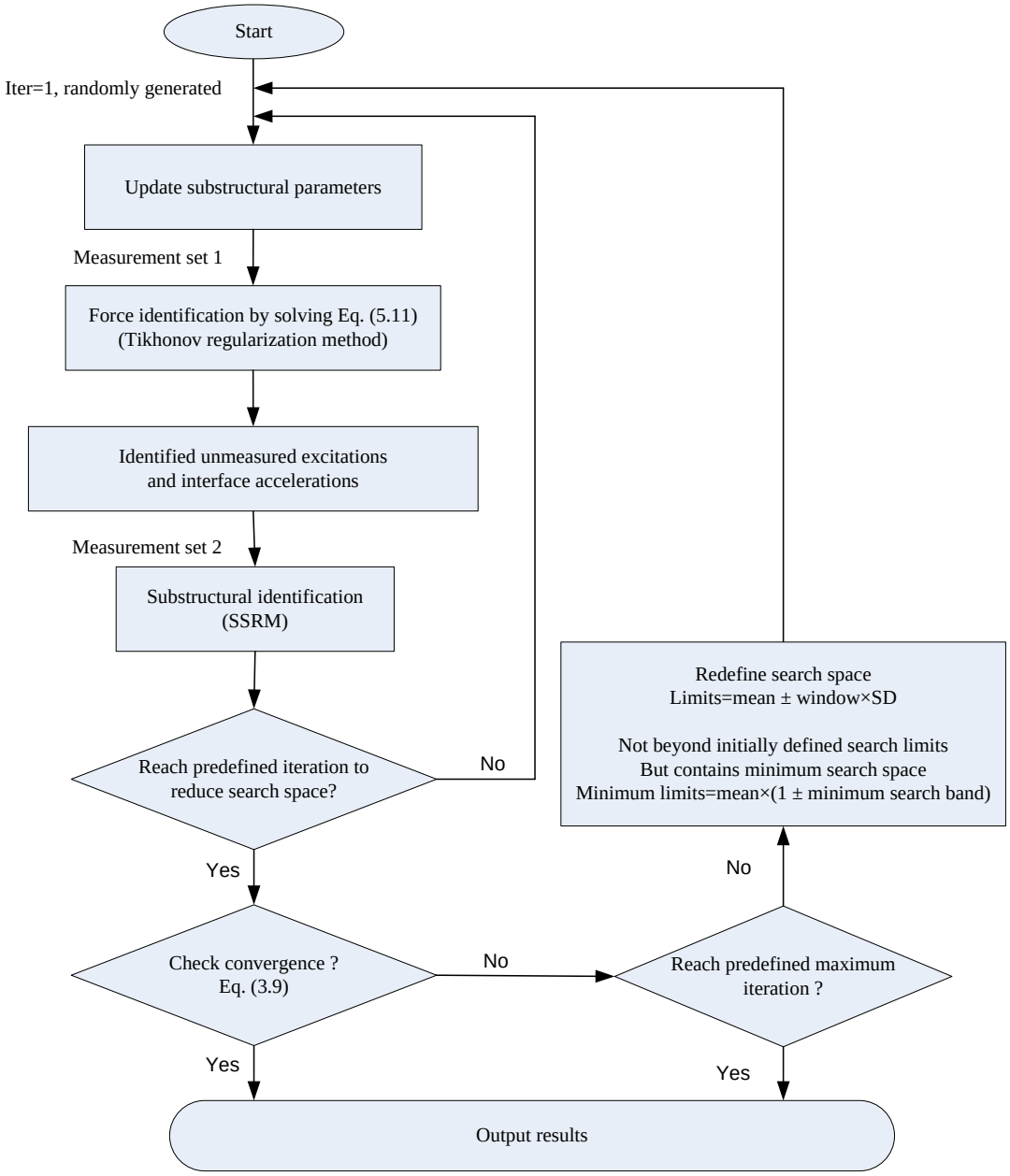


Figure 5.1 Flowchart of the proposed strategy for substructural identification with incomplete interface measurements

The numerical procedure for implementation of this strategy is as follows.

Step 1: Initialization of the unknown substructural parameters in a random way within their search space.

Step 2: Computation of $[H_1]$ and $[H_3^*]$ in Eq. (5.9) from the FE model of the substructure according to measurement set 1.

Step 3: Partitioning of $[H_3^*]$ into $[H_3^*]_m$ and $[H_3^*]_u$, according to the corresponding measured and unmeasured interface accelerations.

Step 4: Identification of unknown input forces and unmeasured interface accelerations by solving Eq. (5.10) with Tikhonov regularization method.

Step 5: Identification of unknown substructural parameters with SSRM, based on the identified excitation forces as well as interface accelerations from step 4.

Step 6: Replacement of substructural parameters with results from step 5. Then go to step 2.

Step 7: Repetition of step 2 to step 6 until the convergence criterion in Eq. (3.9) is satisfied or the predefined maximum iteration number is reached.

## 5.3 Numerical examples

Parameter identification is carried out for substructures in Fig. 5.2 and Fig. 5.6 to examine the performance of the proposed strategy with incomplete interface measurements as well as without measurements of excitations. In these two numerical examples, the unknown substructural parameters include the flexural rigidity or Young's modulus and the two damping coefficients. A broad search space for these substructural parameters is initially defined as [0.5, 2] of their exact values. The same GA parameters as in Table 2.1 are adopted herein. It is assumed that

location of the applied unknown excitation and mass matrix are known. 20 iterations of identification are implemented and the tolerance is set as 0.02. The noise effect is also investigated by introducing 0%, 5% and 10% noise into the measurements.

### 5.3.1 Damage identification on a simply supported beam

The same simply supported beam as in Fig. 2.5 is considered in this numerical example. An unknown excitation force is applied at node 8, shown in Fig 5.2. SS3 indicated in Fig. 5.2, is selected as the substructure of concern, containing elements 5-11 and resulting in 9 unknown substructural parameters inclusive of the flexural rigidities for 7 elements and two damping coefficients. There are 8 accelerometers installed on SS3 and each measured signal is of 0.4 s duration with sampling rate of 5,000.

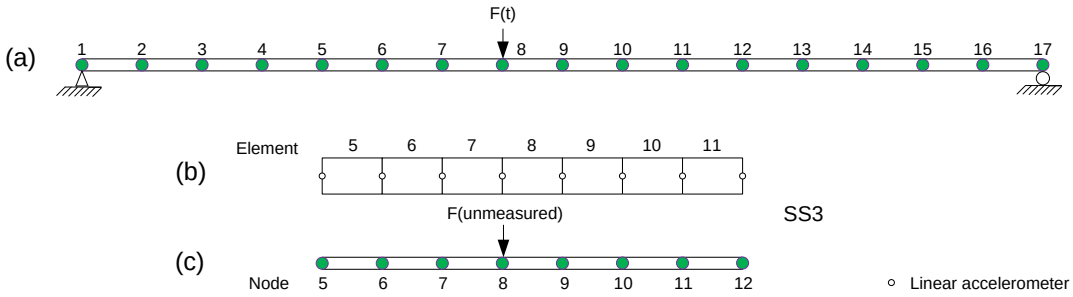


Figure 5.2 (a) Numerical model of the simply supported beam, (b) SS3 and the sensor placement and (c) Numerical model of SS3

From Fig. 5.2, complete interface measurements are not available because angular accelerations are not measured at nodes 5 and 12, located at the interface of SS3. To identify the unknown angular accelerations at interface nodes as well as the unmeasured excitation at node 8, Tikhonov regularization method is employed with measurement set 1 including the translational acceleration responses at nodes 6, 8, 10 and 11. SSRM is employed to identify the 9 unknown substructural parameters

with measurement set 2 including the linear acceleration data at nodes 7, 9 and 10. The damage identification results of SS3 for 0%, 5% and 10% noise cases are plotted in Fig. 5.3, and the substructural identification errors of undamaged and damaged SS3 are summarized in Table 5.1.

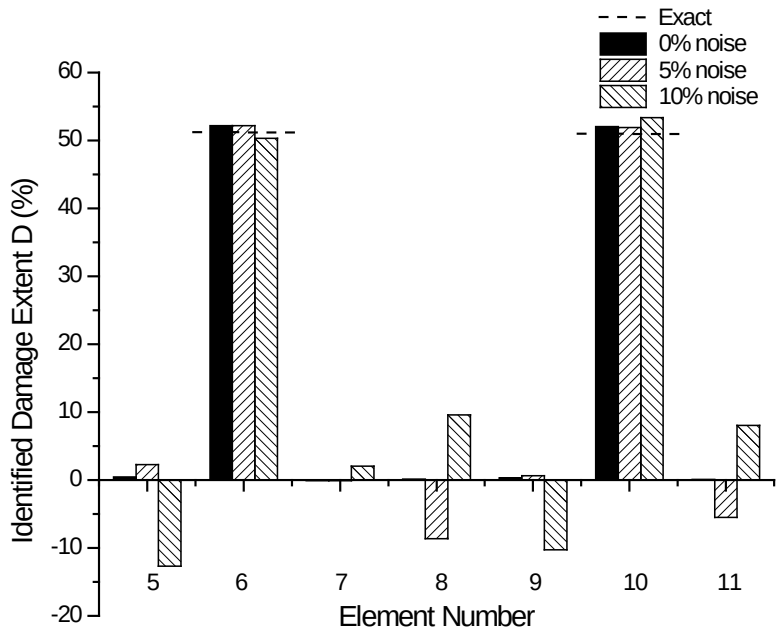


Figure 5.3 Identified damage extent of SS3

Table 5.1 Absolute identification errors of undamaged and damaged SS3

| Beam state | Noise level | Mean error (%) | Max error (%) |
|---|---|---|---|
| Undamaged | 0% | 0.32 | 0.65 |
| | 5% | 3.80 | 7.01 |
| | 10% | 8.65 | 14.49 |
| Damaged | 0% | 0.45 | 0.81 |
| | 5% | 2.68 | 6.34 |
| | 10% | 7.95 | 15.04 |

As seen in Fig. 5.3, for 0%, 5% and 10% noise cases, damage in element 6 is identified as 52.19%, 52.16% and 50.31% reduction in the flexural rigidity, very close to the exact value 52%. Similarly, for the damaged element 10, with 0%, 5% and 10% noise contaminated measurements, the detected 52.03%, 51.90% and 53.34% reduction of the flexural rigidity are also in very good agreement with the exact solution 52%. In addition, the maximum false identified damages are less than 13% for the 10% noise case. As shown in Table.5.1, satisfactory identification results are achieved for both undamaged and damaged SS3 even with noisy measurements. The results in Fig. 5.3 and Table 5.1 demonstrate the excellent performance of the strategy in terms of accuracy. The identification results of undamaged SS3 for each iteration with 10% noise polluted measurements are presented in Fig. 5.4. The identified flexural rigidity in element 8 with corresponding search limits in every iteration is plotted in Fig. 5.5.

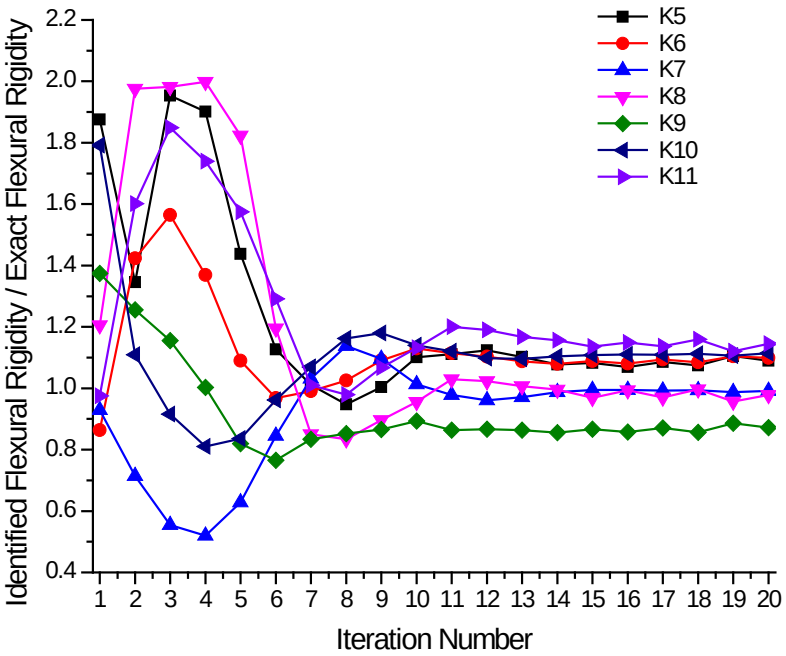


Figure 5.4 Identification results of undamaged SS3, 10% noise

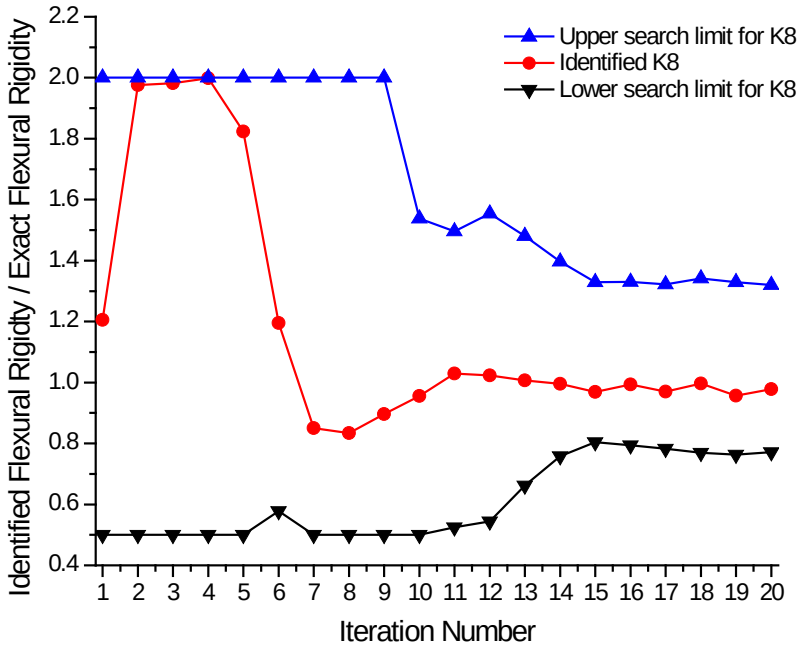


Figure 5.5 Identified flexural rigidity and its search space of element 8 in each iteration, 10% noise

From Fig. 5.4 and Fig. 5.5, the proposed strategy yields stable and converged solution after 20 iterations with 10% noise polluted measurements, which demonstrates excellent performance of the proposed strategy in achieving the converged results.

### 5.3.2 Substructural identification on a cantilever plate

The same substructure SS2 as in Fig. 4.6 is considered as the second numerical study to investigate the effectiveness of the proposed identification strategy. The substructure model and sensor placement is shown in Fig. 5.6.

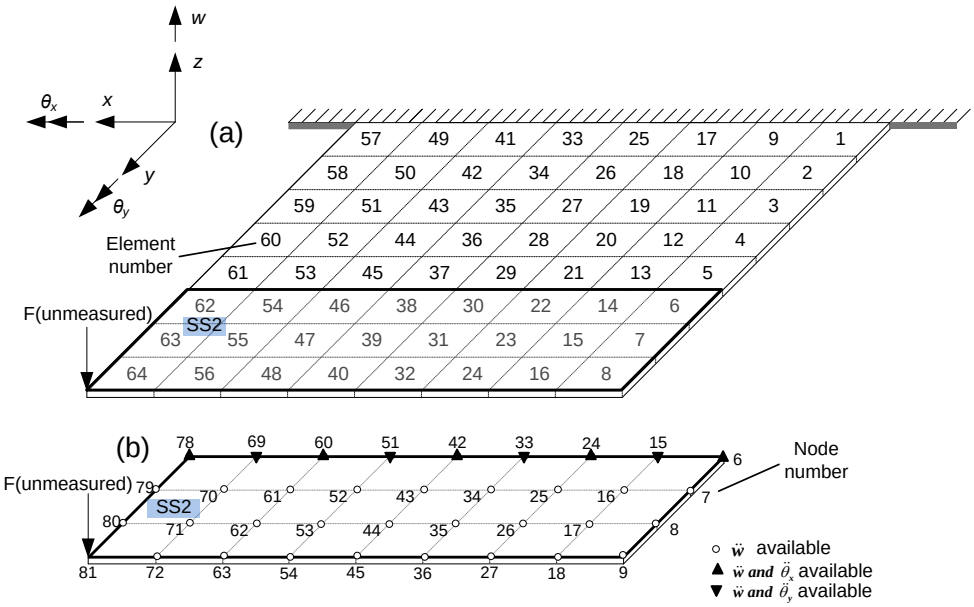


Figure 5.6 (a) The cantilever plate and (b) SS2 and the sensor placement

As shown in Fig. 5.6 (b), there are 24 elements in SS2 and 26 unknowns need to be identified including the unknown Young's modulus of each element and the two Rayleigh damping coefficients. Nine nodes at interface result in 27 interface DOFs in consideration of two translations and one rotation at each node. If there are a large number of unmeasured accelerations at the interface, a considerable number of internal acceleration measurements are necessary for identifying the unmeasured interface responses and excitation forces since the required number of internal measurements should be equal to or larger than the number of absent measurements, namely the unmeasured interface accelerations and excitation forces. In this study, for the purpose of validating the effectiveness of the proposed strategy with incomplete interface measurements, it is assumed that some but not all angular acceleration measurements are available at the interface of SS2, illustrated in Table 5.2.

Table 5.2 Measurements of SS2

| | Available interface measurements at nodes | Available internal measurements at nodes |
|---|---|---|
| Translational acceleration $\ddot{w}$ | 6, 15, 24, 33, 42, 51, 60, 69, 78 | 7, 8, 9, 16, 17, 18, 25, 26, 27, 34, 35, 36, 43, 44, 45, 52, 53, 54, 61, 62, 63, 70, 71, 72, 79, 78 |
| Angular acceleration $\ddot{\theta}_x$ | 6, 24, 42, 60, 78 | |
| Angular acceleration $\ddot{\theta}_y$ | 15, 33, 51, 69 | |

As demonstrated in Fig. 5.6 and Table 5.2, there are 44 available measurements, namely 35 translational accelerations and 9 interface angular accelerations. For different purposes of force identification and parameter identification, the available 26 internal acceleration measurements are grouped into set 1 and set 2, tabulated in Table 5.3.

Table 5.3 Measurement set 1 and set 2

| | Measurement set 1 at nodes | Measurement set 2 at nodes |
|---|---|---|
| Translational acceleration $\ddot{w}$ | 7, 8, 9, 17, 18, 25, 26, 27, 34, 36, 43, 44, 45, 52, 53, 62, 63, 70, 71, 72, 79, 80 | 8, 16, 18 ,26, 34, 35, 46, 45, 52, 54, 61, 63, 71, 79 |

The remaining 9 unmeasured accelerations at the interface and the unmeasured excitation force at node 81 are identified with measurement set 1, listed in Table 5.3. The measurement set 2 is used for fitness function evaluation with the purpose of identifying the 26 unknown substructural parameters. The identified stiffness for the 24 elements in SS2 are presented for the cases of 0%, 5% and 10% noise in Fig. 5.7. The absolute maximum and mean error for the identification results are summarized in Table 5.4.

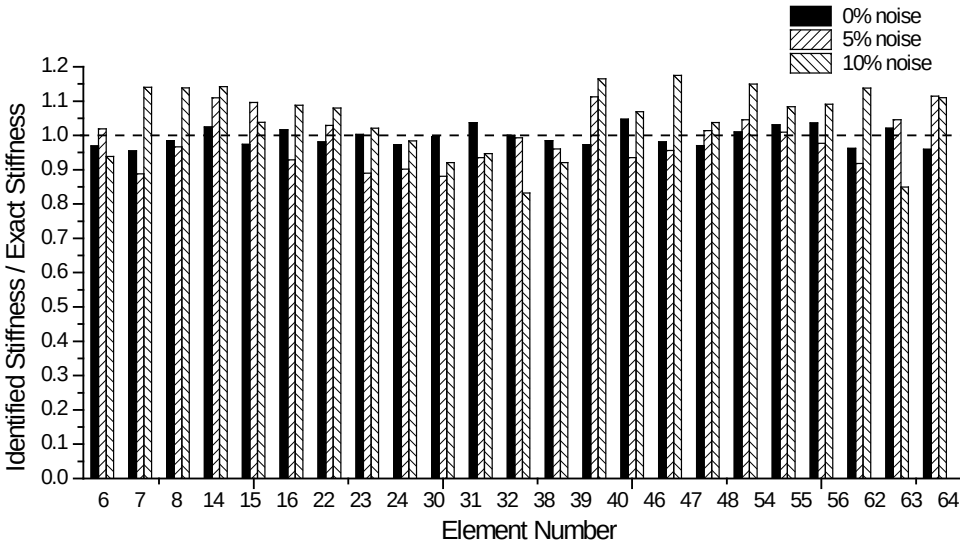


Figure 5.7 Identification results of SS2

Table 5.4 Absolute identification errors of SS2 with respect to noise level

| Noise level | SS2 in plate | |
|---|---|---|
| | Mean error (%) | Maximum error (%) |
| 0% | 2.44 | 4.76 |
| 5% | 6.22 | 11.91 |
| 10% | 9.48 | 17.47 |

From the identification results in Fig. 5.7 and Table 5.4, reasonably accurate results are obtained for the estimated stiffness values of the 24 elements within SS2 with 0%, 5% and 10% noise polluted measurements, which demonstrates the good performance of the proposed strategy for substructural identification with incomplete interface measurements as well as unmeasured excitation forces.

## 5.4 Experimental study

To verify the effectiveness of the proposed strategies for substructural identification without measurements of interface acceleration and excitation located within the

substructure, an experimental study is conducted on a laboratory fabricated small-scale10-storey frame with the same measurement data as Section 3.5.

### 5.4.1 Substructural identification on frame without interface acceleration and excitation force

The same substructure SS1 as in Fig. 4.8, located in the 10-storey frame in Fig 3.10 is considered in this experiment. The identified stiffness of SS1 by static and dynamic test in this substructure are summarized in Table 5.5.

Table 5.5 Stiffness of SS1 by static test and dynamic test

| Storey | Stiffness (kN/m) (static test) | Stiffness (kN/m) (dynamic test ) |
|---|---|---|
| 5 | 267.68 | 252.81 |
| 6 | 396.09 | 393.10 |
| 7 | 378.09 | 391.00 |
| 8 | 263.91 | 271.99 |
| 9 | 252.09 | 285.76 |
| 10 | 362.55 | 402.82 |

SS1 contains storeys 5-10, as shown in Fig. 5.8. Level 4 is the interface of SS1. To investigate the performance of the proposed strategy in substructural identification without complete interface measurements and excitation forces, only the acceleration responses at the $5^{th}$, $6^{th}$, $7^{th}$, $8^{th}$, $9^{th}$ and $10^{th}$ levels are measured for 2 s at a sampling rate of 2,000. These six measurements are divided into two groups, namely set 1 and set 2. Measurement set 1 consists of acceleration measurements at levels 6, 8 and 10 for the purpose of identifying the unmeasured acceleration at level 4 and the unknown excitation force applied at level 10. Measurement set 2 includes acceleration measurement data at levels 5, 7 and 9 for identifying 8 unknown substructural parameters of SS1, namely the stiffness of storeys 5-10 and the two damping coefficients. The search space for these six unknown stiffness values is

defined as half to double of measured values based on static test, demonstrated in Table 5.5. For the two damping parameters, 0-4 and 0-0.0002 are set as their search spaces, respectively. In the proposed identification strategy, the maximum number of iteration and the tolerance of the stopping criterion are set as 20 and 0.02.

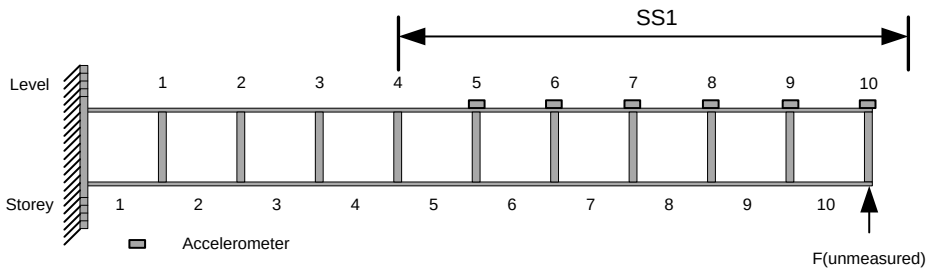


Figure 5.8 SS1 and the sensor placement

Measured acceleration data under three random forces in Fig. 3.17 are employed for stiffness identification of SS1. The corresponding identified stiffness of SS1 compared with the measured values by static test is presented in Fig. 5.9. The identified stiffness of SS1 and the corresponding identification errors are listed in Table 5.6.

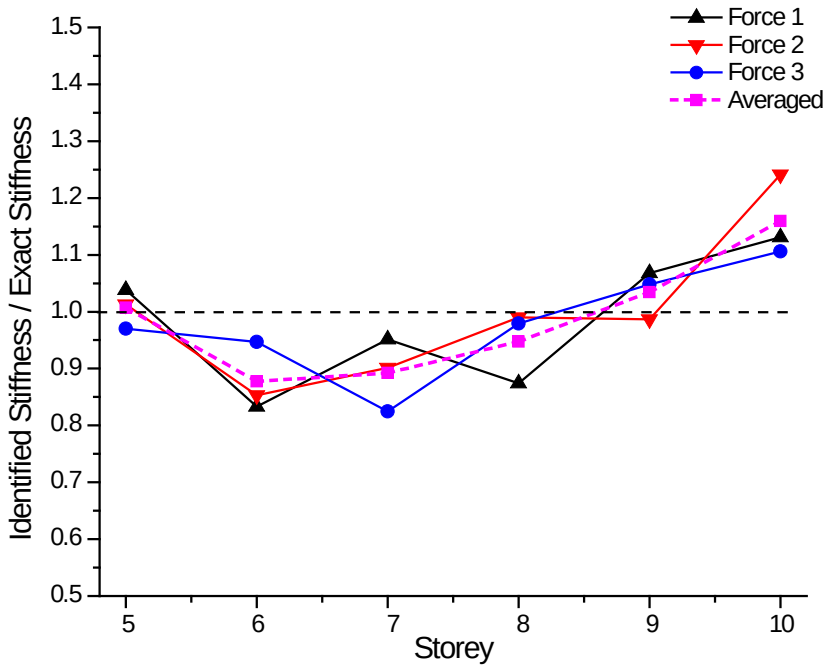


Figure 5.9 Identified stiffness of SS1 with unknown forces and interface accelerations

Table 5.6 Identification errors of SS1 with unknown forces and interface accelerations

| Storey | Stiffness (kN/m) (static test) | Stiffness (kN/m) (dynamic test ) | Stiffness (kN/m) Identified | Error (%) Compared with static test | Error (%) Compared with dynamic test |
|---|---|---|---|---|---|
| 5 | 267.68 | 252.81 | 269.57 | +0.71 | +6.63 |
| 6 | 396.09 | 393.10 | 347.62 | -12.24 | -11.57 |
| 7 | 378.09 | 391.00 | 337.38 | -10.77 | -13.71 |
| 8 | 263.91 | 271.99 | 250.10 | -5.23 | -8.05 |
| 9 | 252.09 | 285.76 | 260.71 | +3.42 | -8.77 |
| 10 | 362.55 | 402.82 | 420.33 | +15.94 | +4.35 |

As shown in Fig. 5.9, reasonably satisfactory identified stiffness values of storeys 5-10 are achieved without interface measurements and excitation force measurements. From Table 5.6, the stiffness of elements in SS1 is accurately identified with absolute mean and maximum error of 8.05% and 15.94% compared with the static test, 8.85% and 13.71% compared with the dynamic test. All these results experimentally validate the effectiveness of the proposed strategy for substructural identification without the measurements of interface accelerations and excitations.

### 5.4.2 Substructural identification on a small-scale jack-up without interface angular accelerations

The second experimental study was carried out on a jack-up, which was designed and tested by Wang (2012), as shown in Fig. 5.10.

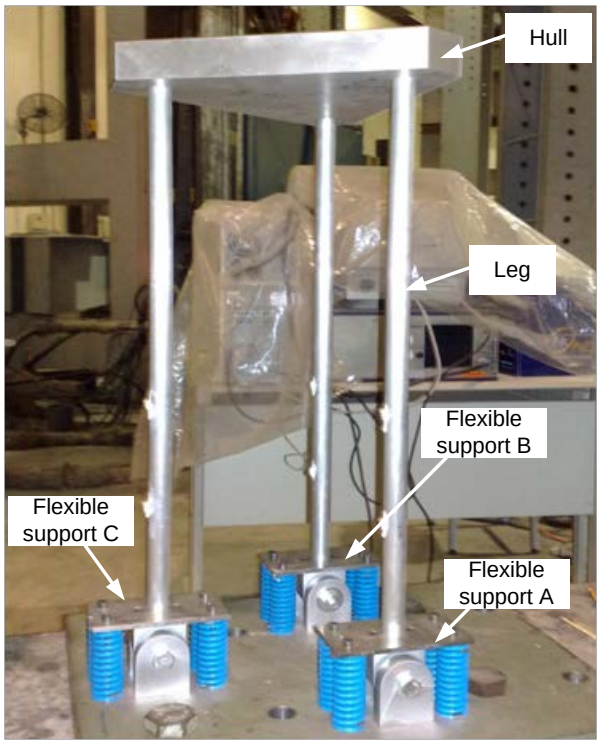


Fig. 5.10 Experiment model for the jack-up

Three legs of the jack-up are made of aluminum tube of the same size, whose length, outer diameter and thickness are 571 mm, 22.2 mm and 1.5 mm, respectively. The hull representing the platform, made with aluminum of approximate density 2,786 kg/m$^3$, weighs 4.84 kg. The layout of the experimental jack-up is shown in Fig. 5.11.

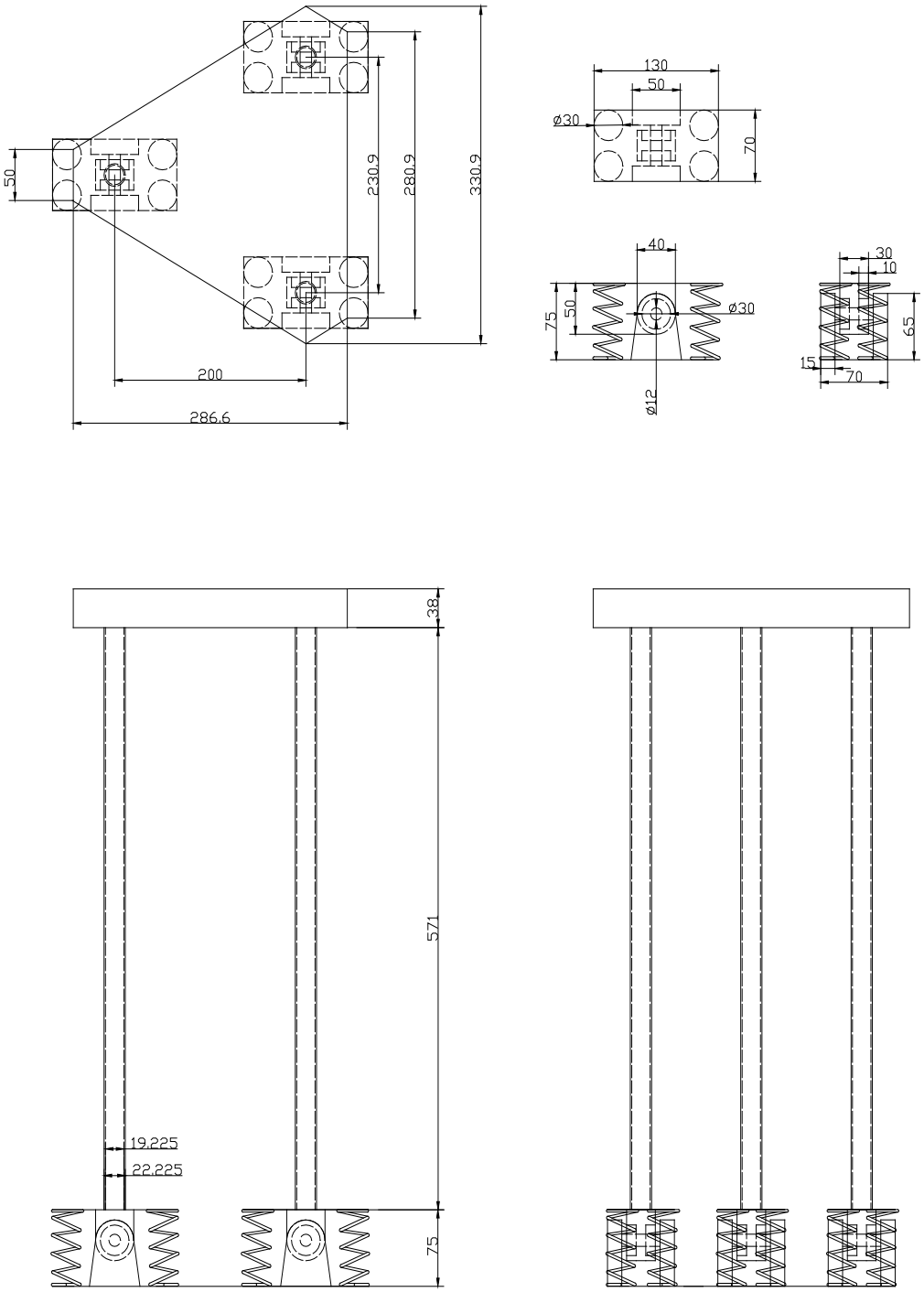


Figure 5.11 Illustration of the experimental jack-up model (Wang, 2012)

Two static tests, respectively measuring the rotational stiffness of three flexible supports and the flexural rigidity of the legs, were conducted by Wang (2012). The main structural parameters for the experimental model are listed in Table 5.7.

Table 5.7 Structural parameters for the experimental model

| Structural parameters of built jack-up model | |
|---|---|
| Length of leg $L$ (m) | 0.571 |
| Young's modulus of leg $E$ (MPa) | 68670 |
| Cross-sectional area moments of inertia for single leg $I$ ($m^4$) | $5.271\times10^{-9}$ |
| Cross-sectional area of single leg $A$ ($m^2$) | $9.766\times10^{-5}$ |
| Measured rotational stiffness $K_\theta$ at flexible support A (N·m/rad) | 550 |
| Measured rotational stiffness $K_\theta$ at flexible support B (N·m/rad) | 584 |
| Measured rotational stiffness $K_\theta$ at flexible support C (N·m/rad) | 574 |
| Measured flexural rigidity for single leg $EI$ ($N\cdot m^2$) | 253.67 |

In this experimental study, one substructure donated as SS1 within one of the flexible legs, shown in Fig. 5.12, is selected to validate the effectiveness of the proposed strategy for substructural identification without angular acceleration measurements at interface. The shaker, shown in Fig. 5.12, is horizontally mounted to the supporting plate. A random force with bandwidth of (0, 1000 Hz) is generated numerically and then applied to one side of the hull to excite the structure. Three accelerometers are installed in SS1 with specifications listed in Table 5.8. The numerical model of SS1 is shown in Fig. 5.13.

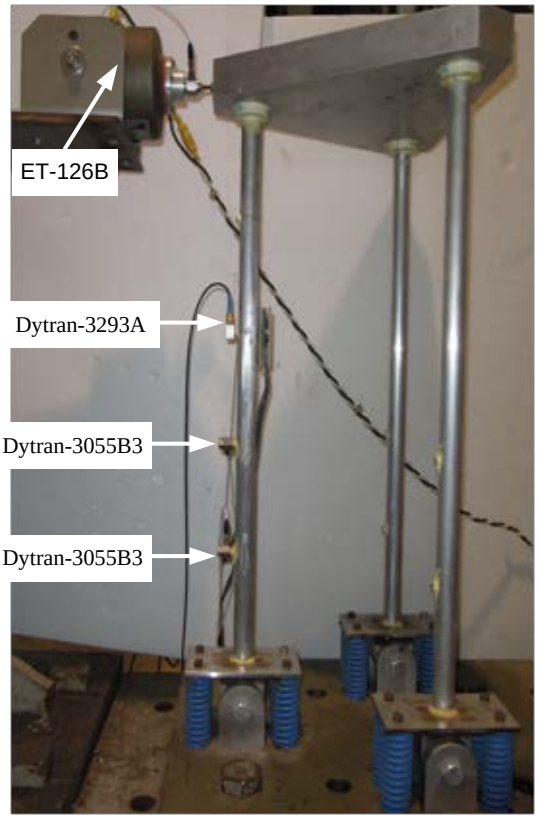


Figure 5.12 Installed accelerometers in SS1

Table 5.8 Specifications of the installed accelerometers on the jack-up

| Model | Node | Measurement Range | Sensitivity | Frequency Range |
|---|---|---|---|---|
| Dytran-3293A (X) | 4 | ±7 g | 524.8 mV/g | 1-4,000 Hz |
| Dytran-3293A (Z) | 4 | ±7 g | 529.3 mV/g | 1-4,000 Hz |
| Dytran-3055B3 | 3 | ±10 g | 494.0 mV/g | 1-10,000 Hz |
| Dytran-3055B3 | 2 | ±10 g | 505.5 mV/g | 1-10,000 Hz |

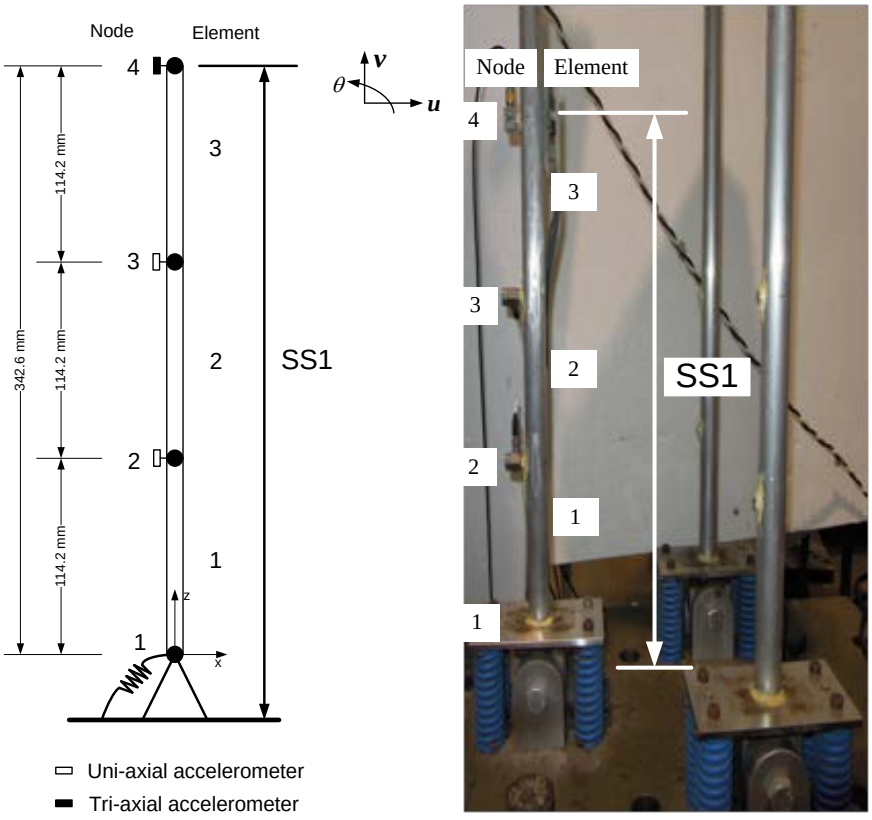


Figure 5.13 Substructure model of SS1 and the sensor placement

As shown in Fig. 5.13, node 4 is the interface between SS1 and the remaining part of the structure. A tri-axial linear accelerometer (Model Dytran-3293A) is installed at node 4 to collect acceleration measurements in x and z directions. Two uni-axial accelerometers (Model Dytran-3055B3) are installed at node 2 and 3 to record acceleration signals in horizontal x direction. All measurements data are recorded at a sampling rate of 2,000 and 4,000 data points of each signal are acquired, and then filtered with frequency band 200-500 Hz for substructural identification.

The flexural rigidities of 3 elements in SS1 are the target parameters of the substructural identification, while FE model of SS1 is established with known rotational stiffness at node 1 by the measured values from static test. The flexural

rigidities of the 3 elements in SS1 and the two damping coefficients are treated as unknown variables in GA. The search limits of these unknown parameters are initially taken as half to double of measured values. In Fig. 5.13, the requirement of complete interface measurements is unsatisfied due to the absence of angular acceleration at node 4. Measurement set 1, involving the horizontal acceleration response at node 3, is employed to identify the angular acceleration at node 4 with Tikhonov regularization method. Measurement set 2, containing the acceleration data at node 2 and 3, is used for substructural parameter identification with SSRM. The maximum number of iterations and tolerance are adopted as 20 and 0.02. The identified flexural rigidities of the 3 elements in SS1 for ten different force signals are compared with measured values from the static test, shown in Fig. 5.14. The corresponding identification errors are tabulated in Table 5.9.

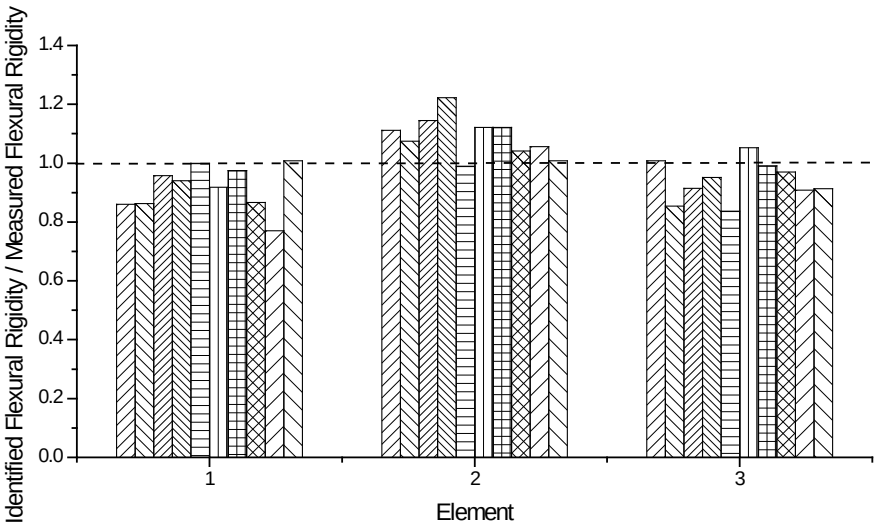


Figure 5.14 Identified flexural rigidities of SS1

Table 5.9 Absolute errors (%) of the identification results of SS1

| Element | Force 1 | Force 2 | Force 3 | Force 4 | Force 5 | |
|---|---|---|---|---|---|---|
| 1 | 13.92 | 13.77 | 4.30 | 5.94 | 0.04 | |
| 2 | 11.20 | 7.45 | 14.48 | 22.20 | 1.06 | |
| 3 | 0.76 | 4.92 | 8.58 | 14.55 | 16.37 | |
| | Force 6 | Force 7 | Force 8 | Force 9 | Force 10 | Mean error |
| 1 | 8.17 | 2.57 | 13.39 | 23.01 | 0.80 | 8.59 |
| 2 | 12.11 | 12.09 | 4.18 | 5.57 | 0.86 | 9.12 |
| 3 | 5.23 | 0.95 | 3.05 | 9.12 | 8.65 | 7.22 |

As shown in Fig 5.14, the identified flexural rigidities of the 3 elements in SS1 are close to the measured values from the static test. Reasonable identification results are achieved with less than 10% mean error, as shown in Table 5.9, which validates that the proposed strategy is effective without requirement of complete interface measurements experimentally.

## 5.5 Estimation of interface acceleration

The proposed strategy is capable of identifying not only the substructural parameters but also the unmeasured interface accelerations and the unknown forces as the by-products. Similar conclusions to Section 3.6 on the identified forces applied in undamaged SS3 shown in Fig.5.2 are reached. With polluted measurements, the strategy yields a ‘drift’ in the identified force as demonstrated earlier in Fig. 3.24 and Fig. 3.25. As shown in Fig. 3.26 and Fig. 3.27, it is also found that the ‘drift’ only contributes to low frequency components of identified forces in frequency domain. The time history of unmeasured excitations can be acquired by filtering out the low frequency components, shown in Fig. 3.28.

The unmeasured interface accelerations are also identified with the presented strategy. With unpolluted measurements, the identified interface angular acceleration at node 12 in undamaged SS3 in Fig.5.2 after 1, 5 and 20 iterations are shown in Fig. 5.15 through Fig. 5.17.

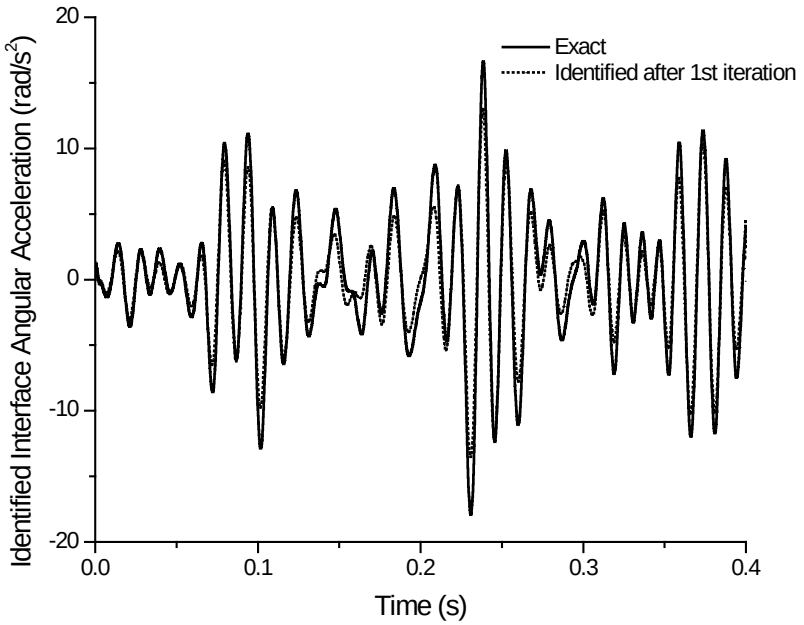


Figure 5.15 Identified angular acceleration at node 12 after 1 iteration, 0% noise

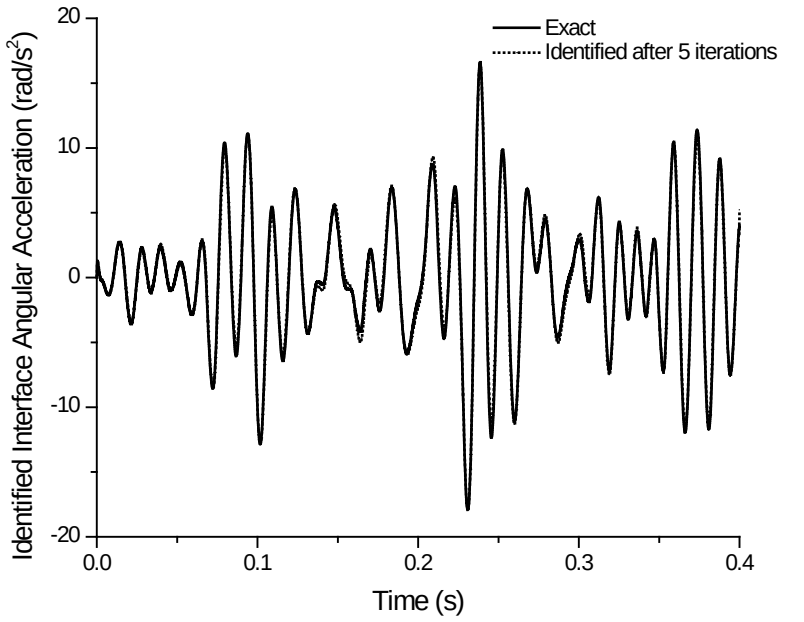


Figure 5.16 Identified angular acceleration at node 12 after 5 iterations, 0% noise

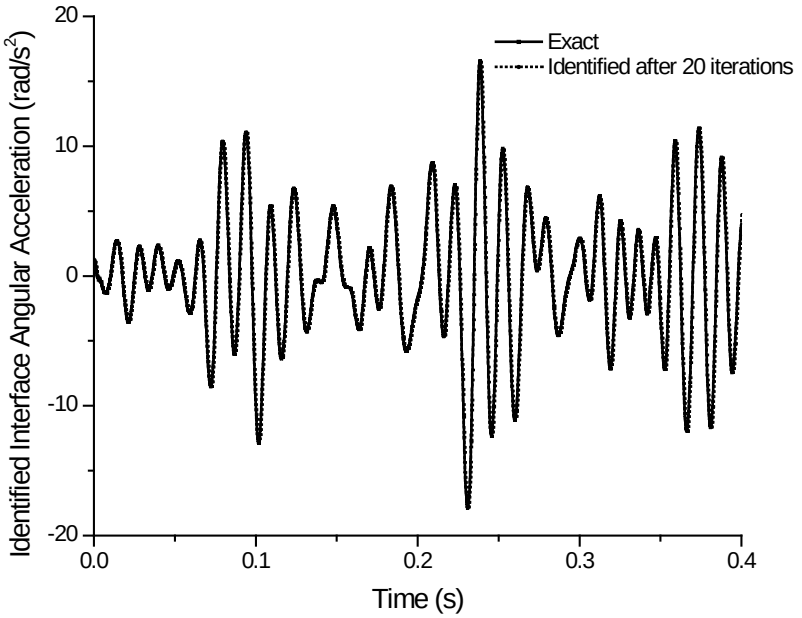


Figure 5.17 Identified angular acceleration at node 12 after 20 iterations, 0% noise

In Fig. 5.15, fairly large identification errors are found in the identified interface angular acceleration after the first iteration due to the inexact estimated substructural parameters. In Fig. 5.16, the identification errors of identified angular acceleration after 5 iterations are significantly reduced and the identified time history is in excellent agreement with their exactness after 20 iterations, shown in Fig. 5.17. These results indicate that the identified angular accelerations at node 12 at the interface of SS3 converge rapidly to the exact values.

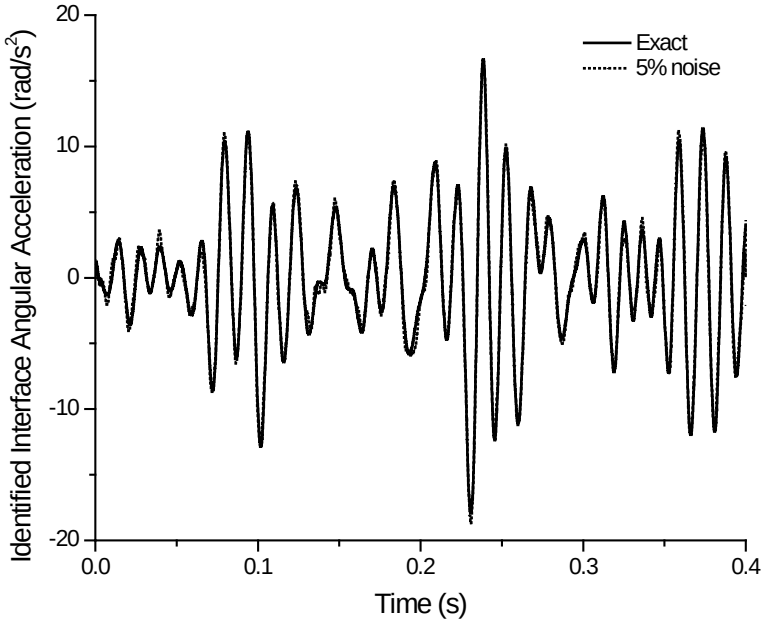


Figure 5.18 Identified angular acceleration at node 12, 5% noise

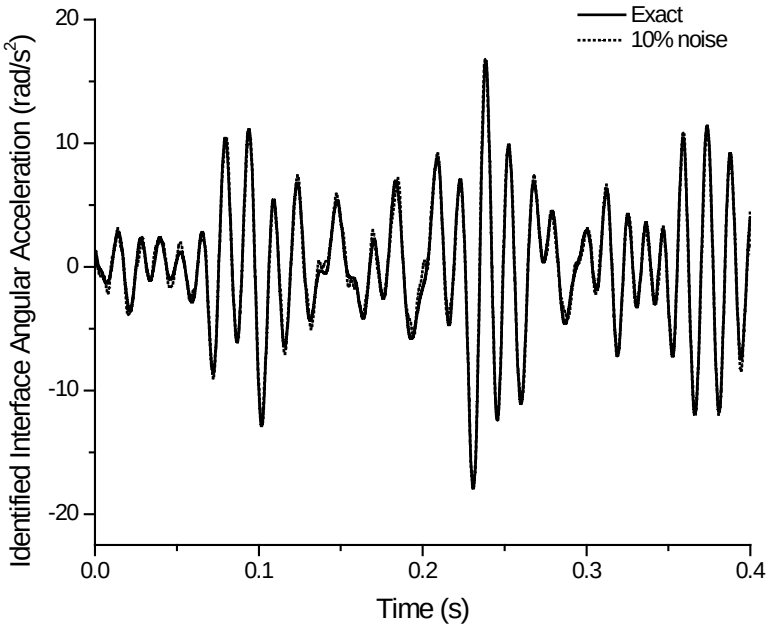


Figure 5.19 Identified angular acceleration at node 12, 10% noise

The noise effect on the identified interface acceleration at the interface is also investigated, shown in Fig. 5.18 and Fig. 5.19. The interface angular acceleration at

node 12 is accurately identified even with 10% noise polluted measurements. In addition to parameter identification of substructures, the proposed strategy is able to directly and accurately identify the unmeasured accelerations at interface.

## 5.6 Summary

In this chapter, an innovative iterative strategy is proposed for substructural identification without complete interface measurements as well as excitation measurements. First, to facilitate force identification with Tikhonov regularization method, the equation of motion for the substructure is derived in a discrete time state space form with the trapezoidal rule. Then unmeasured accelerations at the interface of substructures are treated in a similar way to the unknown excitations which are iteratively identified together with substructural parameters by employing Tikhonov regularization method and SSRM.

The effectiveness of the proposed strategy is validated by damage detection and parameter identification for substructures on a simply supported beam and a cantilever plate. Numerical results show that the location and severity of damages in the beam are accurately identified and the identified stiffness of the plate is in good agreement with their exact values. Furthermore, two experimental studies are carried out: substructural stiffness identification on a 10-storey frame without measurements of forces and interface responses data, flexural rigidity identification of a substructure in one leg of a small-scale jack-up. The identified parameters of the experiments are in good agreement with the measured values from static test. In

addition, the proposed strategy is also able to accurately identify the unmeasured accelerations at the interface of substructures.

# Chapter 6. Conclusions and Recommendations

## 6.1 Conclusions

Structural health monitoring and damage detection of civil infrastructure systems are very important in evaluating their health status with identified key parameters through structural identification based on observed structural responses and excitation forces. In practice, excitation forces are difficult to be accurately measured or in some cases even immeasurable. The unavailability of excitation force measurements is a big challenge in structural identification since the unknowns include not only structural parameters but also input forces.

Compared with global structural identification, substructural identification is a powerful way to improve accuracy and efficiency due to fewer DOFs and unknown parameters involved. Nevertheless, the required complete measurements at interface largely limit its application, particularly for beam and plate substructures where a considerable number of angular accelerations are required. The incompleteness of interface measurements introduces another challenge in achieving good identification results.

To address these two challenges, the following three novel strategies have been proposed in this thesis.

(1) A substructural identification strategy is proposed with measurements of strains and translational accelerations, which are more easily and economically acquired than angular acceleration measurements in practice. In this strategy, a recovery method is developed to compute angular accelerations based on the measurements of strains and translational accelerations. An improved GA called the search space reduction method (SSRM) is employed as the search engine for substructural identification. Numerical studies of damage detection on a beam substructure and stiffness identification on a plate substructure are carried out to examine the performance of the proposed strategy. The results show that the strategy is able to accurately locate and quantify the damage and stiffness values. The recovery method not only recovers angular accelerations at the interface DOFs but also at some internal DOFs. The accuracy of identification results can be significantly improved by including these recovered internal angular accelerations in the fitness function since internal angular accelerations are more sensitive to change in substructural parameters than internal translational accelerations. Savitzky-Golay differentiation algorithm is employed for the required differentiation of strains. Nevertheless, due to the difficulty of accurately computing derivatives at the beginning and ending parts of signals based on insufficient measurement data, differentiation error will inevitably affect the accuracy of identification results. This problem is overcome by excluding the initial and ending part of simulated and measured signals in fitness function.

(2) To address the challenge posed by lack of excitation force measurement, an iterative identification strategy is proposed, which involves the use of Tikhonov regularization method for force identification and SSRM for parameter identification. The proposed strategy is tested through global structural identification on the same two numerical examples of beam and plate. Numerical studies show that satisfactory identification results are achieved after 20 iterations. To substantiate the numerical findings, an experimental study of global structural identification of a laboratory fabricated 10-storey frame is carried out without measurement of applied force. Acceptable stiffness values of the experimental frame are identified when compared with the benchmark values obtained from static and dynamic tests. The iterative strategy is then developed for substructural identification without measurement of excitation force if there is any within the substructure. Two numerical studies of parameter identification of beam and plate substructures validate the effectiveness of the proposed identification strategy, followed by an experimental study on substructural identification of a 10-storey frame without force measurements.

(3) An iterative strategy is developed for dealing with both issues of incomplete interface measurements and unknown excitations in substructural identification. Essentially the unmeasured interface accelerations are identified together with the unknown excitations by Tikhonov regularization method. Numerical study for damage detection on a beam substructure shows that the location and severity of damages in a beam substructure are accurately identified without

measurements of interface angular accelerations and excitation forces. The strategy is also successfully applied for parameter identification of a plate substructure with incomplete interface measurements as well as without force measurements. The performance of the proposed strategy is further demonstrated through two experimental studies, i.e., substructural stiffness identification on a 10-storey frame without interface measurements and force measurements as well as substructural identification on a small-scale jack-up without measurements of angular acceleration at the interface.

## 6.2 Recommendations for future study

Based on the numerical and experimental findings obtained in this thesis, some recommendations for further investigation are suggested as follows.

(1) The identification strategy proposed in Chapter 2 is applied for beam and plate substructures, which are modeled by Euler beam and Kirchhoff plate element, respectively. This strategy can be extended to substructural identification of thick beams and thick plates accounting for shear strains.

(2) The study assumes that the locations of unmeasured applied forces are stationary. In cases of moving loads such as bridges with traffic load, it is suggested to further develop the proposed identification strategies for identifying structures and substructures subjected to unknown moving forces.

(3) In Chapter 5, a considerable number of internal measurements are required if a large number of unmeasured responses at the interface are encountered. It is beneficial to introduce some condensation methods, such as Guyan reduction (Guyan, 1965), dynamic condensation (Paz, 1984, 1989) and iterated improved reduced system (Friswell et al., 1995, 1998) to reduce the required number of internal measurements.

(4) The performance of SSRM can be significantly improved by incorporating initial sampling, such as random uniform distribution, Latin hypercube, orthogonal array and Hammersley sequence sampling (Zhang et al., 2010a) as well as local search such as conjugate gradient method, Broyden-Fletcher-Goldfarb-Shanno method and simulated annealing (Zhang et al., 2010b). It is recommended to include some appropriate initial sampling methods and local search methods in the proposed identification strategies to further improve the identification accuracy and computational efficiency.

# References

Abdalla, M. O. (2009), 'Particle swarm optimization for structural damage detection', *Proceeding of 3rd International Conference on Applied Mathematics, Circuits, Systems and Signals*, Vouliagmeni, Greece, 43-48

Adeli, H. and Park, H. S. (1995a), 'A neural dynamics model for structural optimization - theory', *Computers & Structures*, 57(3), 383-390

Adeli, H. and Park, H. S. (1995b), 'Optimization of space structures by neural dynamics', *Neural Networks*, 8(5), 769-781

Adeli, H. and Karim, A. (1997), 'Neural network model for optimization of cold-formed steel beams', *Journal of Structural Engineering-ASCE*, 123(11), 1535-1543

Adeli, H. (2001), 'Neural networks in civil engineering: 1989-2000', *Computer-Aided Civil and Infrastructure Engineering*, 16(2), 126-142

Agbabian, M. S., Masri, S. F., Miller, R. K. and Caughey, T. K. (1991), 'System identification approach to detection of structural changes', *Journal of Engineering Mechanics-ASCE*, 117(2), 370-390

Aizawa, T., Kimura, T., Matsuoka, T., Takeda, T. and Asano, Y. (2008), 'Application of MEMS accelerometer to geophysics', *International Journal of the JCRM*, 4 (2), 33-36

Alrashidi, M. R. and El-Hawary, M. E. (2009), 'A survey of particle swarm optimization applications in electric power systems', *IEEE Transactions on Evolutionary Computation*, 13(4), 913-918

Alvandi, A. and Cremona, C. (2006), 'Assessment of vibration-based damage identification techniques', *Journal of Sound and Vibration*, 292, 179-202

Bagis, A. (2006), 'Performance comparison of genetic and tabu search algorithms for system identification', *Proceedings of Knowledge-based Intelligent Information and Engineering Systems*, Book Series: Lecture Notes in Artificial Intelligence, 4251, 94-101

Bakhary, N., Hao, H. and Deeks, A. J. (2010a), 'Damage detection using neural network with multi-stage substructuring', *Advances in Structural Engineering*, 13(1), 95-110

Bakhary, N., Hao, H. and Deeks, A. J. (2010b), 'Substructuring technique for damage detection using statistical multi-stage artificial neural network', *Advances in Structural Engineering*, 13(4), 619-639

Balling, R. J. (1991), 'Optimal steel frame design by simulated annealing', *Journal for Structural Engineering-ASCE*, 117, 1780–1795

Bayissa, W. L. and Haritos, N. (2007), 'Structural damage identification using a global optimization technique', *2nd International Conference on Structural Condition Assessment, Monitoring and Improvement*, Changsha, P. R. China, 530-536

Begambre, O. and Laier, J. E. (2009), 'A hybrid particle swarm optimization-simplex algorithm (PSOS) for structural damage identification', *Advances in Engineering Software*, 40(9), 883-891

Bennage, W. A. and Dhingra, A. K. (1995), 'Optimization of truss topology using tabu search', *International Journal for Numerical Methods in Engineering*, 38(23), 4035-4052

Bland, J. A. (1998), 'Structural design optimization with reliability constraints using tabu search', *Engineering Optimization*, 30(1), 55-74

Blum, C. and Roli, A. (2003), 'Metaheuristics in combinatorial optimization: Overview and conceptual comparison', *ACM Computing Surveys*, 35(3), 268-308

Blum, C. and Sampels, M. (2004) 'An ant colony optimization algorithm for shop scheduling problems', *Journal of Mathematical Modeling and Algorithms*, 3(3), 285-308

Camp, C. V. and Bichon, B. J. (2004), 'Design of space trusses using ant colony optimization', *Journal of Structural Engineering-ASCE*, 130(5), 741-751

Camp, C. V., Bichon, B. J. and Stovall, S. P. (2005), 'Design of steel frames using ant colony optimization ', *Journal of Structural Engineering-ASCE*, 131(3), 369-379

Caravani, P., Watson, M. L. and Thomson, W. T. (1997), 'Recursive least-squares time domain identification of structural parameters', *Journal of Applied Mechanics-Transactions of the ASME*, 44(1), 135-140

Carden, E. P. and Fanning, P. (2004), 'Vibration based condition monitoring: A review', S*tructural Health Monitoring-An International Journal*, 3(4), 355-377

Chang, C. C., Chang, T. Y. P., Xu, Y. G. and To, W. M. (2002), 'Selection of training samples for model updating using neural networks', *Journal of Sound and Vibration*, 249(5), 867-883

Chen, H. M., Tsai, K. H. and Qi, G. Z. (1995), 'Neural-network for structure control', *Journal of Computing in Civil Engineering*, 9(2), 168-176

Chen, H. P. and Bicanic, N. (2000), 'Assessment of damage in continuum structures based on incomplete modal information', *Computers & Structures*, 74(5), 559-570

Chen, J. and Li, J. (2004), 'Simultaneous identification of structure parameters and input time history from output-only measurements', *Computational Mechanics*, 33, 365-374

Chou, J. H. and Ghaboussi, J. (2001), 'Genetic algorithm in structural damage detection', *Computers & Structures*, 79(14), 1335-1353

Chu, S. Y. and Lo, S. C. (2011), 'Application of the on-line recursive least-squares method to perform structural damage assessment', *Structural Control & Health Monitoring*, 18(3), 241-264

Clerc, M. and Kennedy, J. (2002), 'The particle swarm - explosion, stability, and convergence in a multidimensional complex space', *IEEE Transactions on Evolutionary Computation*, 6(1), 58-73

Coello, C. A. C., Pulido, G. T. and Lechuga, M. S. (2004), 'Handling multiple objectives with particle swarm optimization', *IEEE Transactions on Evolutionary Computation*, 8(3), 256-279

Cole, H. A. (1971), 'Methods and apparatus for measuring the damping characteristics of a structure', *United States Patent* No. 3,620,069

del Valle, Y., Venayagamoorthy, G. K., Mohagheghi, S., Hernandez, J. C. and Harley, R. G. (2008), 'Particle swarm optimization: basic concepts, variants and applications in power systems', *IEEE Transactions on Evolutionary Computation*, 12 (2), 171-195

Di Caro, G. and Dorigo, M. (1998), 'AntNet: distributed stigmergetic control for communications networks', *Journal of Artificial Intelligence Research*, 9, 317-365

Doebling, S. W., Farrar, C. R., Prime, M. B. and Shevitz, D. W. (1996), 'Damage identification and health monitoring of structural and mechanical systems from changes in their vibration characteristics: a literature review.' *A report LA-13070-MS*, Los Alamos National Laboratory, University of California for the United States Department of Energy

Doebling, S. W., Farrar C. R. and Prime, M. B. (1998), 'A summary review of vibration-based damage identification methods', *Shock and Vibration Digest*, 30 (2), 91-105

Dorigo M. (1992), 'Optimization, learning and natural algorithms', *PhD Thesis*, Politecnico di Milano, Italy

Dorigo, M. and Gambardella, L. M. (1997), 'Ant colony system: a cooperative learning approach to the traveling salesman problem', *IEEE Transactions on Evolutionary Computation*, 1(1), 53-66

Dorigo, M. and Blumb, C. (2005), 'Ant colony optimization theory: a survey', *Theoretical Computer Science*, 344(2-3), 243-278

Dougherty, D. E. and Marryott, R. A. (1991), 'Optimal groundwater-management: 1. simulated annealing', *Water Resources Research*, 27(10), 2493-2508

Fan, W. and Qiao, P. Z. (2011), 'Vibration-based damage identification methods: a review and comparative study', *Structural Health Monitoring - An International Journal*, 10(1), 83-111

Farrar, C. R. and James III, G. H. (1997), 'System identification from ambient vibration measurements on a bridge', *Journal of Sound and Vibration*, 205(1), 1-18

Farrar, C. R., Doebling, S. W. and Nix, D.A. (2001), 'Vibration-based structural damage identification', *Philosophical Transactions: Mathematical, Physical and Engineering Sciences, Experimental Modal Analysis*, 359, 131-149

Fiechter, C. N. (1994), 'A parallel tabu search algorithm for large traveling salesman problems', *Discrete Applied Mathematics*, 51(3), 243-267

Flood, I. and Kartam, N. (1994a), 'Neural networks in civil engineering .I: principles and understanding', *Journal of Computing in Civil Engineering*, 8(2), 131-148

Flood, I. and Kartam, N. (1994b), 'Neural networks in civil engineering .II: systems and application', *Journal of Computing in Civil Engineering*, 8(2), 149-162

Fourie, P. C. and Groenwold, A. A. (2002), 'The particle swarm optimization algorithm in size and shape optimization', *Structural and Multidisciplinary Optimization*, 23(4), 259-267

Franklin, C. H. (2005), 'Maximum Likelihood Estimation', *Encyclopedia of Social Measurement*, 2, 653-664

Gaing, Z. L. (2004), 'A particle swarm optimization approach for optimum design of PID controller in AVR system', *IEEE Transactions on Energy Conversion*, 19(2), 384-391

Gambardella, L.M. and Dorigo, M. (2000), 'Ant colony system hybridized with a new local search for the sequential ordering problem', *Informs Journal on Computing*, 12(3), 237-255

Gendreau, M., Hertz, A. and Laporte, G. (1994), 'A tabu search heuristic for the vehicle-routing problem', *Management Science*, 40(10), 1276-1290

Gendreau, M., Laporte, G. and Seguin, R. (1996), 'A tabu search heuristic for the vehicle routing problem with stochastic demands and customers', *Operations Research*, 44(3), 469-477

Gendreau, M., Laporte, G. and Semet, F. (1998), 'A tabu search heuristic for the undirected selective travelling salesman problem', *European Journal of Operational Research*, 106(2-3), 539-545

Gens, A., Ledesma, A. and Alonso, E. E. (1996), 'Estimation of parameters in geotechnical backanalysis -II. Application to a tunnel excavation problem', *Computers and Geotechnics*, 18(1), 29-46

Glover, F. and McMillan, C. (1986), 'The general employee scheduling problem - an integration of MS and AI', *Computers & Operations Research*, 13(5), 563-573

Glover F. (1990), 'Tabu search - a tutorial', *Interfaces*, 20(4), 74-94

Gonz´alez, A., Rowley, C. and Obrien, E. J. (2008), 'A general solution to the identification of moving vehicle forces on a bridge', *International Journal for Numerical Methods in Engineering*, 75, 335-354

Han, X., Xu, D., Yap, F. F. and Liu, G. R. (2002), 'On determination of the material constants of laminated cylindrical shells based on an inverse optimal approach', *Inverse Problems in Engineering*, 10(4), 309-322

Hansen, P. C. (1992), 'Analysis of discrete ill-posed problems by means of the L-curve.', *SIAM*, 34(4), 561-580

Hansen, P. C. and O´leary, D. P. (1993), 'The use of the L-curve in the regularization of discrete ill-posed problems', *SIAM*, 14(6), 1487-1503

He, R. S. and Hwang, S. F. (2006), 'Damage detection by an adaptive real-parameter simulated annealing genetic algorithm', *Computers & Structures*, 84(31-32), 2231-2243

He, S., Prempain, E. and Wu, Q. H. (2004), 'An improved particle swarm optimizer for mechanical design optimization problems', *Engineering Optimization*, 36(5), 585-605

Hoshiya, M. and Saito, E. (1984), 'Structural identification by extended Kalman filter', *Journal of Engineering Mechanics-ASCE*, 110(12), 1757-1770

Hoshiya, M. and Sutoh, A. (1992), 'Extended Kalman filter-weighted local iteration method for dynamic structural identification', *Proceedings of the tenth world conference on Earthquake Engineering*, 3715-3720

Hoshiya, M. and Sutoh, A. (1993), 'Kalman filter-finite element method in identification', *Journal of Engineering Mechanics-ASCE*, 119(2), 197-210

Hou, J. L., Jankowski, L. and Ou, J. P. (2011), 'A substructure isolation method for local structural health monitoring', *Structural Control & Health Monitoring*, 18(6), 601-618

Hu, M. Y. and Zhang, L. X. (2011), 'Application of optimization analysis on structure damage identification based on ACO algorithm', *3rd International Conference on Advanced Design and Manufacture*, Nottingham Trent University, Nottingham, England, Sep 08-10, 450, 506-509

Huang, C. S., Yang Y. B., Lu L. Y. and Chen, C. H. (1999), 'Dynamic testing and system identification of a multi-span highway bridge', *Earthquake Engineering & Structural Dynamics*, 28, 857-878

Hwang, H. Y. and Kim, C. (2004), 'Damage detection in structures using a few frequency response measurements', *Journal of Sound and Vibration*, 270, 1-14

Ibrahim, S. R. (1977), 'Random decrement technique for modal identification of structures', *Journal of Spacecraft and Rockets-AIAA*, 14 (11), 696-700

Jeong, I. K. and Lee, J. J. (1996), 'Adaptive simulated annealing genetic algorithm for system identification', *Engineering Applications of Artificial Intelligence*, 9 (5), 523-532

Juang, J. N. and Pappa, R. S. (1985), 'An eigensystem realization algorithm for modal parameter identification and model reduction', *Journal of Guidance Control and Dynamics*, 8(5), 620-627

Kalman, R. E. (1960), 'A new approach to linear filtering and prediction problems', *Journal of Basic Engineering-Transactions of the ASME*, 82(1), 35-45

Kameyama, K. (2009), 'Particle swarm optimization - a survey', *IEICE Transactions on Information and Systems*, E92-D (7), 1354-1361

Kargahi, M., Anderson, J. C. and Dessouky, M. M. (2006), 'Structural weight optimization of frames using tabu search. I: Optimization procedure', *Journal of Structural Engineering-ASCE*, 132(12), 1858-1868

Kargahi, M. and Anderson, J. C. (2006), 'Structural weight optimization of frames using tabu search. II: Evaluation and seismic performance', *Journal of Structural Engineering-ASCE*, 132(12), 1869-1879

Karunanithi, N., Grenney, W. J., Whitley, D. and Bovee, K. (1994), 'Neural networks for river flow prediction', *Journal of Computing in Civil Engineering*, 8(2), 201-220

Katkhuda, H. and Haldar, A. (2008), 'A novel health assessment technique with minimum information', *Structural Control & Health Monitoring*, 15(6), 821-838

Kaveh, A. and Talatahari, S. (2010), 'An improved ant colony optimization for contrained engineering design problems', *Engineering Computations*, 27 (1-2), 155-182

Kennedy, J. and Eberhart, R. (1995), 'Particle swarm optimization', *Proceeding of IEEE International Conference on Neural Networks*, University of Western Australia, Perth, Australia, 1942-1948

Kersey, A. D., Davis, M. A., Patrick, H. J., LeBlanc, M., Koo, K. P., Askins, C. G., Putnam, M. A. and Friebele, E. J. (1997), 'Fiber grating sensors', *Journal of Lightwave Technology*, 15 (8), 1442-1463

Khiat, A., Lamarque, F., Prelle, C., Bencheikh, N., and Dupont, E. (2010), 'High-resolution fibre-optic sensor for angular displacement measurements', *Measurement Science & Technology*, 21(2), 025306

Kim, J. T., Ryu, Y. S., Cho, H. M. and Stubbs, N. (2003), 'Damage identification in beam-type structures: frequency-based method vs mode-shape-based method', *Engineering Structures*, 25(1), 57-67

Kirkpatrick, S., Gelatt, C. D. and Vecchi, M. P. (1983), 'Optimization by simulated annealing', *Science*, 220(4598), 671-680

Koh, C. G., See, L. M. and Balendra, T. (1991), 'Estimation of structural parameters in time domain - a substructure approach', *Earthquake Engineering & Structural Dynamics*, 20(8), 787-801

Koh, C. G., Chen, Y. F. and Liaw, C. Y. (2003a), 'A hybrid computational strategy for identification of structural parameters', *Computers & Structures*, 81(2), 107-117

Koh, C. G., Hong, B. and Liaw, C. Y. (2003b), 'Substructural and progressive structural identification methods', *Engineering Structures*, 25(12), 1551-1563

Koh, C. G. and Shankar, K. (2003), 'Substructural identification method without interface measurement', *Journal of Engineering Mechanics-ASCE*, 129(7), 769-776

Koh, C. G., Tee, K. F. and Quek, S. T. (2006), 'Condensed model identification and recovery for structural damage assessment', *Journal of Structural Engineering-ASCE*, 132(12), 2018-2026

Koh, C. G. and Perry, M. J. (2010), 'Structural Identification and Damage Detection using Genetic Algorithms', *Taylor & Francis Group*, London

Kosmas, O. T. and Vlachos, D. S. (2012), 'Simulated annealing for optimal ship routing', *Computers & Operations Research*, 39(3), 576-581

Kumar, R. K. and Shankar, K. (2009), 'Parametric identification of structures with nonlinearities using global and substructure approaches in the time domain', *Advances in Structural Engineering*, 12(2), 195-210

Law, S. S. and Zhu, X. Q. (2000), 'Study in different beam models in moving force identification', *Journal of Sound and Vibration*, 234(4), 661-679

Law, S. S. and Lu, Z. R. (2005), 'Time domain responses of a prestressed beam and prestress identification', *Journal of Sound and Vibration*, 288, 1011-1025

Law, S. S., Zhang, K. and Duan, Z. D., 'Structural damage detection from coupling forces between substructures under support excitation', *Engineering Structures*, 32(8), 2221-2228, 2010

Ledesma, A., Gens, A. and Alonso, E. E. (1996), 'Estimation of parameters in geotechnical backanalysis -I. Maximum likelihood approach', *Computers and Geotechnics*, 18(1), 1-27

Li, S. J., Liu, Y. X., He, X. and Zhou, Y. P. (2003), 'Parameter identification procedures for the concrete dam based on ant colony optimization', *International Conference on Advances in Concrete and Structures*, Xuzhou, China, 32, 1428-1433

Liang, H., Hao, F. and Ju, P. G. (2010), 'Development of novel high precision angular displacement sensor', *Advanced Materials Research*, 97-101, 4332-4336

Lin, C. C. Wang, J. F. and Ueng, J. M. (2001), 'Vibrational control identification of seismically excited m.d.o.f. structure-PTMD systems', *Journal of Sound and Vibration*, 240(1), 87-115

Liu, G. R. and Chen, S. C. (2001), 'Flaw detection in sandwich plates based on time-harmonic response using genetic algorithm', *Computer Methods in Applied Mechanics and Engineering*, 190(42), 5505-5514

Liu, G. R., Han, X. and Lam, K. Y. (2002a), 'A combined genetic algorithm and nonlinear least squares method material characterization using elastic waves', *Computer Methods in Applied Mechanics and Engineering*, 191(17-18), 1909-1921

Liu, G. R., Lam, K. Y. and Han, X. (2002b), 'Determination of elastic constants of anisotropic laminated plates using elastic waves and a progressive neural network' *Journal of Sound and Vibration*, 252(2), 236-259

Liu, G. R., Ma, H. J. and Wang, Y. C. (2005), 'Material characterization of composite laminates using dynamic response and real parameter-coded micro genetic algorithm', *Engineering with Computers*, 20(4), 295-254

Lu, D. and Weng, Q. (2007), 'A survey of image classification methods and techniques for improving classification performance', *International Journal of Remote Sensing*, 28(5), 823-870

Lu, Q., Ren, G. and Zhao, Y. (2002), 'Multiple damage location with flexibility curvature and relative frequency change for beam structures', *Journal of Sound and Vibration*, 253(5), 1101-1114

Lu, Z. R. and Law, S. S. (2007), 'Identification of system parameters and input force from output only', *Mechanical System and Signal Processing*, 21, 2099-2111

Lu, Z. R., Huang, M. and Liu, J. K. (2011), 'State-space formulation for simultaneous identification of both damage and input force from response sensitivity', *Smart Structures and Systems*, 8(2), 157-172

Lundy, M. and Mees, A. (1986), 'Convergence of an annealing algorithm', *Mathematical Programming*, 34(1), 111-124

Luo, J. W., Ying, K., He, P. and Bai, J. (2005), "Properties of Savitzky-Golay digital differentiators", *Digital Signal Processing*, 15, 122-136

Maniezzo, V. and Colorni, A. (1999), 'The ant system applied to the quadratic assignment problem', *IEEE Transactions on Knowledge and Data*, 11(5), 769-778

Mantawy, A. H., Abdel-Magid, Y. L. and Selim, S. Z. (1999), 'Integrating genetic algorithms, tabu search, and simulated annealing for the unit commitment problem', *IEEE Transactions on Power Systems*, 14(3), 829-836

Misevicius, A. (2005), 'A tabu search algorithm for the quadratic assignment problem', *Computational Optimization and Applications*, 30(1), 95-111

Myung, I. J. (2003), 'Tutorial on maximum likelihood estimation', *Journal of Mathematical Psychology*, 47(1), 90-100

Oreta, A. W. C. and Tanabe, T. (1993), 'Localized identification of structures by Kalman filter', *Structural Engineering/Earthquake Engineering*, Japan Society of Civil Engineers, 9(4), 217-225

Oreta, A. W. C. and Tanabe, T. (1994), 'Element identification of member properties of framed structures', *Journal of Structural Engineering-ASCE*, 120(7), 1961-1976

Ovaska, S. J. and Valiviita, S. (1998), 'Angular acceleration measurement: a review', *IEEE Transactions on Instrumentation and Measurement*, 47(5), 1211-1217

Ozcelik, O., Luco, J. E. and Conte, J. P. (2008), 'Identification of the mechanical subsystem of the NEES-UCSD shake table by a least-squares approach', *Journal of Engineering Mechanics-ASCE*, 134 (1), 23-34

Pandey, A. K., Biswas, M. and Samman, M. M. (1991), 'Damage detection from changes in curvature mode shapes', *Journal of Sound and Vibration*, 145 (2), 321-332

Pantelides, C. P. and Tzan, S. R. (1997), 'Simulated annealing for the design of structures with time-varying constraints', *Structural Optimization*, 13(1), 36-44

Park, H. S. and Adeli, H. (1995), 'A neural dynamics model for structural optimization - application to plastic design of structures', *Computers & Structures*, 57(3), 391-399

Park, H. S. and Sung, C. W. (2002), 'Optimization of steel structures using distributed simulated annealing algorithm on a cluster of personal computers', *Computers & Structures*, 80(14-15), 1305-1316

Parloo, E., Verboven, P., Guillaume, P. and Van Overmeire, M. (2002), 'Autonomous structural health monitoring - Part II: Vibration-based in-operation damage assessment', *Mechanical Systems and Signal Processing*, 16(4), 659-675

Peeters, F., Pintelon, R., Schoukens, J., Rolain, Y., Gutierrez, E. S. and Guillaume, P. (2001a), 'Identification of rotor-bearing systems in the frequency domain part I: Estimation of frequency response functions', *Mechanical Systems and Signal Processing*, 15(4), 759-773

Peeters, F., Pintelon, R., Schoukens, J. and Rolain, Y. (2001b), 'Identification of rotor-bearing systems in the frequency domain part II: Estimation of modal parameters', *Mechanical Systems and Signal Processing*, 15(4), 775-788

Perera, R. and Torres, R. (2006), 'Structural damage detection via modal data with genetic algorithms', *Journal of Structural Engineering-ASCE*, 132(9), 1491-1501

Perera, R., Fang, S. E. and Ruiz, A. (2010), 'Application of particle swarm optimization and genetic algorithms to multiobjective damage identification inverse problems with modelling errors', *Meccanica*, 45(5), 723-734

Perez, R. E. and Behdinan, K. (2007), 'Particle swarm approach for structural design optimization', *Computers & Structures*, 85(19-20), 1579-1588

Perry, M. J., Koh, C. G. and Choo, Y. S. (2006), 'Modified genetic algorithm strategy for structural identification', *Computers & Structures*, 84(8-9), 529-540

Perry, M. J. and Koh, C. G. (2008), 'Output-only structural identification in time domain: Numerical and experimental studies', *Earthquake Engineering & Structural Dynamics*, 37(4), 517-533

Phillips, D. (1962), 'A technique for the numerical solution of certain integral equation of the first kind', *Journal of the Association for Computing and Machinery*, 9, 84-97

Puangdownreong, D., Areerak, K. N., Srikaew, A., Sujitjorn, S. and Totarong, P. (2002), 'System identification via adaptive tabu search', *Proceedings of International Conference on Industrial Technology*, 915-920

Rafiq, M. Y., Bugmann, G. and Easterbrook, D. J. (2001), 'Neural network design for engineering applications', *Computers & Structures*, 79(17), 1541-1552

Ramkumar, B., Schoen, M. P. and Lin, F. (2011), 'Hybrid enhanced continuous tabu search and genetic algorithm for parameter estimation in colored noise environments', *Expert Systems with Applications*, 38(4), 3909-3917

Rani, D. and Moreira, M. M. (2010), 'Simulation-optimization modeling: a survey and potential application in reservoir systems operation', *Water Resources Management*, 24(6), 1107-1138

Rao, Y. J. (1999), 'Recent progress in applications of in-fiber Bragg grating sensors', *Optics and Lasers in Engineering*, 31, 297-324

Rao, M. A., Srinivas, J. and Murthy, B. S. N. (2004), 'Damage detection in vibrating bodies using genetic algorithms', *Computers & Structures*, 82(11-12), 963-968

Ratcliffe, C. P. (1997), 'Damage detection using a modified laplacian operator on mode shape data', *Journal of Sound and Vibration*, 204(3), 505-517

Reich, G. W. and Park, K. C. (2001), 'A theory for strain based structural system identification', *Journal of Applied Mechanics-Transactions of the ASME*, 68(4), 521-527

Rolland, E., Pirkul, H. and Glover, F. (1996), 'Tabu search for graph partitioning', *Annals of Operations Research*, 63, 209-232

Rowley, H. A., Baluja, S. and Kanade, T.(1998), 'Neural network-based face detection', *IEEE Transactions on Pattern Analysis and Machine Intelligence*, 20(1), 23-38

Ruotolo, R., Surface, C. and Mares, C. (1997), 'Damage identification using simulated annealing', *Proceedings of SPIE-The International Society for Optical Engineering*, 3089, 954-960

Salawu, O. S. (1997), 'Detection of structural damage through changes in frequency: a review', *Engineering Structures*, 19(9), 718-723

Sampaio, R. P. C., Maia, N. M. M. and Silva, J. M. M. (1999), 'Damage detection using the frequency-response function curvature method', *Journal of Sound and Vibration*, 226(5), 1029-1042

Sandesh S. and Shankar K. (2009), 'Time domain identification of structural parameters and input time history using a substructural approach', *International Journal of Structural Stability and Dynamics*, 9(2), 243-265

Sandesh S. and Shankar K. (2010), 'Application of a hybrid of particle swarm and genetic algorithm for structural damage detection', *Inverse Problems in Science and Engineering*, 18(7), 997-1021

Savitzky, A. and Golay, M. J. E. (1964), 'Smoothing and differentiation of data by simplified least squares procedures', *Analytical Chemistry*, 36, 1627-1639

Schutte, J. F. and Groenwold, A. A. (2003), 'Sizing design of truss structures using particle swarms', *Structural and Multidisciplinary Optimization*, 25(4), 261-269

Seyedpoor, S. M. (2011), 'Structural damage detection using a multi-stage particle swarm optimization', *Advances in Structural Engineering*, 14(3), 533-549

Seyedpoor, S. M. (2012), 'A two stage method for structural damage detection using a modal strain energy based index and particle swarm optimization', *International Journal of Non-Linear Mechanics*, 47(1), 1-8

Shi, Z. Y., Law, S. S. and Zhang, L. M. (1999), 'Structural damage detection from modal strain energy change', *Journal of Engineering Mechanics-ASCE*, 126(12), 1216-1222

Shi, T. H., Jones, N. P., and Ellis, J. H. (2000), 'Simultaneous estimation of system and input parameters from output measurements', *Journal of Engineering Mechanics-ASCE*, 126(7), 746-753

Shi, Z. Y., Law, S. S. and Zhang, L. M. (2002), 'Improved damage quantification from elemental modal strain energy change', *Journal of Engineering Mechanics-ASCE*, 128(5), 521-529

Siringoringo, D. M. and Fujino, Y. (2008), 'System identification of suspension bridge from ambient vibration response', *Engineering Structures*, 30, 462-477

Socha, K. (2004), 'ACO for continuous and mixed-variable optimization', *4th International Workshop on Ant Colony Optimization and Swarm Intelligence*, Brussels, Belgium, SEP 05-08, 3172, 25-36

Sohn, H., Farrar, C. R., Hemez, F. M., Shunk, D. D., Stinemates, D. W., Nadler, B. R. and Czarnecki, J. J. (2004), 'A review of structural health monitoring literature: 1996-2001', *Los Alamos National Laboratory Report*, LA-13976-MS

Tfaili, W. and Siarry, P. (2008), 'A new charged ant colony algorithm for continuous dynamic optimization', *Applied Mathematics and Computation*, 197(2), 604-613

Thompson, J. M. and Dowsland, K. A. (1998), 'A robust simulated annealing based examination timetabling system', *Computers & Operations Research*, 25(7-8), 637-648

Tee, K. F., Koh, C. G. and Quek, S. T. (2005), 'Substructural first- and second-order model identification for structural damage assessment', *Earthquake Engineering & Structural Dynamics*, 34(15), 1755-1775

Tee, K. F., Koh, C. G. and Quek, S. T. (2009), 'Numerical and experimental studies of a substructural identification strategy', *Structural Health Monitoring-An International Journal*, 8(5), 397-410

Tikhonov, A. N., Leonov, A. S. and Yagola, A. G. (1995), 'Nonlinear Ill-Posed Problems, V. 1, V. 2', Chapman & Hall

Trujillo, D. M and Busby, H. R. (1989), 'Optimal regularization of the inverse heat-conduction problem', *Journal of Thermophysics and Heat Transfer*, 3(4), 423-427

Thanh, T. N. (2010), 'Evolutionary divide-and-conquer strategy for identification of structural systems and moving forces', *PhD dissertation*, National University of Singapore

Vandiver, J. K., Dunwoody, A. B., Campbell, R. B. and Cook, M. F. (1982), 'A mathematical basis for the random decrement vibration signature analysis technique', *Journal of Mechanical Design-Transactions of the ASME*, 104(2), 307-313

Verboven, P., Parloo, E., Guillaume, P. and Van Overmeire, M. (2002), 'Autonomous structural health monitoring - Part 1: Modal parameter estimation and tracking', *Mechanical Systems and Signal Processing*, 16(4), 637-657

Wahab, M. M. A. and Roeck, G. D. (1999), 'Damage detection in bridges using modal curvatures: application to a real damage scenario', *Journal of Sound and Vibration*, 226(2), 217-235

Wang, D. and Haldar, A. (1994), 'Element-level system identification with unknown input', *Journal of Engineering Mechanics-ASCE*, 20(1), 159-176

Wang, D. and Haldar, A. (1997), 'System identification with limited observations and without input', *Journal of Engineering Mechanics-ASCE*, 123(5), 504-511

Wang, X. M. (2012), 'System identification of jack-up platform by genetic algorithms', *PhD dissertation*, National University of Singapore

Wang, Z., Lin, R. M. and Lim, M. K. (1997), 'Structural damage detection using measured FRF data', *Computer Methods in Applied Mechanics and Engineering*, 147, 187-197

Wolfaardt, H. J. (2005), 'Theory of the microfluidic channel angular accelerometer for inertial measurement applications', *Thesis*, University of Pretoria

Wu, M. L. and Smyth, A. W. (2007), 'Application of unscented Kalman filter for real-time nonlinear structural system identification', *Journal of Structural Control and Health Monitoring*, 14(7), 971-990

Wu, X., Ghaboussi, J. and Garrett, JR. J. H. (1992), 'Use of neural networks in detection of structural damage'. *Computers & Structures*, 41(4), 649-659

Xu, B. and Du, T. (2006), 'Direct substructural identification methodology using acceleration measurements with neural networks', *Proceedings of the Society of Photo-optical Instrumentation Engineers (SPIE)*, San Diego, CA, 17804-17804

Xu, Y. G., Liu, G. R., Wu, Z. P. and Huang, X. M. (2001), 'Adaptive multilayer perception networks for detection of cracks in anisotropic laminated plates', *International Journal of Solids and Structures*, 38(32-33), 5625-5645

Yang, J. N. and Lin, S. (2005), 'Identification of parametric variations of structures based on least squares estimation and adaptive tracking technique', *Journal of Engineering Mechanics-ASCE*, 131(3), 290-298

Yang, J. N, Lin, S., Huang, H. W. and Zhou, L. (2006), 'An adaptive extended Kalman filter for structural damage identification', *Structural Control & Health Monitoring*, 13(4), 849-867

Yang J. N., Pan S. and Huang H. (2007), 'An adaptive extended Kalman filter for structural damage identifications II: unknown inputs', *Structural Control & Health Monitoring*, 14(3), 497-521

Yu, L. and Wan, Z. Y. (2008), 'An improved PSO algorithm and its application to structural damage detection', *Proceeding of 4th International Conference on Natural Computation*, 1, 423-427

Yu, L. and Xu, P. (2010), 'An ACO-based algorithm for structure health monitoring', *Prognostics and System Health Management Conference*, Macao, China, 209-215

Yu, L. and Xu, P. (2011), 'Structural heath monitoring based on continuous ACO method', *Microelectronics Reliability*, 51(2), 270-278

Yuen, K. V. and Katafygiotis, L. S. (2006), 'Substructure identification and health monitoring using noisy response measurements only', *Computer-Aided Civil and Infrastructure Engineering*, 21, 280-291

Yun, C. B. and Lee, H. J. (1997), 'Substructural identification for damage estimation of structures', *Structural Safety*, 19(1), 121-140

Yun, C. B. and Bahng, E. Y. (2000), 'Substructural identification using neural networks', *Computers & Structures*, 77, 41-52

Yun, C. B., Yi, J. H. and Bahng, E. Y. (2001), 'Joint damage assessment of framed structures using a neural networks technique', *Engineering Structures*, 23(5), 425-435

Zamani, M., Ghartemani, M. K., Sadati, N. and Parniani, M. (2009), 'Design of a fractional order PID controller for an AVR using particle swarm optimization', *Control Engineering Practice*, 17 (2), 1380-1387

Zhang, K. and Law, S. S. (2009), 'Condition assessment of structures under unknown support excitation', *Earthquake Engineering and Engineering Vibration*, 8(1), 103-114

Zhang, Z. (2009), 'A uniformly sampled genetic algorithm with gradient search for system identification', *PhD dissertation*, National University of Singapore

Zhang, Z., Koh, C. G. and Duan, W. H. (2010a), 'Uniformly sampled genetic algorithm with gradient search for structural identification - Part I: Global search', *Computers & Structures*, 88(15-16), 949-962

Zhang, Z., Koh, C. G. and Duan, W. H. (2010b), 'Uniformly sampled genetic algorithm with gradient search for structural identification - Part II: Local search', *Computers & Structures*, 88(19-20), 1149-1161

Zheng, C. and Wang, P. (1996), 'Parameter structure identification using tabu search and simulated annealing', *Advances in Water Resources*, 19(4), 215-224

Zhou, Y. and Yi, W. J. (2007), 'Physical parameter identification for a RC frame structure on elastic foundation by genetic simulated annealing algorithm', *Structural Condition Assessment, Monitoring and Improvement*, 447-455

Zhu, X. Q. and Law, S. S. (2000), 'Identification of vehicle axle loads from bridge dynamic responses', *Journal of Sound and Vibration*, 236(4), 705-724

Zhu, X. Q. and Law, S. S. (2001), 'Identification of moving loads on an orthotropic plate', *Journal of Vibration and Acoustics*, 123, 238-244

Ziad, K. A., Thiru, A., Yan, Z. G. and Felipe, G. (2012), 'A review of optimization techniques used in the design of fibre composite structures for civil engineering applications', *Materials & Design*, 33, 534-544

Zou, Y., Tong, L. and Steven, G. P. (2000), 'Vibration-based model-dependent damage (delamination) identification and health monitoring for composite structures-a review', *Journal of Sound and Vibration*, 230(2), 357-378

# Appendix A Tikhonov Regularization Method with L-curve for Determination of Regularization Parameter

Consider a linear system as follows

$$y = Ax \tag{A.1}$$

When $A$ is severely ill-conditioned and the data $y$ is contaminated by noise, it is not easy to obtain a stable solution. The direct solution of least-square method leads to unbound solution $x$ that is severely contaminated by noise. Tikhonov regularization method (Tikhonov et al., 1995) is one of the most popular approaches to solve discrete ill-posed problems with error-contaminated data by

$$\min \quad \|Ax - y\|^2 + \lambda^2 \|Lx\|^2 \tag{A.2}$$

where $\lambda$ and $L$ are regularization parameter and regularization operator, respectively. $\|Ax - y\|^2$ and $\lambda^2 \|Lx\|^2$ in Eq. (A.2) are least square or residual norm and regularized norm. The solution of Eq. (A.2) is

$$\hat{x} = \left(A^T A + \lambda^2 L^T L\right)^{-1} A^T y \tag{A.3}$$

Based on the fact that log-log parametric plot of the residual norm $\|Ax - y\|^2$ to regularized norm $\|Lx\|^2$ often has a distinct L-shape. L-curve method (Hansen, 1992; Hansen and O´leary, 1993) is to find the value of regularization parameter between

$\log\|Ax-y\|^2$ and $\log\|Lx\|^2$ by plotting their relationship in the graph. They found that the corner point of the L-curve corresponds to a good balance between the residual norm and the regularized norm. Therefore, the optimal regularization parameter $\lambda$ is characterized at the corner of L-curve in the graph by seeking the point with the maximum curvature, while the curvature is defined as (Hansen and O´leary, 1993)

$$\hat{c} = 2\frac{\hat{\rho}'\hat{\xi}'' - \hat{\rho}''\hat{\xi}'}{\left(\left(\hat{\rho}'\right)^2 + \left(\hat{\xi}'\right)^2\right)^{3/2}} \tag{A.4}$$

where $'$ denotes the differentiation with respect to the regularization parameter $\lambda$; $\hat{\xi} = \log\|Lx\|^2$ and $\hat{\rho} = \log\|Ax-y\|^2$.

# Appendix B Strain-to-Displacement Relation in Beam Element

For a plane beam element based on Euler-Bernoulli formulation, the bending strain at the top is expressed as

$$\varepsilon\left(\xi,\frac{h}{2}\right)=-\frac{h}{2}\left(\frac{2}{L}\right)^2\left[\frac{3}{2}\xi \quad -\frac{L}{4}+\frac{3L}{4}\xi \quad -\frac{3}{2}\xi \quad \frac{L}{4}+\frac{3L}{4}\xi\right]\begin{Bmatrix}w_1\\ \theta_1\\ w_2\\ \theta_2\end{Bmatrix} \tag{B.1}$$

where $L$ and $h$ are the length and thickness of beam element. $\{w_1 \quad \theta_1 \quad w_2 \quad \theta_2\}^T$ is the nodal displacement while $\xi\in[-1 \quad 1]$ specifies the location of installed strain gauges. As shown in the numerical study in Section 2.5.1, there are two strain gauges ($\xi_1=-1/\sqrt{3}$, $\xi_2=1/\sqrt{3}$) settled in each element, therefore

$$\begin{Bmatrix}\varepsilon\left(\xi_1=-\frac{1}{\sqrt{3}},\frac{h}{2}\right)\\ \varepsilon\left(\xi_1=\frac{1}{\sqrt{3}},\frac{h}{2}\right)\end{Bmatrix}=-\frac{h}{L^2}\begin{bmatrix}-\sqrt{3} & -\frac{L}{2}-\frac{\sqrt{3}}{2}L & \sqrt{3} & \frac{L}{2}-\frac{\sqrt{3}}{2}L\\ \sqrt{3} & -\frac{L}{2}+\frac{\sqrt{3}}{2}L & -\sqrt{3} & \frac{L}{2}+\frac{\sqrt{3}}{2}L\end{bmatrix}\begin{Bmatrix}w_1\\ \theta_1\\ w_2\\ \theta_2\end{Bmatrix} \tag{B.2}$$

where

$$[S]=-\frac{h}{L^2}\begin{bmatrix}-\sqrt{3} & -\frac{L}{2}-\frac{\sqrt{3}}{2}L & \sqrt{3} & \frac{L}{2}-\frac{\sqrt{3}}{2}L\\ \sqrt{3} & -\frac{L}{2}+\frac{\sqrt{3}}{2}L & -\sqrt{3} & \frac{L}{2}+\frac{\sqrt{3}}{2}L\end{bmatrix} \tag{B.3}$$

According to Eq. (2.16)

$$\left[\Phi_s\right]=\frac{L}{6h\left(L^2+4\right)}\begin{bmatrix} 2\sqrt{3}L & -2\sqrt{3}L \\ 12+\left(3+\sqrt{3}\right)L^2 & 12-\left(-3+\sqrt{3}\right)L^2 \\ -2\sqrt{3}L & 2\sqrt{3}L \\ -12+\left(-3+\sqrt{3}\right)L^2 & -12-\left(3+\sqrt{3}\right)L^2 \end{bmatrix}$$

The elemental rigid-body modes consist of one translation and one rotation, which are

$$\Phi_\alpha^T=\begin{bmatrix} 1 & 0 & 1 & 0 \\ -L & 2 & L & 2 \end{bmatrix} \tag{B.4}$$

Therefore, the nodal displacement can be represented as

$$\begin{Bmatrix} w_1 \\ \theta_1 \\ w_2 \\ \theta_2 \end{Bmatrix}=\frac{L}{6h\left(L^2+4\right)}\begin{bmatrix} 2\sqrt{3}L & -2\sqrt{3}L \\ 12+\left(3+\sqrt{3}\right)L^2 & 12-\left(-3+\sqrt{3}\right)L^2 \\ -2\sqrt{3}L & 2\sqrt{3}L \\ -12+\left(-3+\sqrt{3}\right)L^2 & -12-\left(3+\sqrt{3}\right)L^2 \end{bmatrix}\begin{Bmatrix} \varepsilon\left(\xi_1=-\frac{1}{\sqrt{3}},\frac{h}{2}\right) \\ \varepsilon\left(\xi_1=\frac{1}{\sqrt{3}},\frac{h}{2}\right) \end{Bmatrix} + \begin{bmatrix} 1 & -L \\ 0 & 2 \\ 1 & L \\ 0 & 2 \end{bmatrix}\begin{Bmatrix} \alpha_1 \\ \alpha_2 \end{Bmatrix} \tag{B.5}$$

Therefore, the rigid-body amplitudes and the rotational displacements can be computed through the measurements of strains and translational displacements

$$\begin{Bmatrix}\alpha_1\\ \alpha_2\\ \theta_1\\ \theta_2\end{Bmatrix}=\begin{bmatrix}-1 & L & 0 & 0\\ -1 & -L & 0 & 0\\ 0 & -2 & 1 & 0\\ 0 & -2 & 0 & 1\end{bmatrix}^{-1}\left\{\begin{matrix}\dfrac{L}{6h\left(L^2+4\right)}\begin{bmatrix}2\sqrt{3}L & -2\sqrt{3}L\\ -2\sqrt{3}L & 2\sqrt{3}L\\ 12+\left(3+\sqrt{3}\right)L^2 & 12-\left(-3+\sqrt{3}\right)L^2\\ -12+\left(-3+\sqrt{3}\right)L^2 & -12-\left(3+\sqrt{3}\right)L^2\end{bmatrix}\\ \times\begin{Bmatrix}\varepsilon\left(\xi_1=-\dfrac{1}{\sqrt{3}},\dfrac{h}{2}\right)\\ \varepsilon\left(\xi_1=\dfrac{1}{\sqrt{3}},\dfrac{h}{2}\right)\end{Bmatrix}-\begin{bmatrix}1 & 0\\ 0 & 1\\ 0 & 0\\ 0 & 0\end{bmatrix}\begin{Bmatrix}w_1\\ w_2\end{Bmatrix}\end{matrix}\right\} \tag{B.6}$$